

UNIVERSITY OF CALIFORNIA, SAN DIEGO

Endothelial Influences Enhance Human Pluripotent Stem Cell-derived Cardiomyocyte Maturation

A dissertation submitted in partial satisfaction of the
requirements for the degree Doctor of Philosophy

in

Bioengineering

by

Karen A. Wei

Committee in charge:

Professor Andrew D. McCulloch, Chair
Professor Mark Mercola, Co-Chair
Professor Shu Chien
Professor Karen L. Christman
Professor Karl Willert

2011

Copyright

Karen A. Wei, 2011

All rights reserved.

The dissertation of Karen A. Wei is approved, and it is acceptable in quality and form for publication on microfilm and electronically:

Co-Chair

Chair

University of California, San Diego

2011

DEDICATION

To my parents.

EPIGRAPH

Do not go where the path may lead, go instead where there is no path and leave a trail.

Ralph Waldo Emerson

TABLE OF CONTENTS

Signature Page	iii
Dedication	iv
Epigraph.....	v
Table of Contents	vi
List of Figures.....	xi
List of Tables.....	xviii
Acknowledgements	xix
Vita	xxiii
Abstract of the Dissertation	xxiv
1 Introduction	1
1.1 The Myocardium.....	2
1.2 Regenerative Medicine.....	5
1.2.1 Current Approaches to Myocardial Regeneration	6
1.2.2 Major Limitations to Myocardial Regeneration	9
1.3 Heart Development	10
1.3.1 Embryological Perspective of Cardiac Development.....	11
1.3.2 Stem Cells: Cardiac Specification and Differentiation	12
1.4 Cardiomyocyte Maturation	14
1.4.1 Cardiomyocyte Morphology.....	17
1.4.2 Cardiomyocyte Mechanobiology	19
1.4.3 Cardiomyocyte Electrophysiology	22
1.4.4 Cardiomyocyte Ca ²⁺ Handling	25
1.4.5 Exploiting Endogenous Mechanisms of CM maturation.....	27
1.4.6 Field Limitations	30
1.5 The Endothelial-Cardiomyocyte Relationship	31
1.5.1 Endothelial-Cardiomyocyte Interactions in Development.....	32
1.5.2 Endothelial-Cardiomyocyte Interactions in Normal Cardiac Function	33

1.5.3	Endothelial Influences on hPSC-derived Cardiomyocytes	34
1.6	Scope of the Dissertation	36
2	Co-culture of Endothelial Cells and Human Embryonic Stem Cell (hESC)-derived Cardiomyocytes	38
2.1	Abstract	38
2.2	Introduction.....	39
2.3	Methods.....	42
2.3.1	Cells	42
2.3.2	Media Comparison for Long-term culture of ECs	44
2.3.3	Dissociation of cardiospheres for multi-well formats	45
2.3.4	Co-culture of hESC-derived CMs and Endothelial Cells	46
2.3.5	Electrophysiology: Intracellular (IC) Recordings.....	48
2.3.6	Pharmacology	49
2.3.7	Quantitative Polymerase Chain Reaction (qPCR).....	49
2.3.8	Immunostaining	51
2.4	Results	52
2.4.1	Media comparison for Long-term Culture of ECs	52
2.4.2	Dissociation of cardiospheres for multi-well formats	56
2.4.3	Co-culture of hESC-derived CMs and Endothelial Cells	57
2.4.3.1	Co-culture of hESC-derived CSs with HUVECs (CCE1)	57
2.4.3.2	Co-culture of dissociated hESC-derived CMs and Disparate Endothelial Sources (CCE2 and CCE3).....	61
2.5	Discussion	64
2.5.1	Media Comparison for Long-term Culture of ECs	64
2.5.2	Dissociation of cardiospheres for multi-well formats	65
2.5.3	Co-culture of hESC-derived CMs and Endothelial Cells	66
2.5.3.1	Co-culture of hESC-derived CSs with HUVECs (CCE1)	66
2.5.3.2	Potential Limitations to Evaluating CSs in Biological Assays.....	69
2.5.3.3	Co-culture of dissociated hESC-derived CMs and Disparate Endothelial Sources (CCE2 and CCE3).....	70
2.5.3.4	Technical Limitations of CCE2 and CCE3.....	72

2.6	Conclusions.....	73
2.7	Acknowledgements	75
3	Endothelial Paracrine Factors Enhance Maturation of Human Induced Pluripotent Stem Cell-derived Cardiomyocytes	76
3.1	Abstract	76
3.2	Introduction.....	77
3.3	Methods.....	79
3.3.1	Cells	79
3.3.2	Conditioned Media	80
3.3.3	Time course of Endothelial Paracrine Effects on CM Maturation	81
3.3.4	Fluo4 Loading of Cardiomyocytes for Ca ²⁺ Transient Imaging.....	82
3.3.5	Pharmacology	82
3.3.6	Kinetic Imaging Cytometer (KIC) for High-throughput Acquisition of Cardiomyocyte Ca ²⁺ Transient Generation	83
3.3.7	Cyteseer Analysis of Ca ²⁺ Transient Imaging Data	84
3.3.8	Quantitative Polymerase Chain Reaction (qPCR).....	86
3.3.9	Immunostaining	88
3.4	Results	88
3.4.1	High-throughput analysis of cardiac Ca ²⁺ -handling parameters enables large-scale evaluation of heterogeneous hiPSC-derived CM populations	88
3.4.2	Maturation of hiPSC-derived CMs correlates with lower nFWHM values....	94
3.4.3	Treatment with HUVEC conditioned media enhances pacing ability of hiPSC-derived CMs.....	98
3.4.4	Treatment with HUVEC conditioned media enhances Ca ²⁺ transient kinetic parameters towards a more mature phenotype.	99
3.4.5	Inhibition of the L-type Ca ²⁺ channel eradicates contractile activity of hiPSC-derived CMs	102
3.4.6	Treatment with HUVEC conditioned media enhances Na _v 1.5 function in hiPSC-derived CMs.....	104
3.4.7	Exposure to endothelial paracrine factors increases functionality of SERCA2 in a larger proportion of CMs.....	109

3.5	Discussion	115
3.5.1	High-throughput analysis of cardiac Ca ²⁺ -handling parameters enables large-scale evaluation of heterogeneous hiPSC-derived CM populations	116
3.5.2	Maturation of hiPSC-derived CMs correlates with lower nFWHM values..	118
3.5.3	Treatment with HUVEC conditioned media enhances Ca ²⁺ transient kinetic parameters towards a more mature phenotype.	119
3.5.4	Inhibition of the L-type Ca ²⁺ channel eradicates contractile activity of hiPSC-derived CMs in all experimental subsets.....	120
3.5.5	Treatment with HUVEC conditioned media enhances Na _v 1.5 function in hiPSC-derived CMs.....	122
3.5.6	Exposure to endothelial paracrine factors increases functionality of SERCA2 in a larger proportion of CMs.....	124
3.6	Conclusions.....	128
3.7	Acknowledgements	131
4	Summary and Future Directions.....	132
	Appendix A Technical Tables.....	136
A.1	Table of Media Formulations	137
A.2	Table of qPCR Primers.....	138
A.3	Table of Cardiac Markers Modulated with CM Maturation.....	139
	Appendix B Generation of a Tie2 Reporter Line for Genetic Selection of ECs from Human Pluripotent Stem Cells	140
B.1	Rationale.....	141
B.1	Cloning of the Tie2-Selectable Lentiviral Construct	142
B.2	Methods.....	148
B.2.1	Cells.....	148
B.2.2	Lentivirus Production and Infection of hESCs.....	150
B.2.3	Fluorescence Activated Cell Sorting (FACS)	152
B.2.4	Quantitative Polymerase Chain Reaction (qPCR)	152
B.2.5	Immunostaining.....	154
B.3	Tie2 Construct Validation.....	154
B.3.1	Validation of T2P Construct in HUVECs	154

B.3.2	Validation of T2M Construct in HUVECs	155
B.3.3	Validation of Tie2 Constructs in hESCs	156
B.4	Tie2 Upregulation Trials	161
B.4.1	Endothelial Differentiation Conditions	161
B.4.2	Shear Experiments	163
B.4.3	Hypoxia Experiments	164
B.4.4	FoxC2/Etv2 Induction of Tie2 Expression	166
B.4.5	Teratoma Formation	168
B.5	Conclusions	170
B.6	Acknowledgements	171
References	172

LIST OF FIGURES

Figure 1 Multi-scale nature of the myocardium. [4]	2
Figure 2 Prominent tissue engineering strategies to date. [23]	8
Figure 3 Schematic of sequential steps involved in cardiomyocyte development in hESCs. [92]	13
Figure 4 Longitudinal section of isolated rabbit myocytes of varying developmental stages. (A) Adult CM and (B) 3-week-old CM. Myofibril organization is much less regular in (B). Scale bar = 10µm. [111]	16
Figure 5 The cardiac action potential. (A) Illustrations of representative cardiac action potential and the associated ion currents [140] (B) Action potentials characteristic of the various myocardial cell subtypes [6]	23
Figure 6 Schematic of CM Ca ²⁺ handling systems and major membrane machinery. [141]	25
Figure 7 HUVEC media testing 8 days of culture versus 22 days of culture. Different medias were tested with HUVEC cultures: EGM-2, 2% hEB differentiation media, 0.25% Neonatal CM media, and neonatal CM media with no serum. (Rows 1 and 3) For each time point, 50/50 EGM-2 media to the four different types of media were also tested (Rows 2 and 4), 10X.	54
Figure 8 Immunostaining of D22 HUVEC cultures. Staining is as follows: CD31 (green), lectin (red), To-Pro-3 (blue), 10X. White arrowheads indicate representative localization of EC markers to intracellular junctions.	55
Figure 9 Dissociation of cardiosphere to a contractile CM monolayer in multi-well formats. (A) Cardiosphere (10X), (B) 24-well, 3.5x10 ⁵ cells plated (20X), and (C) 384-well, 2x10 ⁴ cells plated (20X. Stained with α-actinin (Red) and DAPI (Blue).	56
Figure 10 Immunostainings of CS-HUVEC co-culture, 57 days. CS only cultures are shown in panels (A1) and (A2). CS-HUVEC co-cultures are shown in panels (B1) and (B2). Cultures were stained with α-actinin (Red), CD-31 (green), and DAPI (blue).	57
Figure 11 Gene expression profile of key cardiac markers during CM development of co-cultured CSs versus CS only controls. The panel of genes surveyed represents	

key cardiac markers that are active at different points of CM development. All expression values are expressed as fold change over control values (dashed red line = 1).	59
Figure 12 Electrophysiological parameters from IC recordings for co-cultured CS and CS only subsets. The parameters measured were as follows: (A) maximum diastolic potential (MDP), (B) V_{max} , (C) cycle length between APs (RR), (D) action potential amplitude (APA), and (E) action potential duration (APD90). (G) and (H) are representative tracings from each subset.	60
Figure 13 Pharmacology profile of co-cultured CSs versus CS only controls. Depression of beating frequency in comparison to control CS only conditions are compared with exposure to TTX (1 μ M, 5 μ M) and ryanodine (10 μ M).	61
Figure 14 Live fluorescence imaging of dissociated CM:HUVEC co-culture (10X), Day 48 of co-culture. (A) CM only, (B) 1:1 HUVEC:CM co-culture, and (C) 2:1 HUVEC:CM co-culture. CMs are represented by mCherry expression (Red) and GFP-positive nuclei. HUVECs are detected by fluorescein-conjugated lectin shown in green (non-nuclear pattern). ECs are only detected in (B) and (C) as indicated by the arrows.	62
Figure 15 Gene expression profile from qPCR of key cardiac markers during CM development with HUVECs and dissociated CM co-culture versus CM only controls. Here, CMs seeded with HUVECs in a 1:1 HUVEC:CM ratio (n=2) are shown in black and CMs seeded with HUVECs in a 2:1 HUVEC:CM ratio (n=2) are shown in grey. All expression values are expressed as fold change over control values (n=1; dashed red line = 1).	64
Figure 16 Diagram of Ca^{2+} transient parameters extracted by Cyteseer.	86
Figure 17 Comparison of population sampling capabilities between traditional versus high-throughput methods of assaying CM maturation.	89
Figure 18 Number of individual CMs analyzed at week 1 (n=780) and week 2 (n=830) time points.	90
Figure 19 Cyteseer processing of representative well (D05) of baseline CMs. (A) Single cells were segmented and assigned a unique cell ID. (B) CMs were identified as cell segments that could generate spontaneous or electrically stimulated Ca^{2+} transients (grey). Cells that were unresponsive or exhibited low quality transients	

(noise or drifting baseline) were not included in analyses (black). (C) By week 2 of culture, CM contractions were synchronous across the entire well as evidenced by the uniform Ca^{2+} trace when time series data for each CM was averaged. (D)-(F) are Ca^{2+} traces for representative cells that were included in analyses (blue, D-E) or excluded (yellow, F)..... 90

Figure 20 Frequency distributions of Ca^{2+} kinetic parameters, (A) nFWHM, (B) rise velocity, and (C) decay velocity, and lognormal transformation of each parameter, respectively (B), (D), and (F). 92

Figure 21 Time course characterization of Ca^{2+} kinetic parameters. Percentile distributions of kinetic parameters, (A) peak value (B) nFWHM (C) rise velocity, and (D) decay velocity, based on Table 3 and corresponding fold changes of Week 2 cell percentages over Week 1 for each percentile. 93

Figure 22. CMs were spontaneously contractile and could respond to electrical stimulation. (A) Spontaneous beating frequency at 1- and 2-week time points were about 0.5Hz and 1Hz, respectively. (B) Baseline CMs could respond to 2 and 3Hz electrical stimulation regimes after 2 weeks in culture (D50 of differentiation)..... 95

Figure 23 Pacing ability of 2-week (D50 of differentiation) hiPSC-derived CMs. (A) Spontaneous, (B) 2Hz, 12 stimulations, and (C) 3Hz, 12 stimulations..... 96

Figure 24 Correlation of 3Hz pacing responsiveness with nFWHM values suggest response to pacing signifies increased maturity can be reflected by lower nFWHM values. Data is from one representative control well (Well D05). 97

Figure 25 3Hz pacing ability of hiPSC-derived CMs was evaluated in all CMs from each subset (A). (B) A proportion of CMs from each experimental sample could respond to all 12 stimulations at 3Hz. Total CM number is listed above each bar. 98

Figure 26 Correlation of CM responsiveness to 3Hz pacing and nFWHM values for each experimental subset: (A) untreated, (B) HUVEC, (C) HMEC, and (D) hESC-derived fibroblast conditioned media treated hiPSC-derived CMs after 2 weeks of culture. The first column represents the cell number of responders versus total CM number in each percentile. The second column shows the percentage of

responding CMs from the total number of CMs in each percentile range. The third column gives representative traces from each well.....	100
Figure 27 Mean values of Ca kinetic parameters over all CMs assayed. (SEM, **p<0.01, ***p<0.0001)	101
Figure 28 Evaluation of Ca ²⁺ transient kinetics, nFWHM (A, B), rise velocity (C, D), and decay velocity (E, F) for conditioned media treated CMs versus untreated CMs. Both frequency distributions (A, C, E) and percentile-based (B, D, F) evaluations are represented to quantify differences between conditioned media treated and untreated samples.....	101
Figure 29 Representative Ca ²⁺ transient tracings of diltiazem (DTZ)-treated (red) and untreated (black) hiPSC-derived CMs. DTZ inhibition of L-type Ca ²⁺ channels eradicates Ca ²⁺ flux and contractile activity for all conditions. (A) Stimulated (B) 1Hz, 6 stimultions.....	103
Figure 30 Expression levels of Cav1.2 expression normalized to GAPDH for each experimental subset after 2 weeks of culture.	103
Figure 31 Representative Ca ²⁺ transient traces from individual wells treated with TTX (red) versus untreated CMs (black) for (A) control CMs, (B) HUVEC, (C) HMEC, and (D) hESC-derived fibroblast conditioned media treated CMs after 2 weeks.	106
Figure 32 Effect of TTX treatment on beating frequency after 2 weeks in culture. Beating frequency is depressed with TTX treatment (red) versus untreated controls (black).....	106
Figure 33 Percentile characterization of TTX treatment versus untreated CMs for each experimental subset, namely (A) control, (B) HUVEC, (C) HMEC, and (D) hESC-derived fibroblast conditioned media treated CMs. For each subset, overlays of percentile distributions for TTX-treated (red) and untreated (black) CMs are shown.....	107
Figure 34 Characterization of CMs with rise velocities below the 45 th percentile. (A) Percentage of CM population with rise velocities below the 45 th percentile for untreated CMs (black) and TTX-treated (red) (B) Fold change of TTX-treated CMs with rise velocities below the 45 th percentile over untreated CMs.....	108

Figure 35 Fold change comparison of Nav1.5 channel expression between experimental subsets and control CMs.....	108
Figure 36 Immunostaining of Na _v 1.5 (green) in each experimental subset (A) Control (B) HUVEC conditioned media (C) HMEC conditioned media (D) hESC-derived fibroblast conditioned media. CMs are mCherry-positive (red) and nuclei are stained with DAPI (blue), 20X.	109
Figure 37 Representative Ca ²⁺ transient traces from individual wells treated with TSG (red) versus DMSO-treated CMs (black) for (A) control CMs, (B) HUVEC, (C) HMEC, and (D) hESC-derived fibroblast conditioned media treated CMs after 2 weeks.	111
Figure 38 Effect of thapsigargin (TSG, 1 μm) on beating frequency of hiPSC-derived CMs in all experimental subsets at 2 weeks. (SEM) Beating frequency is depressed in TSG-treated (red) samples compared to untreated controls (black) in all cases.	111
Figure 39 Percentile characterization of TSG-treated versus DMSO-treated CMs for each experimental subset, namely (A) control, (B) HUVEC, (C) HMEC, and (D) hESC-derived fibroblast conditioned media treated CMs. For each subset, overlays of percentile distributions for TSG-treated (red) and untreated (black) CMs are shown.	112
Figure 40 Characterization of CMs with decay velocities below the 45 th percentile. (A) Percentage of CM population with decay velocities below the 45 th percentile for untreated CMs (black) and TSG-treated (red) (B) Fold change of TSG-treated CMs with decay velocities below the 45 th percentile over untreated CMs.	113
Figure 41 Fold change of Ca ²⁺ -handling protein expression of conditioned media treated CMs over controls for SERCA2 (A), NCX1(B), PLB(C), IP3R2(D), RYR2(E), CASQ2(F), and CaI _R (G).....	114
Figure 42 Plasmid map of Sin18 Tie2-Puro ^r -Rex-Neo ^r (T2P) construct.	145
Figure 43 Plasmid map of Sin18 Tie2-mCherry-Rex-Neo ^r (T2M) construct.	146
Figure 44 Lipofectamine transfection of T2P construct into HUVECs with 4 hour and 8 hour transfection protocols. Cultures were then exposed to puromycin for 48 hours at 0.35, 0.25, and 0.125 ug/ml concentrations. Red squares outline the viable cells. (x10 magnification).	155

Figure 45 Lipofectamine transfection of T2M construct into HUVECs using a 4 hour transfection protocol. Phosphoglycerate kinase (PGK) is expressed at basal levels in all cells and used as a transfection control. mCherry expression is only seen in the HUVEC transfections signifying the functionality of the construct. . 156

Figure 46 Neomycin selection of T2P-infected H9 hESCs. A) hESC colonies on mouse embryonic fibroblast feeder layer, pre-neomycin exposure. B) Cultures were exposed to a half dose of typically 0.2856 ug/ml of neomycin for 4 days. Elimination of non-neomycin resistant fibroblast feeders shows the resistance of the hESC colonies. (x4)..... 157

Figure 47 D17 hEB differentiation cultures of both (A) T2M and (B) T2P hESC lines, 10X. Bright field (A1 and B1) panels demonstrate the morphology of hEB cultures. Fluorescent imaging of differentiation cultures (A2 and B2) shows networks of lectin-stained ECs (green) but no cellular mCherry expression (red). Both cell lines exhibit EC differentiation. 158

Figure 48 Evaluation of T2M functional specificity in HUVECs 7 days post-infection, 10X. L-cells (A) infected with the T2M construct do not express mCherry, whereas HUVECs (B) show expression of mCherry (red) in some of the cells. This evaluation shows that the T2M construct is not only functional, but also endothelial-specific to cells that express Tie2. 159

Figure 49 Evaluation of puromycin sensitivity in T2P-infected HUVECs, 10X. A comparison of untreated (A) and 24-hour puromycin-treated T2P-infected HUVECs shows that the construct can confer puromycin sensitivity in mature ECs..... 159

Figure 50 Gene expression of Tie2 and CD31 normalized to GAPDH in D25, T2P EB differentiation cultures. T2P-modified hESCs were differentiated to D25 to ensure an EC presence (confirmed with lectin staining). Untreated (white), 24-hour puromycin (1mg/ml) treated (black), and HUVEC controls (grey) EB cultures were processed for qPCR and probed for expression of EC markers. 160

Figure 51 Comparison of traditional versus endothelial differentiation conditions, 10X. (A1) and (B1) depict T2M and T2P hESCs, respectively, differentiated with serum conditions. (A2) and (B2) depict T2M and T2P hESCs, respectively, differentiated

with EC conditions. All cultures were stained with lectin (green) and evaluated for mCherry expression (red). mCherry could not be resolved.....	162
Figure 52 Gene expression profile of T2P hESCs differentiated in both traditional serum (white) and endothelial (black) differentiation protocols. Gene expression of endothelial markers, although upregulated in EC differentiation conditions, did not confer mCherry expression or puromycin resistance. α MHC expression was also tested.....	162
Figure 53 Gene expression of EC markers for D35, T2M differentiation cultures subjected to 48- and 72-hour shear stress. Fold change of expression over static controls is shown for Tie2, CD31, and mCherry expression.	164
Figure 54 mCherry expression in D37 T2M differentiation cultures in static (A), 48-hour shear (B), and 72-hour shear (C) conditions, 20X. ECs were stained with lectin (green). mCherry expression (red) could not be detected in the cells. Non-specific red signal was detected in (B), but the same expression pattern was seen in all other channels as well.....	164
Figure 55 Gene expression of T2M hESC differentiation cultures (D17) in response to 1% hypoxia conditions. Cultures were dissociated and exposed to 24- and 48-hour hypoxic conditions. Samples were fixed and processed immediately at each time point. One sample was then returned to normoxic conditions for 24 hours. No upregulation of EC markers or reporter genes were observed, except in the expression of the positive control, Glut1.	166
Figure 56 Activation of T2M reporter with FoxC2/Etv2 co-expression in transfected L-Cell fibroblasts. Coexpression of FoxC2 and Etv2 factors enhances the activation of the T2M reporter when transfected in non-endothelial L-Cell fibroblasts by almost 2-fold.	168

LIST OF TABLES

Table 1 Table of CM plating densities for various tissue culture plating formats.	46
Table 2 Table of co-culture experiments and cell constituents.	48
Table 3 Table of percentile gates based on Week 1 median values (50 th percentile) for each Ca ²⁺ kinetic parameter.	93
Table 4 Table of percentile gates based on Week 2 median values (50 th percentile) for each Ca ²⁺ kinetic parameter.	96
Table 5 Table of percentile gates for decay velocity (V_{decay}) based on Week 2 median values (50 th percentile) for DMSO-treated control CMs.	112
Table 6 PCR primers used for cloning Tie2-Puro ^r -Rex-Neo ^r construct.	147
Table 7 PCR programs for cloning Tie2-Puro ^r -Rex-Neo ^r construct.	147
Table 8 Table of Restriction Enzymes used from New England Biosciences, Inc. (Ipswich, MA).	147
Table 9 Table of transfection conditions for FoxC2/Etv2 upregulation of Tie2 expression.	167

ACKNOWLEDGEMENTS

The completion of this dissertation would not have been possible without the concerted effort of many individuals. As a Bioengineering student at the University of California, San Diego, I embraced the multidisciplinary approach of this field and formed collaborations cross-departments and cross-institutions. Over the past 7 years, my graduate student career has been spent jointly in the Cardiac Mechanics Research Group (CMRG) and in the Mercola laboratory at the Sanford-Burnham Medical Research Institute (SBMRI). I will be forever grateful for this experience, which has not only helped me gain the scientific proficiency I aspired to when I began this journey but has also equipped me with the professional toolset that I know will be instrumental for all future endeavors.

Each step in my graduate career would not have been possible without those who helped me build and execute my ideas. I would first like to acknowledge my co-advisors, Andrew McCulloch and Mark Mercola, for supporting and encouraging my research interests. The evolution of my project from creating 3D cardiac grafts to characterizing the cues that govern cardiac maturation has required a unique flexibility and openness that has enabled scientific exploration and my development into an independent researcher. I am thankful to both advisors for their mentorship, insight, wisdom, and discussion throughout this process. My committee members, Shu Chien, Karen Christman, and Karl Willert, have also been instrumental in offering important perspectives and suggestions that have really helped shape my research.

Moreover, collaborators from both academic institutions and industry have contributed significantly to my research progress. First, I would like to thank Vincent

Chen for his clinical insight and technical expertise with electrophysiological characterization of cardiomyocytes. I would also like to thank Fabio Cerignoli, who first introduced me to KIC and Cyteseer. Fabio's technical assistance and counsel not only prompted the collaborations with both Vala Sciences, Inc. and Cellular Dynamics International, Inc. but also directed the emphasis of this work towards Ca^{2+} -handling as an indicator for cardiomyocyte maturation. Thank you both for your time and patience throughout this process.

Throughout my graduate career, I was lucky enough to have a number of post-doctoral research associates take me under their wing. Maria Barcova taught me the ins and outs of human embryonic stem cell culture and differentiation into cardiomyocytes. She also initiated my foray into molecular cloning, which was later continued and expanded upon by Hiroko Kita-Matsuo. As my project evolved, discussions and brainstorming sessions with Natalia Kan have been instrumental in terms of experimental design as well as subsequent data analysis. I will be forever thankful for her mentorship and friendship. I am also extremely grateful to Ramon Diaz-Trelles, who has acted as a sounding board and resource in all things science and life for the past 7 years. I thank him for his perpetual honesty, infectious vigor, and Spanish-inspired humor. Finally, I would like to thank Andy Edwards for taking the time to teach me the fundamentals of Ca^{2+} -handling in cardiomyocytes, help me synthesize experimental data, and brainstorm analysis approaches. In a very short amount of time, we were able to plough through what seemed to me was an insurmountable volume of experimental data and generate meaningful conclusions.

Due to the large scale of most of my experiments, the technical aid of many individuals was necessary and extremely appreciated. From sample cultivation,

maintenance, and acquisition to data processing and analysis, the following people have contributed considerably to my dissertation research: Sean Spiering, Herman Davidovics, Margaret Choi, Ana Rioja, and Scott Karney-Grobe. I would like to thank each individual for undertaking my research interests with the same dedication and enthusiasm as his or her own. Also from the Mercola Laboratory, I would like to acknowledge Masanao Tsuda, Alexandre Colas, and Wenqing Cai for their support, humor, and clarity. I would also like to thank Denise Carroll for maintaining the sanity (or INsanity) from reagent requests to interpretive dances inspired by scientific discovery.

Moreover, I am grateful to two funding organizations, UC BREP and ARCS, which have provided notable financial support during my graduate studies. The Graduate Research and Education in Adaptive BioTechnology (GREAT) fellowship not only helped forge the multidisciplinary character of my dissertation but also afforded my participation in various conferences, industry visits, and networking opportunities. I am also thankful for the generosity of the ARCS foundation. Specifically, I would like to thank Paula Ray and Doug Dawson, from the Ellen Browning Scripps Foundation, for their kind visits and avid interest in my research and personal endeavors.

Finally, I would not have been able to complete this journey without the continual support and encouragement from my family and friends. The unconditional and unlimited love that effortlessly emanates from my parents has fueled me my entire life. I thank them for their innumerable sacrifices, eternal optimism, and belief in me. To my friends from San Diego and beyond, thanks for providing constant laughter and perspective throughout this roller coaster ride. I would particularly like to acknowledge Aric Joneja, who started this Ph.D. journey with me in 2004 and without whom I would have never made it through. Words alone do not suffice in expressing my appreciation for his

considerable patience, candor, and reassurance. (Persistence!) Last but not least, I would like to thank Riki Suzuki for his unlimited zen supply and always providing the salmon belly at the end of the tunnel. I am lucky to have you in my life.

Chapter 3 is in preparation for publication with authors Wei KA, Savtchenko A, Cerignoli F, McCulloch AD, Mercola M. The dissertation author is the primary investigator and author of this material.

VITA

1982 Born, San Jose, California

2004 Sc.B., Biomedical Engineering, Brown University

2006 M.S., Bioengineering, University of California, San Diego

2011 Ph.D., Bioengineering, University of California, San Diego

HONORS AND AWARDS

- ARCS Foundation, Ellen Browning Scripps Scholar, 2006-2011
- UCBREP GREAT Grant, 2006-2008
- NSF GFRP, Honorable Mention, 2004, 2006
- Medtronic Graduate Fellowship, 2004

ABSTRACTS AND PUBLICATIONS

Jacot JG, Kita-Matsuo H, Wei KA, Chen HS, Omens JH, Mercola M, McCulloch AD. *Cardiac myocyte force development during differentiation and maturation*. Ann NY Acad Sci. 2010 Feb;1188:121-7.

Kim C, Majdi M, Xia P, Wei KA, Talantova M, Spiering S, Nelson B, Mercola M, Chen HS. *Non-cardiomyocytes influence the electrophysiological maturation of human embryonic stem cell-derived cardiomyocytes during differentiation*. Stem Cells Dev. 2009 Dec 10.

Kita-Matsuo H, Barcova M, Prigozhina N, Salomonis N, Wei K, Jacot JG, Nelson B, Spiering S, Haverslag R, Kim C, Talantova M, Bajpai R, Calzolari D, Terskikh A, McCulloch AD, Price JH, Conklin BR, Chen HS, Mercola M. *Lentiviral vectors and protocols for creation of stable hESC lines for fluorescent tracking and drug resistance selection of cardiomyocytes*. Plos One. 2009; 4(4):e5046.

Wei KA, McCulloch AD, and Mercola M. A genetic selection-based co-culture method exploring the effects of endothelial-cardiomyocyte interactions on cardiomyogenesis of human embryonic stem cells. Georgia Tech Regenerative Medicine Workshop, 2008. Poster and Abstract.

Wei KA, Gallagher JO, Jacot JG, Mercola M, and McCulloch AD. *Characterizing mechanical strains in a novel three-dimensional tissue culture platform*. California Tissue Engineering Meeting, 2006. Poster and Abstract.

ABSTRACT OF THE DISSERTATION

Endothelial Influences Enhance Human Pluripotent Stem Cell-derived Cardiomyocyte Maturation

by

Karen A. Wei

Doctor of Philosophy in Bioengineering
University of California, San Diego, 2011

Professor Andrew D. McCulloch, Chair
Professor Mark Mercola, Co-Chair

Cardiac tissue engineering has the potential to develop regenerative therapies for damaged myocardium, but due to the complex structure and composition of the tissue in both healthy and diseased states, a clinical solution has not been realized. Human embryonic stem cells (hESCs) and human induced pluripotent stem cells (hiPSCs) are self-renewing, pluripotent cell sources that can potentially generate an unlimited number of cardiomyocytes (CMs). However, the clinical application of these cells is hampered by the limited knowledge of 1) the long-term ability of transplanted cells to maintain a therapeutic effect and 2) the eventual fate of these still very immature cells. Identifying

the biochemical and physical factors that govern cardiac maturation and understanding how they influence this process will be imperative to propel this field forward. This dissertation describes the influence of endothelial cells on major aspects of hiPSC-derived CM physiology and their functional maturation.

To date, neither repopulation of lost myocardial mass nor functional recovery of cardiac infarct regions has been demonstrated after transplantation of human pluripotent stem cell (hPSC)-derived CMs. Strikingly, even after long-term incubation, transplanted CMs remain morphologically and physiologically immature. To this end, we postulate the importance of endothelial influences on CM maturation based on their intimate association from the formation of the early heart tube through adulthood.

In the subsequent chapters, we demonstrate the maturative influences of co-culture hESC-derived CMs with human umbilical vein endothelial cells (HUVECs) on the electrophysiology and gene expression profiles towards a more mature phenotype. Moreover, we investigate the specific effect of endothelial paracrine factors on Ca^{2+} -handling machinery by evaluating changes in kinetic parameters and pharmacological sensitivity. Ultimately, we demonstrate that treatment of hiPSC-derived CMs with endothelial conditioned media increases 3Hz pacing ability, Ca^{2+} transient kinetics, and sensitivity to pharmacological agents that affect the functionality of Ca^{2+} reuptake and initiation of the Ca^{2+} transient. We argue that the functional maturation of hPSC-derived CMs and elucidating the mechanisms that govern these processes will significantly contribute to the therapeutic efficacy and safety of cell-based therapies for myocardial repair.

1 Introduction

Chronic congestive heart failure is the leading cause of death in developed nations.[1] Coronary heart disease, which encompasses myocardial infarction (MI), is responsible for 1 in 5 deaths in the United States. Typically, MI results from coronary artery occlusion of major cardiac vessels, which leads to tissue death, subsequent impairment of contractile function, and, in many cases, mortality. Tissue engineering has the potential to generate more effective methods of replacing damaged myocardium [2, 3], but lack of understanding and inability to recapitulate the complexity of the tissue has hampered clinical progress of tissue-engineered cardiac therapies. [3] In addition to the challenges of developing healthy tissue *in vitro*, myocardial analogs must survive the harsh, post-insult environment, defined by hypoxic, fibrotic, and necrotic conditions. In order to progress further in this field, it is imperative to first elucidate the intricate relationships and interactions between cardiomyocytes (CMs) and their physical environments and understand how these relationships correlate with myocardial structure and function.

1.1 The Myocardium

The heart is an organ of utmost complexity and consequence. This intricate muscular pump is responsible for the continuous circulation through our body that allows for delivery of nutrients and removal of wastes from each organ as well as transporting messenger proteins between various regions of the body. In order to accomplish these formidable tasks requires a synchronized orchestra of contractile, electrical, vascular, and structural components that never rests. Problems occur when these elaborate systems are compromised.

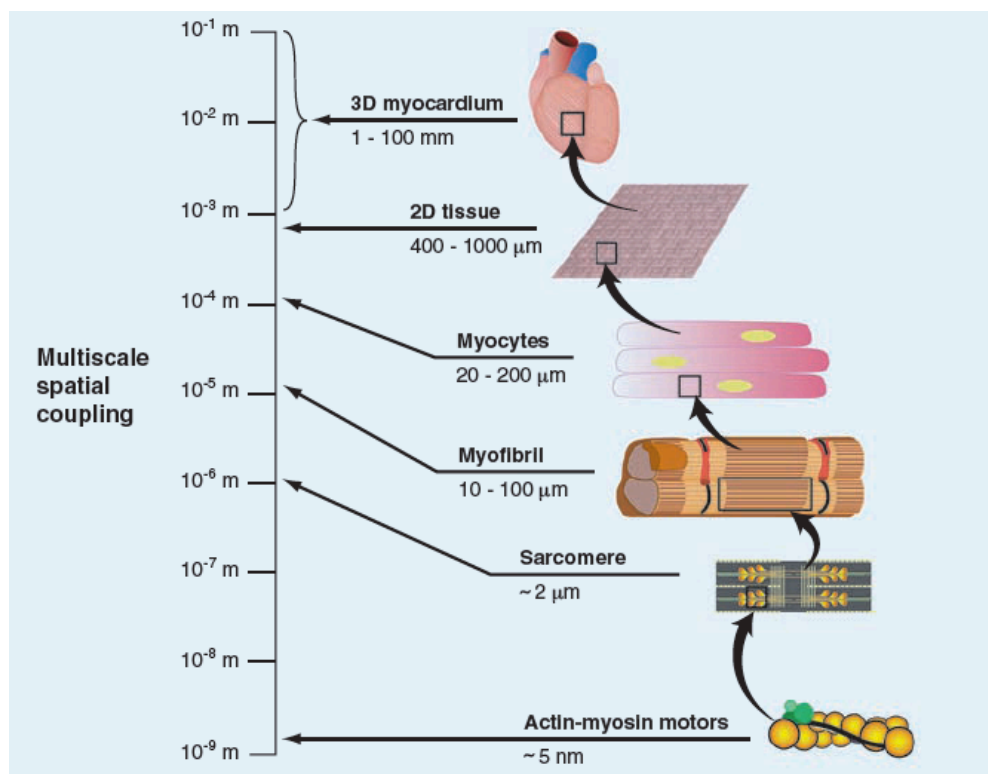


Figure 1 Multi-scale nature of the myocardium. [4]

In order to fully appreciate the complexity of the heart, segregation of each of the major tissue components using a multi-scale approach is imperative. (Figure 1) [4, 5] On a molecular scale, junctional connections between cardiomyocytes, the voltage-gated channels and ion pumps that populate the plasma membrane (PM) and cellular compartments, as well as the actin/myosin motors that are responsible for contraction are the fundamental units responsible for CM physiology. [6] These nanometer scale actin/myosin motors are further organized into the sarcomeres ($\sim 2\mu\text{m}$), the basic contractile units of CMs. Junctional connections are concentrated at the ends of CMs and the machinery that regulates movement of ions are concentrated in regions of the t-tubules and intercalated disks to propagate action potentials across cardiac tissue. [6-8]

Sarcomeres are aligned end-to-end within the CM and together form the myofibrils ($\sim 10\text{-}100\mu\text{m}$) that run along the long axis of the cell. Myofibrils compose 47% of the CM volume and give CMs ($\sim 200\mu\text{m}$) their characteristic striated appearance due to the organization of the contractile proteins into thick and thin filaments aligned in parallel across the long axis of the CM. [6] Myofibrillogenesis is an important hallmark of CM maturation as young myocytes must be able to assemble these functional units before contraction can occur. [9] CMs are concentrated in heart tissue at a density of 10^8 cells/cm³ and supported by a dense vascular network with intercapillary distances on the order of $20\mu\text{m}$. [5]

At a tissue scale (millimeter range), rod-shaped, elongated CMs exhibit an anisotropic organization. In two dimensions (2D), myofibrils are arranged in parallel and serially aligned. As mentioned, each CM is coupled to its neighbors with concentrations of junctional complexes at the longitudinal ends of the cells. Each of these specific elements influences the directional propagation of electrical signals as well as the

uniformity in contraction of the tissue as a whole. [10, 11] As a three-dimensional (3D) tissue, the myocardial wall is composed of layers of cardiomyocytes with fiber angles varying across the layers that span the endocardium to the epicardium. [12] Interspersed between CMs and the muscle layers exists a vast extracellular matrix (ECM) network that provides structural support and contributes to the mechanical properties of the heart. [6, 12] Moreover, the matrix constituents, including collagen, fibronectin, and laminin, and 3D architecture of the ECM serve important signaling roles that dictate cell morphology and physiology.[6, 13]

Although CMs constitute the bulk of the myocardial mass and volume, 70% of myocardial cells are smaller non-myocytes. [6, 14, 15] Endothelial cells and fibroblasts outnumber CMs by about 3:1 [16] and 7:3 [14], respectively. In addition, these cells have distinctive roles as cardiac endothelial cells make up the vasculature that innervate the heart [16] and cardiac fibroblasts are responsible for secreting ECM proteins that contribute to the 3D structure and mechanical compliance of the myocardium [17]. Furthermore, both myocardial homeostasis as well as pathological remodeling of the heart can be influenced by the interplay between CMs and these non-myocyte cell types. [16-19]

The heart is a dynamic organ that is extremely sensitive to environmental cues. Understanding how the organ changes structurally at each organizational level throughout development and in response to different pathologies will be consequential to the creation of effective therapeutic strategies. Specifically in the context of cell-based repair, determining how to capitalize on endogenous repair and remodeling mechanisms in concert with in vitro-designed repair strategies will be necessary to efficiently address the severe implications of cardiovascular disease.

1.2 Regenerative Medicine

Regenerative medicine is the process of developing therapies to repair or replace deficient tissue or organ function due to age, disease, damage, or congenital defects. [20, 21] Thus far, this field has made the most clinical impact in the development of therapies that use cytokines and growth factors to stimulate endogenous cell repair as well as with some cell-based therapies, such as bone-marrow transplantation and skin grafting. [21, 22] Ultimately, the greatest promise of regenerative medicine lies in the prospect of generating complex organs and tissue analogs to alleviate the surging demands for organ transplantation. [22, 23] One reason why the heart has received so much attention and holds so much potential for this field is because this vital organ is minimally regenerative, with CM turnover averaging less than 1% annually over one's lifetime. [24, 25] In the event of a myocardial infarction, approximately 25% of the myocardial mass (25-50g; 10^9 CMs) can be eradicated within a few hours [23, 26, 27], which the body cannot replenish on its own. To highlight the mounting needs for donor-transplant alternatives, around 2,500 out of an estimated 250,000 end-stage heart failure patients will receive a heart replacement. [1, 28] For the majority of patients who will not receive a donor organ, their futures are bleak. Of the patients who do receive a transplant, graft and patient survival average 70% after 5 years. [1, 29] Therefore, the immense therapeutic potential of a non-immunogenic, scalable, readily available tissue analog for infarcted myocardium fuels research efforts in this field.

1.2.1 Current Approaches to Myocardial Regeneration

Myocardial regeneration strategies have generally been divided between cell transplantation and engineering tissue constructs. The overall clinical goals for these distinct approaches are 1) to prevent or attenuate late-stage remodeling due to MI and 2) to restore cardiac function that is lost after bulk tissue death through healthy tissue regeneration. [30, 31] Cellular cardiomyoplasty using a myriad of cell types, ranging from hESC-derived cardiomyocytes, neonatal cardiomyocytes, skeletal myoblasts, to bone marrow stem cells (BMCs), has displayed functional improvement in animal-MI models, exemplified by attenuated deterioration of heart contractility, ejection fraction and stroke volume observed at 4-week to 6-month time-points post-MI. [32-38] It is important to note that, in studies that compared transplantation of myocyte derivatives versus various non-contractile cell types, greatest improvements in left ventricular function were observed when transplanting contractile cell types. [35, 39-41]

Despite the positive suggestion that regenerating damaged myocardium is feasible in animal models, clinical trials transplanting BMCs and skeletal myoblasts, have reported conflicting results, reporting small improvements to insignificant differences between experimental and sham groups.[31, 42-45] At present, the conclusions from these pre-clinical and clinical studies have been: 1) despite some positive indications that cell transplantation improves myocardial function, little is still understood about the underlying mechanisms, optimal cell types, and best methods for therapeutic delivery, 2) the functional improvements that have been observed, although important, do not involve efficient regeneration of the myocardium lost after MI reflected by minimal long-term benefits, and 3) in addition to the therapeutic characteristics of the transplanted cell type alone, graft performance and viability may depend on other

factors, such as paracrine factors, vascularity, and matrix architecture, to name a few. [31, 35, 36, 40, 45, 46]

Whereas cellular cardiomyoplasty relies on endogenous mechanisms to guide transplanted cells to repopulate the infarct, form intercellular connections for electromechanical synchrony, and assume proper organization, tissue-engineering methods aim to restore the functional deficiencies of damaged myocardium by addressing many of these issues before transplantation. From the tissue engineer's perspective, cardiac regeneration is a multi-scale problem, where each hierarchical level is associated with specific structural and functional characteristics that must be identified, understood, and recapitulated in order to create therapeutically effective constructs. [4, 21-23, 30] The success of this approach is contingent upon advances within and collaborations between a myriad of disciplines, spanning cell biology, developmental biology, physiology, biochemistry, and molecular biology to materials science, instrumentation design, mathematical modeling, and engineering. [21, 22, 47] Thus far, tissue engineering efforts have primarily focused on 1) creating thick and compact tissue, while balancing the metabolic needs of three-dimensional cell culture with sufficient nutrient delivery [48-52], 2) developing biomaterials that provide the proper structural and mechanical support for three-dimensional cell culture [13, 53-58], 3) recreating myocardial anisotropy and spatial organization using material patterning and mechanical stimulation cues [11, 59-61], 4) identifying cell sources capable of a mature myocardial phenotype and mass production [62-64], and 5) combining the lessons learned in each specific research area to create a functional whole. Figure 2 surveys the five most prominent tissue-engineering strategies in the field to date.

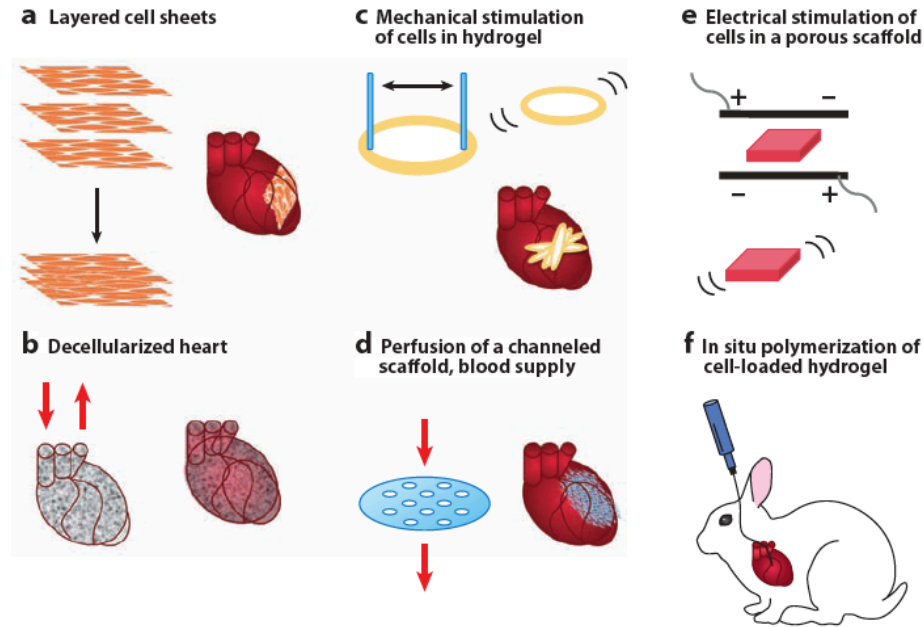


Figure 2 Prominent tissue engineering strategies to date. [23]

With concerted efforts across several disparate disciplines, various designs of tissue-engineered myocardial constructs have been employed in animal infarct studies with encouraging results. In 2006, Zimmerman et al transplanted mechanically-conditioned, 3D neonatal rat cardiomyocyte constructs suspended in collagen/Matrigel hydrogel matrices into a rat infarct model and reported functional electrical coupling of graft CMs to the host, prevention of dilatation, induced systolic wall thickening of infarct areas, and improved fractional area shortening of infarcted hearts compared to sham controls 4 weeks after transplantation. [2] Miyagawa et al demonstrated similar results 4 and 8 weeks post-transplantation using 100 μ m-thick, layered sheets of neonatal rat CMs in a rat infarct model. [65] More recently, in a head-to-head comparison between direct injection of cells into injured myocardium versus epicardial transplantation of tissue constructs, Hamdi et al reported that transplantation of skeletal myoblasts seeded in

three-dimensional Gelfoam collagen scaffolds demonstrated significantly higher recovery of left ventricular function, graft cell retention, and reduction of tissue fibrosis at 1-month post-procedure. [66] Translation of these successful strategies into clinical applications is now a realistic possibility, yet significant challenges still remain.

1.2.2 Major Limitations to Myocardial Regeneration

Although disparate in fundamental approach, cell transplantation and tissue engineering are complementary disciplines that share the same goal and many of the same challenges. For a cell-based myocardial therapy to be clinically effective, it must demonstrate excitability, ability to generate force, functional integration with host tissue through electromechanical coupling as well as vascularization, and remain functionally viable post-transplantation. Although inextricably linked, research in this field is bifurcated into furthering our understanding of the biology behind myocardial development and developing new technologies to not only probe the biology but direct tissue formation.

Surveying the current literature in the field, the primary limiting factor to the progress of both cell transplantation and tissue engineering is the cell source. The specifications for the optimal cell type to use in cell-based therapies are 1) unlimited numbers, 2) myogenic, 3) ability to integrate electromechanically with endogenous tissue, 4) functionally therapeutic, and 5) non-immunogenic. [23, 67, 68] The advent of hESCs and human induced pluripotent stem cells (hiPSCs) as an unlimited, self-renewing cell source with myocardial potential has solidified the promise of cell-based heart repair. Recently, the ability to generate cardiomyocytes from these pluripotent sources at reasonable numbers for myocardial repair has been reported by many

groups. [35, 69-74] In addition, transplantation of hESC-derived CMs specifically in cell suspension or as tissue constructs into animal models have confirmed the therapeutic relevance of these cells.[3, 32, 40, 75-79] The pitfall of many of these studies is that, although some functional recovery, integration, and CM maturation is evidenced, substantial regeneration of myocardial mass remains elusive. With the intent to restore lost myocardial function post-insult with bulk replacement of tissue, the influence of any transplanted therapy will be significant to the proper functioning of the heart. Thus, characterizing the functional properties and understanding the maturative process of human pluripotent stem cell (hPSC)-derived CMs is also crucial in terms of therapy optimization and long-term patient safety.

1.3 Heart Development

With the demonstration that cell-based therapies are beneficial to the post-infarcted, failing heart in animal models [2, 55, 80], determining the optimal cell source for the human patient has stirred controversy within the field. From a therapeutic standpoint, an autologous cardiomyocyte would satisfy functional and immunogenic concerns. [39, 41, 68] However, the technical feasibility of isolating cardiomyocytes from a human source that are also amplifiable relegated these efforts as proof-of-concept only. When Thomson et al first reported the ability to isolate pluripotent stem cells from human blastocysts in 1998, cell-based repair became a clinical reality. [81] hESCs provided a cell source that could be directed towards the cardiomyocyte fate and can, in theory, propagate boundlessly. Furthermore, the introduction of hiPSC technology in 2006, where pluripotency could be induced from plentiful human fibroblast sources,

diminished the ethical and immunogenic concerns that plagued hESCs. [82-85] Harnessing the full potential of these pluripotent cell sources for cardiomyocyte repair will require new methodology and technologies to not only isolate and mass produce the cardiac cells of interest but also direct their maturation reproducibly and efficiently.

1.3.1 Embryological Perspective of Cardiac Development

The ability to translate the potential of hPSCs from a research tool to a clinical reality will require understanding how endogenous cardiomyocytes develop and form functional myocardium. In the developing embryo, all cells of the eventual organism can be traced to a single pluripotent cell source. As this single cell embryo begins to divide, replicate, and specify, differentiation potential of individual cells diminishes and adult stem cells that are capable of producing specific cell types replenish tissues upon necessity. The inner cell mass of the developing blastocyst provides the pluripotent cells that give rise to the developing embryo and are the same cells used in deriving hESCs. [81] During development, these cells rapidly divide and, after gastrulation, form the three germ layers, the endoderm, mesoderm, and ectoderm, which are responsible for organogenesis. [86, 87] Accordingly, hPSCs are deemed pluripotent once the ability to form all three germ layers is demonstrated.

In mammals, the heart is the first organ to form during embryogenesis. Cardiomyocytes descend from a multipotent mesodermal lineage that also gives rise to vascular, connective, non-cardiac muscular, osteogenic, and cartilaginous tissues. [67] As gastrulation occurs, differential spatial and temporal patterning of key signaling pathways results in the formation of a sub-mesodermal region termed the cardiac mesoderm or cardiac crescent. Differentiation of these cardiac precursor cells results in

endothelial, atrial myocyte, ventricular myocyte, and nodal cell fates. [86, 88] In conjunction with different morphogenetic regulators and effectors, the heart transitions from a contractile primitive heart tube with a myocardial outer layer and endothelial lining (3 weeks in human gestation) to a four-chambered organ with valvular components and inflow and outflow tracks to coordinate nutrient exchange and blood flow (3 months in human gestation). [86] Although the major players in cardiac specification and heart formation are relatively established, the interplay between these parts remains to be clarified. [89]

The plasticity of hPSCs allows for the generation of hundreds of cell types but simultaneously also renders these cells difficult to control. Understanding the different signaling components active at each stage of cardiac development, from mesodermal specification to early cardiac precursor commitment to cardiac differentiation and morphogenesis, will influence regulation strategies for hPSC culture. As discussed in the next sections, the lessons from developmental biology have been an instrumental guide to optimize protocols for specification of particular lineages of interest. In effect, hPSCs cannot only benefit from the lessons learned in embryology but can also serve as an in vitro model to test many of the hypotheses that arise in developmental biology.

1.3.2 Stem Cells: Cardiac Specification and Differentiation

Differentiation of hPSCs into bona-fide cardiomyocytes has now been demonstrated routinely in the field. Traditionally, undifferentiated cells are withdrawn from conditions that promote pluripotency and encouraged to aggregate into differentiating clusters called embryoid bodies (EBs). Spontaneous differentiation of different cell lineages occurs in this model. CMs arise as one of many cell types,

constituting typically about 1-2% of the spontaneously differentiating culture. [90] Using mechanical dissection methods as well as genetic manipulation, groups have been able to extract cardiac cells of interest for further study. [74, 91]

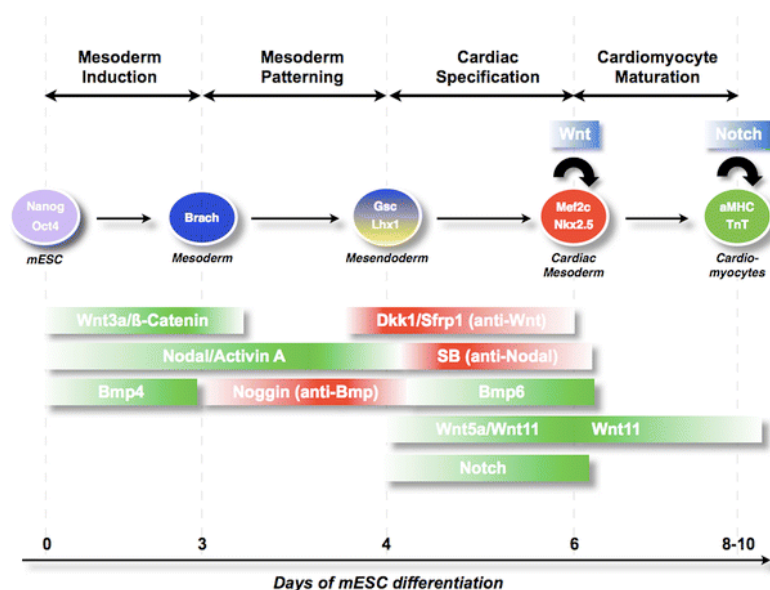


Figure 3 Schematic of sequential steps involved in cardiomyocyte development in hESCs. [92]

With lessons from developmental biology, researchers have been able to pinpoint specific media components that promote the appearance of cells derived from the three germ layers. [93-95] Of notable importance to the cardiac lineage is exposure to bone morphogenic proteins 2 and 4 (BMP-2 and -4), activin A, fibroblast growth factors (FGFs), various Wnt antagonists, and transforming growth factor β (TGF- β) signaling molecules. (Figure 3) [70, 96, 97] Tailored programs of morphogen exposure seem to dictate levels of cardiac lineage specification. Using these serum-free protocols of CM differentiation, groups have reported CM incidence between 40-60%. [35, 70, 98] Groups have also shown that modulating the physical microenvironment (e.g. substrate stiffness,

ECM selection, or selective matrix patterning) can direct pluripotent and multipotent cell sources towards a myogenic fate. [99-101] The expression of a number of specific transcription factors, such as Nkx2.5, GATA-4, Mef2c, and Isl1, have been shown to define the cardiac precursor population. [96, 102]

Once cardiac specification occurs, CMs arising from PSC origins display the defining characteristics of immature cardiomyocytes. [103-106] One of the first signs of CM presence in heterogeneous PSC differentiation cultures is contractile activity. CMs spontaneously contract as early as Day 5 (D5) post-differentiation with peak numbers of contractile areas arising around D15-20 after differentiation. hPSC-derived CMs also express specific cardiac structural markers, which form the myocardial contractile apparatus, such as cardiac troponins I and T (cTnI and cTnT), alpha myosin heavy chain (α MHC), beta myosin heavy chain (β MHC), and sarcomeric alpha actinin (α -actinin). [90, 95, 107] In addition, the three major CM cell types, atrial, ventricular, and pacemaker, have been evidenced by gene profiling and electrophysiological assessment of these cell types. [108] Finally, as previously mentioned, hPSC-derived CMs also show the ability to functionally integrate in vivo, with the formation of host-graft junctions and non-arrhythmic electromechanical activity, in both normal and post-infarct environments. [3, 32, 35, 40, 77, 78, 109] Together, these data suggest that these myogenic cells derived from hPSCs in vitro are bona-fide CMs.

1.4 Cardiomyocyte Maturation

The specific processes that govern CM maturation from embryonic specification to adulthood are relatively unclear. Although rapid progress has been made in

understanding CM specification from hPSCs, hPSC-derived CMs are phenotypically immature and it is unclear whether endogenous mechanisms that promote maturation exist or will suffice for long-term therapeutic applications. To create functional CMs in vitro, it is important to understand the normal processes of maturation in vivo.

The transition in cardiac phenotype from fetal to neonatal and subsequently to adult is not immediate as various aspects of CM development can occur from birth through the early stages of adulthood. Focusing on the CMs themselves, human CMs are typically mononucleated in newborns with increases in binucleation to about 33% in infancy and early childhood and a subsequent decrease to 5-13% in adult myocytes. Furthermore, the CM content of the human newborn heart is about half that of the adult heart, but adult values are reached on average around the age of four months. Although CMs cease proliferating early in post-natal development, heart weight continues to increase rapidly, doubling within the first 6 months, tripling within the first year, and growing proportionally with body weight for the first half of life. Specifically, myocyte diameter will increase from 5 μ m at birth to 8 μ m by 6 weeks to 13 μ m by 15 years and 14 μ m in adults. [110] In comparing 3-week old CMs with their adult counterparts, cell shape changes also occur as a doubling in length values occur, evidenced by a morphological transition from short and rounded to long and rod-like cells. Finally, intracellular changes in organization and density of the myofibrillar apparatus (Figure 4) are paired with increases in sarcoplasmic reticulum (SR) Ca²⁺ stores, which translate to functional increases in CM contractility. [111]

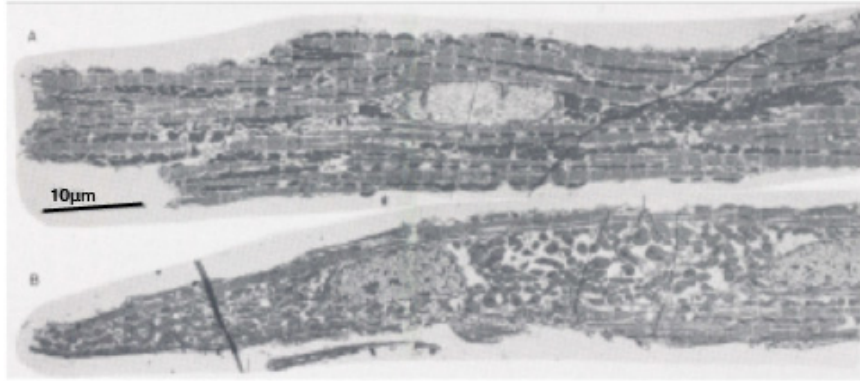


Figure 4 Longitudinal section of isolated rabbit myocytes of varying developmental stages. (A) Adult CM and (B) 3-week-old CM. Myofibril organization is much less regular in (B). Scale bar = 10 μ m. [111]

Physiologically, the resting heart rate of newborns and infants are dramatically higher than in the adult. In newborns, the mean basal heart rate averages 138 beats/min, peaking around 150 beats/min at the age of 2 months and decreasing to about 120 beats/min in early childhood. Adult levels of 55-85 beats/min are achieved around the age of 12 years.

Metabolically, CMs switch from a carbohydrate to a lipid energy metabolism prior to birth. Interestingly, concentrations of calcium, sodium, magnesium, and potassium, the major electrolytes that govern CM physiology, remain relatively unchanged from neonatal stages to senescence. [112]

On the other hand, vascularization and innervation of cardiac tissue continues to mature considerably after birth. In a human newborn, large vascular structure density and thickness are relatively unchanged between newborns and adults, with vascular growth stemming mostly from arteriolar and capillary expansion. However, vascular maturation continues with modifications in vessel organization, morphology, and biochemistry through childhood and early adulthood. [113] Innervation of the heart is functionally and morphologically immature in human newborns as well. As the heart

develops, the cardiac nervous system forms and matures, hallmarked by a functional transition between a predominantly sympathetic neural supply towards a co-dominant sympathetic and parasympathetic nervous system. [110]

This macroscopic overview of cardiac maturation from fetal to adult developmental stages underscores the complexity and varied timing of changes that occur for the heart to fully mature. In devising regenerative strategies for cardiac repair, it becomes apparent that the immature CM is drastically disparate from its adult counterpart in both structure and function. CMs derived from hPSC sources have been shown to be relatively immature, resembling more closely human fetal CMs in morphology, expression and localization of junctional proteins, gene expression profiles, and electrophysiology. [90, 91, 95, 114, 115] Thus, the question remains whether the phenotypically immature cells derived from pluripotent cell sources are therapeutically valuable after initial derivation or if more rigorous maturation programs must be employed for these in vitro-derived cells to be useful.

1.4.1 Cardiomyocyte Morphology

CM morphology is inextricably linked to cell function. As mentioned, through development, myocyte architecture changes considerably with increases in volume, shape, and organization. In the healthy heart, CM hypertrophy is a morphological consequence of increasing cardiac loads from both natural developmental processes and athletic conditioning. [6, 111, 116, 117] In situations of myocardial insult, the length-to-width ratio of normal CMs can decrease or increase depending on the specific cardiopathology, which can translate into a loss of contractility and ultimately heart failure. [118] Gopalan et al showed that culturing rat neonatal CMs in micro-patterned

collagen channels of 30 μ m width induces an elongated CM morphology with parallel alignment in comparison to randomly arranged CMs cultured in unpatterned or wider channel controls. [11] Furthermore, as the structure of myocardium is inherently 3D, studies have shown that cells cultured in 3D ECM environments form stronger adhesions, exhibit enhanced migration rates, and display an accelerated rate of acquiring an *in vivo*-like morphology than cells cultured on protein-coated surfaces. [13] Using ECM patterning techniques that restrict myocyte shape, one research group varied the aspect ratio of neonatal rat CMs and demonstrated that as the aspect ratio of single CMs increases, alignment of myofibrils and registration of adjacent sarcomeres can be induced. In addition, a dominant ratio of 7:1 (length to width) exists in healthy myocytes, which translates to peak contractile force generation versus other dimensional ratios. [10, 119]

With traditional differentiation protocols, hPSC-derived CMs exhibit irregular myofibrillar organization with random arrays of striated myofibrils, reminiscent of fetal CMs and a far cry from the highly organized, parallel bundles of myofibrils characteristic of adult tissue. [90, 95] In most cases, undifferentiated hPSC EBs are plated on gelatin-coated tissue culture substrates to initiate differentiation. As spontaneous differentiation occurs, CMs tend to concentrate together with isotropic cellular organization and myofibrillar orientation early on (< 20 days post-differentiation) in differentiation cultures. [90, 95, 120] As these spontaneous differentiation continues *in vitro*, some groups report heterogeneities within differentiating EBs, where some areas displaying myofibrillar alignment are interspersed with randomly organized CMs. [90, 120] No studies have yet been reported on how *in vitro* modulation of hPSC-derived CM shape may affect morphological maturation of CMs.

1.4.2 Cardiomyocyte Mechanobiology

Contractile activity is a hallmark of CMs at no matter which developmental stage. Proper mechanical function of CMs is governed intrinsically, in part, by the expression and organization of myocardial contractile proteins. Expression of different myocardial proteins can be correlated with various developmental stages of the heart as well as CM type. For instance, β -MHC accounts for 90% of cardiac myosin content in a 30-week human fetus, decreases after birth, and reaccumulates in the ventricles of the 2-month human heart. [117] α -MHC predominates in fetal and adult atria with low levels of β -MHC expression. [121] In the same vein, myosin light chain proteins (MLC) also have two cardiac isoforms, one that predominates in the adult atria, MLC2a, and one that predominates in the adult ventricles, MLC2v. However, in embryonic and fetal CMs, expression of these two isoforms is more ambiguous with ventricular expression of a MLC isoform that cannot be distinguished from MLC2a. [111] Troponins and actins are two more classes of contractile proteins that have cardiac-specific varieties. Together, these elements form the contractile machinery of individual CMs and influence the contractile capabilities of the myocardium. In hPSC-derived CMs, expression of the major cardiac contractile proteins, α -MHC, β -MHC, α -actinin, cTnI, cTnT, MLC2a, and MLC2v, can be detected as early as 5-10 days after initiation of differentiation using immunohistochemical and quantitative polymerase chain reaction (qPCR) techniques. [90, 95, 107, 122, 123] However, from gene expression alone, little can be deduced about CM function.

Contractile activity in hPSC-derived CMs is not only a visual indicator to identify a CM presence in heterogeneous cultures but also an indicator of proper CM function. Mature CMs display a repertoire of fundamental mechanical properties. For instance,

one property is a positive force-frequency relationship, where adult myocardium will produce more force with increases in stimulation frequency. When Dolkinov et al probed early (D7-Day 7 post-differentiation) and late (D55) stage hESC-derived CMs, these cells exhibited a negative force-frequency relationship in both subsets, suggesting the immaturity of hESC-derived CMs in mechanical function despite the ability to spontaneously contract. [91] Another fundamental property of CMs is the Frank-Starling law, which states that increases in myocyte length are linearly related to increases in force generation within a physiologic range. [124] Tulloch et al were able to demonstrate that hESC-derived CM constructs could exhibit this physiological phenomenon after applying static mechanical conditioning conditions to immature CMs for 3 weeks. [78]

Myofibrillogenesis, the process that governs myofibril assembly from contractile protein elements, is essential to the proper functioning of CMs. This process is dictated both by chemical and mechanical signaling events. [125] Myocardial structure is intrinsically 3D and defined by a vast ECM network that supports the form and function of the heart. [13, 126] In addition, cardiac cells are constantly subjected to dynamic mechanical loading throughout their lifetime. While myocardial stresses and strains are directly influenced by the contractile function of the myocytes and the structure of the ECM, there is also ample evidence that external mechanical stimuli can directly regulate the structure and function of isolated CMs. [127-131] In particular, studies have shown that subjecting neonatal CMs to cyclic and static mechanical stretch stimulates growth signals, maintains myofibrillar structure, increases protein synthesis, and increases contractile force generation. [11, 125, 127, 129, 131, 132]

In the context of hPSC-derived CM mechanobiology, Tulloch et al. recently reported the first study that shows the influence of exogenous mechanical cues on

hPSC-derived CM maturation. First, this group showed that mechanical loading of hESC- and hiPSC-derived CMs cultured in 3D collagen gels improved myocyte alignment by 2-fold compared to non-stressed controls. Interestingly, mechanical load also improved collagen fiber alignment within the matrix hydrogel by 2+ fold. hiPSC-derived CMs displayed increased spontaneous beating frequency, proliferation rates, hypertrophic growth, and expression of contractile protein markers in response to extrinsic mechanical loading. Aside from the positive effects of mechanical loading, culturing cells in this 3D matrix environment also enhanced other morphological indicators of maturation, such as binucleation and organized sarcomeric banding. Although hPSC-derived CMs appear to be more in vivo-like than when cultured using traditional scaffold-free, non-stressed methods, it is important to note that hPSC-derived CM morphology was still relatively immature when compared to adult myocardial phenotypes. Again, the conclusion that hPSC-CMs most closely resemble fetal CMs was conveyed. [78]

Another mechanobiological property of particular interest is substrate stiffness due to the changes of this property when healthy myocardium is replaced by scar tissue during post-MI remodeling. Infarcted myocardium progressively increases in mechanical stiffness as scar tissue matures, from 18 ± 2 kPa in normal myocardium to 55 ± 15 kPa in central, infarcted tissue. [133, 134] How infarct-like stiffness might affect the subsequent hPSC-CM maturation and myofibril assembly is unclear in the long-term. In a developmental context, it has been reported that myocardial stiffness changes considerably in the transition from embryonic to adult developmental stages in human, murine, and avian models due to changes in collagen type and content. [135-137]

Jacot et al demonstrated that extracellular stiffness that closely resembles that of native myocardium significantly enhances maturation of contractile force generation and

morphologic properties of neonatal rat ventricular cardiomyocytes (NRVCMs). On stiffer gels (50kPa), the functional maturation of NRVCMs seemed to be inhibited with less cytoskeletal structure, unaligned sarcomeres, and stress fiber formation. [138] In a related study, our group showed that late-stage hESC-derived CMs (D50) purified and dissociated from differentiating hESC-derived EB cultures and cultivated on stiff surfaces displayed contractile forces similar to neonatal rat ventricular CMs. Similar values were observed even in CMs cultured for 90 days. [74] Engler et al demonstrated that quail embryonic stem cell (qESC)-derived cardiomyocytes retain contractile ability when cultured on substrates that mirror in vivo tissue elasticity versus CMs cultured on softer or much stiffer, infarct-like substrates. qESC-derived CMs ceased beating after 48 hrs. This study not only suggests the importance of stiffness for proper CM function but also implies that transplantation of PSC-derived CMs into infarct situations may only have transient benefits. [139]

1.4.3 Cardiomyocyte Electrophysiology

One characteristic feature of the heart is its ability to couple electrical signals to a mechanical response. The cardiac action potential (AP), which lasts over 300 milliseconds (ms), describes the changes in voltage in the CM due to electrical stimulation. These changes in voltage are due to fluxes of electrolytes (predominantly Na^+ , Ca^{2+} , and K^+) through voltage-sensitive ion channels on the CM plasma membrane. (Figure 5A) In brief, a rapid upstroke (Stage 1), controlled by influx of Na^+ and Ca^{2+} , is followed by transient repolarization (Stage 2) and a plateau phase (Stage 3), responsible for the prolonged action potential and governed by the K^+ currents, and, finally, return (Stage 4) to a resting membrane potential (-80mV for mature CMs, Stage 0). (Figure 5A)

Although, fundamentally similar in action potential properties, each specialized cell of the myocardium displays different AP configurations that reflect their distinctive electrophysiological roles. [6] (Figure 5B)

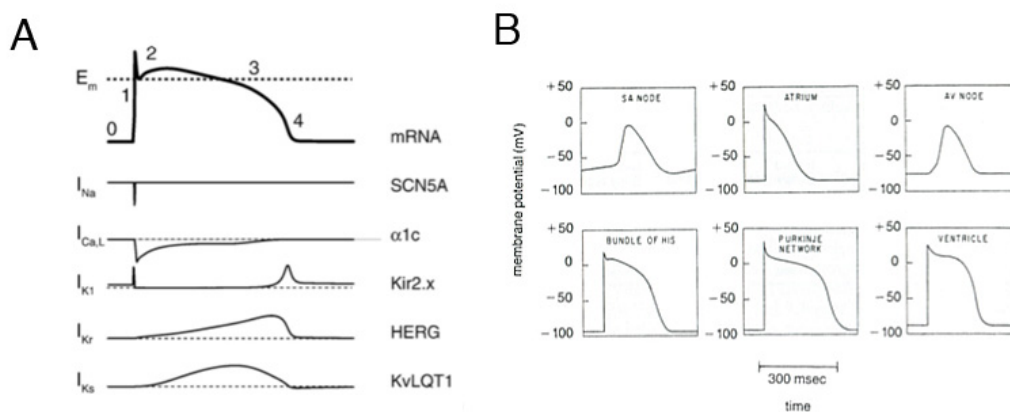


Figure 5 The cardiac action potential. (A) Illustrations of representative cardiac action potential and the associated ion currents [140] (B) Action potentials characteristic of the various myocardial cell subtypes [6]

During development, the resting potential increases, becoming more negative, in mammals. [141-143] Age-related modulation in number and functional properties of calcium, sodium, and potassium channels affect the properties of the AP, reflected in its morphology, kinetics, and quantitative attributes. In general, as CMs mature, increases in the density of calcium and sodium channels occur which account for the larger inward Ca^{2+} current and faster upstroke velocity (governed by the Na^+ current). As a reference, neonatal and adult CMs display an upstroke velocity ranging from 150-350 V/s whereas embryonic CMs typically display much slower depolarization kinetics. [108] In the mature CM, outward rectifying currents (I_{Kr}) initiate repolarization whereas inward rectifying currents (I_{K1}) stabilize the resting membrane potential. [6] As human CMs develop, K^+ channels (K_{ir}) that dictate the inward rectifying current are established by 2.5 years of

age. The outward rectifying K^+ channels (K_v) continue to develop through childhood as adult CMs demonstrate a higher current density and faster recovery kinetics than juvenile CMs. [141]

Electrophysiological characterization of hPSC-derived CMs not only gives insight about the maturity of their function but also perhaps their identity. Mummery et al showed that cultures of hESC-derived CMs are heterogeneous in nature, represented by several electrical phenotypes that were atrial-like (1/33 cells), ventricular-like (28/33), and pacemaker-like (2/33) in morphology. Moreover, AP kinetics, such as upstroke velocity, were relatively slow but similar to fetal CMs in culture. This group also detected gene expression of various K^+ channels and protein expression of RYR2, suggesting an intermediate developmental stage. [95]

He et al reported similar findings in the heterogeneity of hESC-derived CMs based on their electrical phenotypes. The CMs probed in this study were evaluated at D45-D90 of differentiation and exhibited resting membrane potentials of -50 to -60 mV and upstroke velocities of 5-30 V/s, properties that resemble, at most, 7-week-old human embryonic hearts. [108] A physiological property of CMs is the ability to adapt to an increase in heart rate with a decrease in AP duration (APD). [144, 145] Indeed, He et al found that increases in stimulation rate from 1Hz, around natural spontaneous rates, to 2Hz and subsequently to 3Hz translated to APD shortening. Thus, although the AP amplitude and upstroke velocities reflected immature CM properties, these CMs exhibited that they had the proper electrophysiological machinery to exhibit rate adaptation. These analyses were conducted for those CMs that exhibited ventricular-like and atrial-like APs, suggesting that a more mature AP morphology may also correlate with the maturation of CM functional properties. [108] Although the definitive identity of

CMs as atrial, ventricular, or nodal could not be correlated with the respective AP morphologies in either of these studies, these electrophysiological characterizations underscore the heterogeneity and unpredictability of hPSC-derived CM culture composition, in cell type and maturation level, using current methods.

1.4.4 Cardiomyocyte Ca^{2+} Handling

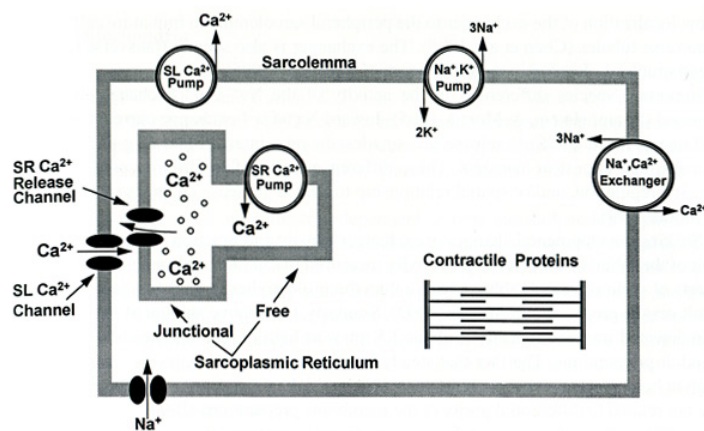


Figure 6 Schematic of CM Ca^{2+} handling systems and major membrane machinery. [141]

The movement of Ca^{2+} in and out of CMs is essential to CM contraction and homeostasis. In brief, extracellular Ca^{2+} enters the cell through passive diffusion down a concentration and electrochemical gradient due to the 1000-fold discrepancy between Ca^{2+} concentration inside and outside of the cell in addition to the natural electronegativity of resting CMs. [6] L-type Ca^{2+} channels are the major contributor to Ca^{2+} influx in the mature CM. Once Ca^{2+} enters the cell, activation of cardiac specific ryanodine receptor (RyR2), the SR Ca^{2+} release channel, leads to high volume release of Ca^{2+} from the SR (Ca^{2+} -induced- Ca^{2+} -release (CICR)) in order for contraction to occur. With a sudden rapid increase in intracellular Ca^{2+} content, specialized pumps on the SR,

SR Ca^{2+} ATPase (SERCA2a), and on the plasma membrane, the sodium-calcium exchanger (NCX-1), are subsequently responsible for Ca^{2+} reuptake to the SR and Ca^{2+} extrusion, respectively, to return CMs to their resting state. [6, 146] (Figure 6) The mature CM also expresses key regulatory proteins that control Ca^{2+} transport and SR Ca^{2+} retention, namely phospholamban (PLB), calsequestrin (CASQ2), and calreticulin (CalR).

The immature CM relies primarily on extracellular Ca^{2+} influx through the sarcolemmal membrane for Ca^{2+} transient generation instead of CICR. [135, 146, 147] Accordingly, immature myocytes display lower force generation capabilities than their adult counterparts. NCX-1 expression levels are also significantly higher in developing CMs, which correlates to the fact that this is the major pathway for Ca^{2+} extrusion in fetal CMs. [148] As maturation occurs, increases in L-type Ca^{2+} channel expression and functionality as well as SR density have been shown. [117, 147] It has also been well documented that SR in fetal CMs is immature in structure and function. [149] In particular, pharmacological studies reveal that Serca2a and RYR2, although can be expressed in fetal CMs, can be non-functional at these early stages. [146] Also, CalR dominates early on in development with a transition towards CASQ2 as the myocyte matures and builds its Ca^{2+} stores.

Conflicting results exist when hPSC-derived CMs are probed for their Ca^{2+} handling maturity. Dolkinov et al suggested that hESC-derived CMs rely on a trans-sarcolemmal influx of Ca^{2+} versus CICR. Functional immaturity was evidenced by marked insensitivity of these CMs to caffeine induced Ca^{2+} expulsion of SR stores, ryanodine inhibition of RYR2, and thapsigargin inhibition of Serca activity. A predominantly immature gene expression profile was also demonstrated with high

expression of NCX-1 and absence of PLB and CASQ2 expression. Overall, the hESC-derived CMs characterized in this study underscored their physiological immaturity. However, this study did report L-type Ca^{2+} channel functionality as contraction was inhibited by exposure to verapamil, an L-type Ca^{2+} channel blocker, and Serca2 gene expression, which together suggest a tendency towards a more mature phenotype. [91]

In contrast, three other groups demonstrated that hESC-derived CMs do indeed express functional SRs and closely resemble fetal CMs. [105, 115, 150] In a subpopulation of hESC-derived CMs (35-40%), Liu et al reported that caffeine, ryanodine, and thapsigargin sensitivity was observed. [105, 115] In addition, expression of Serca2a, NCX, and RYR2 with an absence of CASQ2 and other associated SR structural proteins was noted. [115] Zhu et al suggested that hESC-derived CM exhibit local control of excitation contraction coupling capabilities that mirror human fetal CMs and rival the adult CM phenotype. Specifically, pharmacological evidence demonstrated L-type Ca^{2+} channel, Serca2a, and RYR2 function. Electrophysiological probing of hESC-derived CMs revealed L-type Ca^{2+} current densities and Ca^{2+} transient kinetics that were indistinguishable from similarly probed human fetal CMs. [105] These confounding differences are addressed in Section 1.4.6. However, it is clear that the mechanisms underlying Ca^{2+} handling maturation are still relatively unknown.

1.4.5 Exploiting Endogenous Mechanisms of CM maturation

The true test for the utility of any cell-based therapeutic model is in vivo performance. As recapitulation of function is the overarching intention that fuels the work of tissue engineers, understanding to what extent we must engineer tissue is of utmost importance. Numerous studies thus far have investigated the therapeutic value of hPSC-

derived CMs, in their current immature state. Laflamme et al implanted purified and dissociated hESC-derived CMs into healthy rat myocardium. 4 weeks after injection of hESC-derived CMs, grafts appeared to be predominantly composed of CMs, non-teratomatous, and expressing β -MHC and MLC2v. Graft morphology began to resemble host myocardial tissue organization with sarcomeric banding and alignment with host tissue. In addition, by pre-treating grafted CMs with a heat shock regimen, CM grafts increased by 7-fold and CMs displayed proliferative capabilities even after the 4-week duration. [3] Similarly, Kehat et al implanted contractile EBs derived from hESCs into a porcine animal model and found electromechanical integration with host tissue, exemplified by pace-making activity originating from the transplantation site. However, even after 3 weeks of in vivo conditioning, grafted CM phenotype still resembled their immature in vitro counterparts. [75] From these studies, it is clear that hESC-derived CMs engraft in vivo and can persist over an extended transplantation period and do not have clear pathological consequences. Despite clear evidence of electromechanical integration, some suggestion that physiological mismatch between graft and host CMs may be arrhythmogenic. [151] In addition, the in vivo cardiac environment does not seem to stimulate considerable maturation beyond in vitro culture.

With these findings, safety concerns manifest in terms of simply transplanting hESC-derived CMs without first understanding how to control and induce a more mature functional phenotype. Yet, the question still remains whether transplant of these immature CMs can rescue the pathology of MI. In the context of a rat MI animal model, hESC-derived CMs have been transplanted into infarct regions and compared with media and undifferentiated hESC controls. In all cases, transplanting pluripotent, undifferentiated hESCs resulted in teratoma formation. [152] When the cell source was

pre-differentiated towards a CM fate, teratoma incidence was significantly reduced but in one study 2 out of 16 animals still developed teratomas. [153] With regards to cardiac function, transplantation of hESC-derived CMs improved cardiac function compared to control animals. Yet, in all cases, the therapeutic benefit was attributed to better preservation of left ventricular structure and function rather than direct functional contributions by the graft. [32, 76, 152] van Laake et al. also reported similar positive results 4 weeks after transplantation but noted that the beneficial effects of hESC-derived CM grafts disappeared by 12 weeks. [32]

Thus, like transplanting other potential cell sources surveyed in the previous sections of this chapter, the therapeutic benefits of cell therapies seem to be more paracrine in nature than actual regeneration of cardiac function. Moreover, it seems that the immature phenotype of these CMs may be a serious safety concern when electromechanical integration with mature CMs is intended. As methods of enhancing CM specification have improved in recent years, the ability to generate substantial CM numbers from these hPSC sources is within reach. Also, these reports show that hPSC-derived CMs can remain viable, electromechanically integrate, and even proliferate within infarcted myocardium for an extended period of time.

What is interesting to note is the impact of non-cardiac factors on the performance of hPSC-derived CMs in a transplant setting. For instance, pre-treatments with heat shock or survival factors can ameliorate graft performance. Other studies show the importance of endothelial influences and graft vascularity (discussed in Section 1.5) on the degree of functional improvements seen post-transplantation. [40, 77, 78, 154, 155] Presently, it seems that a major focus in this field will be elucidating how these non-

cardiac factors work and how they will factor into tissue engineering functional and therapeutically valuable myocardium.

1.4.6 Field Limitations

From this brief review, it becomes evident that the conflicting findings when comparing many of these reports on hPSC-derived CM characterization reflect major field limitations. First, a multitude of different sources are being used for the derivation of hPSC lines. Despite similarities in terms of self-renewal, expression of pluripotency markers, and the ability to differentiate, disparate cell origins have been shown to influence differences in the functional properties of their progeny. [156] Second, protocols used to enhance differentiation of cardiac cells are extremely varied in the field. The sensitivity of hPSCs to environmental cues renders differences between how different groups induce CM specification and their further development extremely significant. [105] Different starting points may therefore account for functional differences reported in the literature between research groups. Third, often times CMs are differentiated for different amounts of time before they are probed for functional characteristics. There is no standard in the field in terms of a differentiation time-line, which makes comparisons between studies error prone. Fourth, the caveat of hPSC differentiation is that any cell type can be induced in these cultures. [157] Despite specific methods of isolating CMs from these heterogeneous cultures, 100% purity is still elusive, especially if differentiation periods extend over several months and in-growth of other cell types becomes increasingly prominent. [74, 158] In addition, hPSC-derived CMs are heterogeneous in composition, in terms of CM type and maturation level. [95, 108, 115] Fifth, at present, a good positive control does not exist for human cell models.

Although comparisons can be made to fetal and adult myocardium, access to these tissues is hampered due to ethical concerns and availability. In addition, comparisons to animal models, such as the mouse or rat, are disadvantaged due to species differences in development. [110, 159]

1.5 The Endothelial-Cardiomyocyte Relationship

Intercellular relationships between the different cardiac cell types are critical to the normal functioning of the heart and the development of CMs both in vivo and in vitro. The heart is composed primarily of CMs, fibroblasts, and endothelial cells (ECs). CMs represent the main volume of the heart and are responsible for the unique contractile properties of this organ. As underscored in the previous sections, the spatial organization and physiology of CMs is a major determinant of proper cardiac function. However, it is the extra-cardiac cells that dominate the cellular make-up of the organ, outnumbering CMs by more than 3 times.

In terms of factors that mediate hPSC-derived CM maturation, Kim et al demonstrated that the influence of non-cardiac cells on CM electrophysiological maturation was important. By comparing hESC-derived CMs purified for CMs early on (D20) after differentiation and maintained for 40 additional days in culture without influence from non-CM cell types (D20+40 CMs) versus those CMs that maintained interaction with other cell types continually until functional characterization at D60 (D60 CMs), electrophysiological maturation was more prominent in hESC-CMs that interacted with other cell types. Additionally, add-back of non-cardiomyocyte influences to hESC-derived CMs purified at D20 rescued the more mature phenotypes observed with D60

CMs. [158] However, the identities of the non-cardiac sources that modulated these more mature responses remains unknown.

1.5.1 Endothelial-Cardiomyocyte Interactions in Development

Furthermore, CMs and ECs are intimately associated throughout development. In the developing embryo, cardiomyogenesis and vasculogenesis are complimentary processes that form both the circulatory system and the heart [86]. Cardiomyocytes and endothelial cells originate from a common mesodermal precursor. In response to endoderm-derived growth factors, specification of the mesoderm into cardiac mesoderm, primary myocardium, and endocardium occurs in mice at about E7.5. [160] In vitro, Yang et al have demonstrated that cardiomyocytes, endothelial cells, and vascular smooth muscle cells can all develop from a common KDR⁺ hESC-derived population of cells, hallmarking a shared lineage early on in human development as well. [98] As heart formation proceeds, signaling between the endocardial and myocardial cell layers is imperative for proper cardiac development as demonstrated by numerous murine, cell-type specific knockout models that result in embryonic lethality, cardiac defects, and vascular defects.

Key biochemical factors secreted by endothelial cells influence the proper development of CMs and the heart. Neuregulins are one family of growth factors secreted by endothelial cells early on in development. In early cardiogenesis, signaling from neuregulin-1 is essential for the formation of myocardial trabeculae and cardiac cushions and disruption of this signaling system is embryonic lethal. [161, 162] In addition, treatment of rat neonatal CMs with neuregulin-1 enhances survival, proliferation, and hypertrophic growth of CMs. [163] Other similarly important endothelial-

secreted biochemical regulators of cardiac development are neurofibromatosis type 1 (NF1) and platelet-derived growth factor B (PDGF-B) that influence myocardial formation, growth and cardiac chamber septation. CMs also secrete factors, vascular endothelial growth factor A (VEGF-A) and angiopoietin-1 (ANG-1), which influence vascular proliferation, stabilization, and maturation. [16]

1.5.2 Endothelial-Cardiomyocyte Interactions in Normal Cardiac

Function

In the mature heart, not only does the cardiac vascular system support healthy myocardium with transport of oxygenated blood and nutrients, but biochemical and physical communication between these two cell types also appear to promote cardiomyocyte organization, survival, growth, and proliferation.[16, 154, 164] Narmoneva et al cultured ECs with neonatal CMs on 3D peptide hydrogels and found that ECs promoted spatial organization of the myocytes as well as increased survival and synchronized contraction. [164] The presence of ECs was seen to enhance Cx43 expression that translated into increased synchrony in contraction due to better electrical impulse communication between cells.

Biochemically, two major factors have been shown to regulate the contractile state of CMs, nitric oxide (NO) and endothelin-1 (ET-1). [16] Two different NO synthase isoforms, neuronal NO synthase (nNOS) and endothelial NO synthase (eNOS), are expressed in normal physiologic conditions in the heart. nNOS seems to target the SR and facilitates Ca^{2+} release and positive inotropy. On the other hand, eNOS has a negative inotropic effect by inducing ventricular relaxation. [165] ET-1 seems to induce positive inotropy in rat atrial CMs, inducing increases in intracellular Ca^{2+} concentration.

[166, 167] Neuregulin activity is also detected in the mature myocardium with a negative inotropic effect at normal physiological conditions. [16] In situations of cardiac dysfunction, neuregulin-1 has been seen to have a role in sarcomeric organization, promoting proliferation and survival of CMs, and maintaining Ca^{2+} homeostasis. [168]

1.5.3 Endothelial Influences on hPSC-derived Cardiomyocytes

It is not surprising that hPSC-derived CM maturation may be influenced by relationships with other cell types, as cell-cell interactions cannot be avoided in vivo. Additionally, one of the major limitations to in vitro reconstruction of the myocardium is nutrient delivery to a dense and thick myocardial construct. [16, 23] As the vascular system is composed primarily of endothelial cells, a method of supplying tissue constructs with proper nutrient exchange would be to stimulate vascularization by doping constructs with endothelial cells or factors that promote vasculogenesis once implanted in vivo. Thus, from a biological and technical standpoint, elucidating EC-CM interactions in the context of hPSC-derived CMs has been a major focus in the field.

There has been some evidence supporting the hypothesis that endothelial influences enhance hPSC-derived CM culture. For instance, when human umbilical vein endothelial cells (HUVECs) were co-cultured with hESC-derived CMs and embryonic fibroblasts in 3D polymer scaffolds, Caspi et al found that tri-culture resulted in 1) increased numbers of proliferating CMs, 2) upregulation of some CM maturation markers, and 3) highly vascularized 3D cardiac constructs. [154] Similarly, Stevens et al. created functionally vascularized patches of hESC-derived CMs co-cultured with ECs and mouse embryonic fibroblasts (MEFs). Tri-cultures, in this case, also seemed to promote the formation of vascular networks interspersed with hESC-derived CMs as well

as enhanced CM proliferation. Tri-cultured patches also displayed improved passive mechanical characteristics with stiffness values 5 times that of CM only patches, but still an order of magnitude lower than adult myocardium in vivo. No differences were observed between tri-cultures and CM only patches in response to electrical stimulation; all subsets could synchronously contract and respond to pacing. [155]

The incorporation of endothelial cells into hPSC-derived CM grafts also seems to improve graft performance in vivo. van Laake et al transplanted hESC-derived CMs into infarcted rat hearts and noted that enhancement in cardiac function was correlated to elevated vascular density and not the number of CMs transplanted. [40] Additionally, multiple groups have shown that in pre-vascularized CM grafts, electromechanical integration as well as vascular integration between graft and host CMs and ECs occurs. [77, 78, 155] Stevens et al directly compared transplant of hESC-derived CM only grafts with tri-culture grafts. hESC-derived CM-only grafts exhibited poor survival in vivo with rare, isolated human CMs evident at 1-week post-transplantation. Prevascularization of CM grafts with ECs and fibroblasts resulted in 10-fold larger graft sizes at the time of evaluation. Tulloch et al demonstrated similar results with hESC- and hiPSC-derived CMs. [78, 155]

From these studies, it is clear that intercellular interactions may be important for functionalization of hPSC-derived CMs. At the current state, hPSC-derived CMs alone have mixed results in terms of transplantation survival and therapeutic benefit in an infarct situation. These studies have suggested that functional maturation of hPSC-derived CMs must exceed what these cells exhibit currently. Specifically, which aspects of the CM phenotype must be more mature before transplantation are unknown. In addition, the specific mechanisms that govern maturation from this intermediate

developmental state to one that is more “adult-like” are unknown. Elucidating the relationship between ECs and CMs will be instrumental to the progress of hPSC-derived CMs as a clinical therapy on two accounts: 1) ECs may provide a conduit for maintaining CM survival post-transplantation, particularly in the case of MI, and 2) elucidating EC-CM interactions may lend insight on key factors that govern CM maturation.

1.6 Scope of the Dissertation

The objective of the dissertation was to investigate the role of endothelial cells on hPSC-derived CM maturation. Specifically, we developed and optimized the tools necessary for probing this biological question in a high-throughput manner. In addition, we focused on how conditioned media from endothelial sources modulates CM maturation in terms of 1) Ca^{2+} handling, 2) gene expression, and 3) protein expression.

Chapter 2 describes the development and optimization of methods for co-culture hESC-derived CMs and endothelial cells. We implemented these methods to co-culture of both purified CM clusters and dissociated CM monolayers with two endothelial sources, primary human umbilical vein endothelial cells (HUVECs) and human microvascular endothelial cells (HMEC-1 cell line). We subsequently characterized CMs for both electrophysiological function and gene expression profiles to assess CM maturation.

Chapter 3 describes the effect of paracrine factors secreted by endothelial sources on hiPSC-derived CM maturation. hiPSC-derived CMs were treated with conditioned media from both HUVECs and HMEC-1 cells in addition to fibroblast conditioned media and unconditioned media controls. Using a high-throughput method

for Ca^{2+} imaging and computational single-cell analysis methods, we were able to characterize Ca^{2+} transient parameters, peak amplitude, rise velocity, decay velocity, and transient duration, of hiPSC-derived CMs for cell populations an order of magnitude higher than traditional assays for Ca^{2+} handling. Evaluations of Ca^{2+} transient kinetics were paired with pharmacological evaluation, gene expression profiling, and immunohistochemical analyses to fully characterize the maturative influences of endothelial cells.

Chapter 4 summarizes the major findings of these studies of endothelial influences on CM maturation. In addition, this chapter will address the implications of our conclusions for the field and future directions.

2 Co-culture of Endothelial Cells and Human Embryonic Stem Cell (hESC)-derived Cardiomyocytes

2.1 Abstract

The specific mechanisms that govern CM maturation from cardiac specification to the adult phenotype are relatively obscure. In the context of regenerative medicine, understanding the maturation process is becoming increasingly relevant due to the inability of immature CMs to functionally replace damaged myocardium. We hypothesize that endothelial influences can enhance CM physiology towards a more mature phenotype. In this chapter, we developed and optimized conditions for long-term hESC-derived CM and EC co-culture. Using these methods, we demonstrate that hESC-derived CMs co-cultured with HUVECs exhibit more mature action potential kinetics, in terms of maximum diastolic potential (MDP), action potential amplitude (APA), and

action potential duration (APD₉₀). In addition, co-cultured CMs display functional sensitivity to inhibitors of both the fast Na⁺ channel (Na_v1.5) and ryanodine receptor (RyR2), phenotypes, indicative of increasing maturity. Furthermore, gene expression profiles of co-cultured CMs more closely approach their mature counterparts. Modulation of CM phenotype seems to be cell source specific as HUVECs and HMEC-1 cells spur different results. These studies therefore suggested the significance of intercellular interaction, and more specifically endothelial influences, on CM maturation, but also reveal critical technical limitations that challenge the relevancy of this culture model.

2.2 Introduction

Throughout development, the vascular and cardiac systems are viewed as functional counterparts. The heart acts as the contractile pump that pulses blood through the vascular conduits that permeate the body. [6] Without nutrient delivery, the myocardium, along with any other living tissue or potential tissue analog, suffers and eventually undergoes necrosis, as with MI. Particularly, in the field of cardiac regeneration, the incorporation of ECs has been viewed as a necessary component for this specific function, to supply cardiac grafts with the building blocks of circulation and, in this way, to improve graft survival in the ailing heart. [23, 78, 154, 155] Although groups have demonstrated improvements in graft retention and CM spatial morphology by creating vascularized CM grafts [152, 155], functional replacement of damaged CMs remains elusive due, in large part, to the persistent immaturity of hPSC-derived CM grafts. Thus, understanding how cardiac maturation occurs and the factors at play has become increasingly important for developing new research strategies. [23] Here, we

propose that, in addition to the potential circulatory benefits afforded by the inclusion of ECs with hPSC-derived CM grafts, EC-CM interactions also play a role in CM functional maturation.

Even prior to the development of a functional circulatory system in the human fetus, CM specification, differentiation, and contractile function is already observed. [169] The early heart tube first forms around day 22 in the human embryo and consists of a myocardial outer layer with an endothelial lining which forms the endocardium. Within the myocardial cells of the early heart tube, homogeneous expression of numerous contractile proteins, including α MHC, β MHC, α -actinin, tropomodulin, tropomyosin, MLC1A, and MLC1V, can already be detected and the onset of contraction occurs shortly after heart tube formation at day 23. [169, 170] Further specification of myocyte type and functional maturation continues to occur as the heart changes morphogenically and the physiological needs of the embryo change with subsequent organogenesis and growth.

Little is understood about how CM maturation and specification progresses at the cellular level. [171] Interestingly, throughout cardiac development, the myocardium is closely juxtaposed with endothelial influences from the endocardium to the epicardial-derived coronary vasculature. [169, 171, 172] It has been shown that signals from both the endocardium and epicardium are necessary for proper myocardial development in terms of CM differentiation, proliferation, and localization. [16, 172, 173] In addition, it has been demonstrated through various genetic deletion studies in the mouse that abnormal endothelial development can translate into myocardial disruptions. [174] It is important to note that many of these cardiac developmental processes occur before

circulation is even established, suggesting the importance of intercellular relationships, spatial organization, and morphogenic cues to the developing CM. [86, 169, 171]

Our first insights into the different regulators of the mature CM phenotype at a cellular level have arisen in the literature over the past decade, due to the development of hPSCs as an in vitro model for human development. In particular, Kim et al demonstrated the important role of non-cardiac cell influences on developing CMs in vitro. Not only did maintaining the influence of these extra-cardiac cells enhance ion channel functionality and CM electrophysiology, but this more mature phenotype could be rescued in CM only cultures by adding back the extra-cardiac influences. [158] Although specific cell types and how they regulate the physiological maturation observed was not elucidated, this study suggests the importance of other cell types on CM maturation.

Accordingly, we hypothesize that ECs contribute significantly to the progression of the CM phenotype. Co-culture of CMs with ECs has previously been shown to regulate CM spatial organization, conduction, and survival in neonatal rat CMs. [164] However, it is unclear how endothelial influences affect hESC-derived CM maturation. In this study, we developed the tools and optimized methods for long-term co-culture of ECs and hPSC-derived CMs. We determined that a 50/50 ratio of endothelial growth medium (EGM2) to hESC differentiation maintenance medium could maintain contractile hESC-derived CMs and endothelial cell viability for at least 22 days in culture. In addition, we were able to scale down culture formats to minimize cellular demands and reagent costs.

Using these methods to co-culture hESC-derived CMs and ECs, we observed that hESC-derived CMs co-cultured with primary human umbilical vein endothelial cells

(HUVECs) displayed enhanced action potential kinetics with significant increases in maximum diastolic potential (MDP), action potential amplitude (APA), and action potential duration (APD₉₀). Pharmacological treatment of co-cultured hESC-derived CMs revealed an increased functional sensitivity to TTX, a Na_v1.5 channel blocker, and ryanodine, a ryanodine receptor blocker. Furthermore, co-cultured CMs exhibit higher mRNA expression of key ion channels that regulate Ca²⁺ handling and action potential generation. These findings indicate that endothelial influences enhance CMs towards a more mature phenotype.

2.3 Methods

2.3.1 Cells

H9 Human Embryonic Stem Cell-derived Cardiomyocytes

H9 hESCs (WiCell Research Institute, Cat# WA09, Madison, WI) were used to make the cell lines, (A) α MHC-mCherry α MHC-Puro^r Rex-Neo^r and (B) α MHC-mCherry- α MHC-Puro^r Rex-Neo^r-PGK-H2B-GFP lines, as detailed in [74]. With these genetic modulations, CMs, expressing α MHC, are not only puromycin-resistant but mCherry positive. In addition, pluripotent hESCs expressing the Rex-1 promoter are neomycin resistant. Undifferentiated H9 cells were cultured on Matrigel (0.0625 mg/ml, BD Biosciences, Cat# 354230, San Diego, CA)-coated 6-well plates with an irradiated mouse embryonic feeder (MEF) layer (E13.5 CD-1 mice). The medium used is referenced in Appendix 0. Three days prior to differentiation, cultures were treated with

400 µg/ml of G418 (Invitrogen, Cat# 10131, Carlsbad, CA) to eliminate MEFs. Media changes were performed on differentiating cultures every 2 days.

Embryoid body (EB) differentiation was initiated using serum-based hESC cardiac differentiation protocols. [93] Briefly, undifferentiated H9 hESCs were dissociated using collagenase IV (Invitrogen, Cat# 17104-019, Carlsbad, CA) and mechanical dispersion under 20% serum conditions. (Media is referenced in Appendix 0) EBs were formed once cells were cultured in suspension on ultra low-attachment 6-well plates (Corning, Inc., Cat# 3471, Corning, NY) for 6 days. After EB formation, EBs were plated on 0.1% gelatin-coated (Stem Cell Technologies, Cat# 07903, Vancouver, BC) tissue-culture plates. CMs were purified from differentiating EB cultures around day 20 (D20) of differentiation by 24-hour treatment of puromycin (1 mg/ml, Sigma Aldrich, Cat# P7130, St. Louis, MO). Mechanical excision of contractile areas using 1cc U-100 insulin syringe needles (Becton Dickinson and Company, Cat# 329420, Franklin Lakes, NJ) was also performed to improve purification of CMs. Once mechanically dissected, contractile EBs were plated on 0.1% gelatin-coated tissue culture dishes or 0.1% gelatin-coated glass coverslips (Menzel-Gläser, Cat# CB00110RA1, Braunschweig, Germany) and treated with puromycin as indicated. Purified CMs from EB cultures are termed cardiospheres (CSs).

Endothelial Cells

Human umbilical vein endothelial cells (HUVECs) (Lonza Walkersville, Inc., Cat# C2519A, Lot#6F3251, Walkersville, MD) and human microvascular endothelial cells (HMEC-1) (ATCC, Cat# CRL-10636, Manassas, VA) were used for co-culture studies. For experiments, HUVECs were used experimentally until passage 10 before discarded.

HMEC-1s are an endothelial cell line and thus can be used indefinitely in vitro. HUVECs and HMEC-1s were maintained in endothelial growth medium (EGM-2; Lonza Walkersville, Inc., Walkersville, MD) and media was changed every 2 days. For passage of both endothelial cell types, confluent plates were washed with Dulbecco's phosphate buffered saline, or dPBS, (Mediatech, Inc., Cat# 21-031-CV, Manassas, VA) and treated with 0.25% trypsin-EDTA (Invitrogen, Cat# 25200, Carlsbad, CA) for 2.5 minutes. Once cells detached, cells were resuspended in fresh EGM-2 to stop trypsinization and for transfer into new tissue-culture plates.

L-Cell Fibroblast Cells

L-cell fibroblasts (ATCC, Cat# CRL-2648, Manassas, VA) were used in co-culture experiments as a control comparison for EC-CM co-cultures. L-cells are cultured using 10% fetal bovine serum (Hyclone, Cat# SH30070.03, Logan, UT) in Dulbecco's modified eagle medium/F12 (Gibco, Cat# 1330-057, Carlsbad, CA) with penicillin (100U/ml)/streptomycin (100µg/ml) (Hyclone, Cat# SV30010, Logan, UT) and 20mM L-glutamine (Gibco, Cat# 25030, Carlsbad, CA).

2.3.2 Media Comparison for Long-term culture of ECs

A time-course was set up to compare different medias for long-term endothelial culture. Evaluations were conducted at 8- and 22-day time points for 4 different media conditions. The media conditions were as follows: 1) human embryoid body (hEB) maintenance media with 2% serum (2% hEB medium) [93], 2) neonatal CM maintenance media with 0.25% serum, 3) neonatal CM maintenance medium with no serum, and 4) EGM-2. (Appendix 0) HUVECs were plated at confluency and treated with the

aforementioned media conditions as well as 50/50 mixtures of EGM-2 with each of the other cardiac maintenance medias. Each media condition was performed in triplicate. A similar media comparison experiment was conducted with HMEC-1s as well with only the 2% hEB, EGM-2, and 50/50 EGM2/2% hEB medias for 43 days.

For the HUVEC media comparison experiments, images were taken with bright-field microscopy (10X) to assess cell morphology and viability. In addition, cultures were immunostained for traditional endothelial markers, platelet/endothelial cell adhesion molecule (PECAM-1 or CD31) (Santa Cruz Biotechnology, Inc., Cat# sc-1506, Santa Cruz, CA) and ulex-lectin (Vector Laboratories, Cat# RL-1062/FL-1061, Burlingame, CA), which demarcates endothelial membrane glycoproteins and glycolipids, and a nuclear marker, to-pro-3 iodide (Invitrogen, Cat# T3605, Carlsbad, CA). In the case of the HMEC-1 evaluations, HMEC-1 cells are genetically modified with an H2B-mCherry construct, demarcating nuclei as red, which allows for live fluorescent cell imaging.

2.3.3 Dissociation of cardiospheres for multi-well formats

Cardiospheres (CSs) were dissociated into single-cell format for monolayer hESC-derived CM culture. Once purified, CSs were allowed to recover from puromycin treatment for 48 hours. Subsequently, CSs were dissociated at various stages using 0.25% trypsin-EDTA. CSs were exposed to trypsin for 2 minutes at 37°C. Cultures were then mechanically agitated with a P200 pipet gently five times and returned to 37°C for 2 additional minutes. The previous step was repeated for a maximum of 10 minutes or until CSs were dissociated to single cells. Trypsinization was arrested with the addition of 2% hEB medium at twice the volume of trypsin. Dissociated hESC-derived CMs were then pelleted using a centrifuge (Eppendorf Centrifuge 5702R, Hauppauge, NY) for 5 minutes

at 1,220 x g. The supernatant was aspirated and the hESC-derived CM pellet was resuspended in a known volume. Cell count was obtained using the Countess cell counter (Invitrogen, Cat# C10227, Carlsbad, CA). hESC-CMs were then plated accordingly on 0.1% gelatin-coated 24-, 96-, and 384-well formats at various cell densities. (Table 1) Media was changed 24 hours post-plating and contractile cells were observed between 24-48 hours post plating. Cultures were evaluated for contractility and viability using immunostaining for α -actinin and bright field microscopy, respectively.

Table 1 Table of CM plating densities for various tissue culture plating formats.

Densities (# Cells)	24-well	96-well	384-well
A	7.5×10^5	4.0×10^5	2.0×10^4
B	3.5×10^5	2.0×10^5	1.0×10^4
C		1.0×10^5	5.0×10^3
D		5.0×10^4	

2.3.4 Co-culture of hESC-derived CMs and Endothelial Cells

hESC-derived CMs were co-cultured with HUVECs. Co-culture experiments were initially performed with hESC-derived D20 CSs. HUVECs were added at cell densities of 24,000 and 40,000 cells per well to contractile CS cultures and maintained for 40-54 additional days in 50/50 EGM-2/2% hEB mixed maintenance medias. Media was changed every other day. Controls were CSs alone, HUVECs alone, and CSs with L-cell fibroblasts. Co-cultures were monitored for contractility throughout the culture period. In addition, intracellular recordings and pharmacology studies were conducted on co-cultured CSs. Finally, co-cultures were immunostained with cardiac marker, α -actinin, and endothelial marker, CD31 to demarcate CMs and ECs within the culture.

Electrophysiological characterization and immunostaining protocols are detailed in the following sections.

Additionally, a series of experiments were conducted exploring the effect of ECs on dissociated hESC-derived CMs to test: 1) optimal ratios of ECs to CMs, 2) longevity of co-cultures, and, finally, 3) whether ECs modulate CM development through co-culture. (Table 2) In the first experiment (CCE1), two different ratios of HUVECs to CMs were tested. The goal of these experiments was to determine the proper seeding density on dissociated H9 hESC-derived CM cultures as well as to determine whether CMs and ECs can remain viable over long-term in vitro culture. In these experiments, 387 beating EBs derived from hESC line (A) were mechanically dissected and purified into CSs with 24-hour puromycin exposure. After dissociation, 3.0×10^6 total cells were plated at 5.0×10^5 cells per well in a 24-well plate coated with 0.1% gelatin. Cultures were purified again for CMs with puromycin treatment.

The CMs used in the subsequent co-culture experiment (CCE2, Table 2) were from hESC line (B) and thus express mCherry under an α MHC promoter and H2B-GFP under a ubiquitous phosphoglycerate kinase (PGK) promoter. HUVECs were seeded on D65 hESC-derived CMs at two different densities, 5.0×10^5 (1:1 EC:CM) and 1.0×10^6 (2:1 EC:CM), and compared to CM only controls. Each condition was performed in triplicate. Co-cultures were maintained with 50/50 EGM2:2% hEB media conditions. Media was again changed every other day. Additional HUVECs were added at D71, D88, and D106 post-differentiation of CMs. Lectin staining was used to assess the presence of ECs in co-cultures a couple of days after HUVEC seeding and two weeks after HUVEC seeding to monitor the viability of HUVECs. CMs, which are mCherry-positive, were monitored throughout the culture period with fluorescence microscopy for viability and contractility.

The experiment was completed after 62 days of co-culture (D134 post-differentiation). At the completion of the experiment, IC recording was performed to assess differences in physiology and qPCR was conducted to assess changes in gene expression from exposure to ECs.

A similar co-culture experiment was repeated with HMEC-1 cells (CCE3, Table 2) in lieu of HUVECs. In this case, HMEC-1 cells were plated at a cell density of 1.0×10^5 cells/well on a dissociated monolayer of D35 hESC-derived CMs. CMs were plated at a density of 1.0×10^5 cells/well. After 43 days of co-culture, cultures were probed for gene expression changes by qPCR. Controls were performed in duplicate and experimental conditions in triplicate.

Table 2 Table of co-culture experiments and cell constituents.

Experiment ID	Cardiomyocytes		Endothelial Cells
	CM Format	H9 hESC Cell Line	
CCE1	Cardiospheres	α MHC-mCherry- α MHC-Puro ^r Rex-Neo ^r	HUVEC
CCE2	Dissociated CMs	α MHC-mCherry- α MHC-Puro ^r Rex-Neo ^r / PGK-H2B-GFP	HUVEC
CCE3	Dissociated CMs	α MHC-mCherry- α MHC-Puro ^r Rex-Neo ^r / PGK-H2B-GFP	HMEC-1

2.3.5 Electrophysiology: Intracellular (IC) Recordings

Intracellular (IC) recordings were conducted using a sharp electrode technique detailed in [74, 158]. Briefly, CSs are plated on 0.1% gelatin-coated glass coverslips for the duration of culture. Upon recording, coverslips were transferred to a recording chamber on the stage of an inverted microscope (Olympus IX71). The recording chamber is superfused at 1-2ml/min with Knockout Dulbecco's modified eagle medium (KO-DMEM, Invitrogen, Cat#10829-018, Carlsbad, CA) at 37°C and preoxygenated with

constant 95%O₂/5% CO₂. The electrodes that were used are sharp glass microelectrodes filled with 3M KCl and have resistances of 50-150 MΩ in this configuration. Contractile CSs with mCherry expression were impaled with sharp electrodes to obtain action potentials (APs) at a single cell level. Intracellular recordings were obtained using an AxoPatch 200B amplifier in current clamp mode and pCLAMP-10 software (Molecular Devices, Sunnyvale, CA). Data was sampled at 10kHz using Clampex 10 software (Molecular Devices, Sunnyvale, CA) and low-pass filtered at 5 kHz. From these recordings, AP parameters were measured for APs exhibiting at least 10 seconds of baseline stability. Specifically, we were able to obtain information on AP amplitude (APA), maximum diastolic potential (MDP), maximal upstroke velocity (V_{max}), AP duration at 90% of the repolarization (APD₉₀), and the cycle-length between two spontaneous APs (RR).

2.3.6 Pharmacology

For the pharmacology studies, CSs in HUVEC co-cultured and non-co-cultured conditions were exposed to three different drugs diluted in KO-DMEM, tetrodotoxin (TTX, 1μM or 5μM, Tocris, Cat# 1069, Ellisville, MO) and ryanodine, a blocker of the RYR2 channel, (10μM, Tocris, Cat# 1329, Ellisville, MO). The effect of these pharmacological agents on the spontaneous beating frequency of CSs was observed compared to CS only controls.

2.3.7 Quantitative Polymerase Chain Reaction (qPCR)

Prior to qPCR processing, co-cultures were treated with 1mg/ml of puromycin for 36 hours to eliminate non-cardiac cells from the analysis. Total RNA was extracted using Trizol reagent (Invitrogen, Cat# 15596-018, Carlsbad,CA) in conjunction with the

protocol provided by the manufacturer for cells in a monolayer. Further homogenization of CS samples was performed by passing samples through 1cc insulin syringes until homogenization was complete. Samples incubated in Trizol were either stored at -80°C or processed immediately. Once RNA extraction was complete, RNA was resuspended in 10µl distilled, deionized water (ddH₂O) (Mediatech, Inc., Cat# 25-055-CV, Herndon, CA). RNA concentrations were measured using the Nanodrop spectrophotometry system (Thermo Scientific, Inc., Cat# ND-1000, Wilmington, DE). cDNA was synthesized using the QuantiTect Reverse Transcriptase (RT) Kit (Qiagen, Inc., Cat# 205314, Valencia, CA). cDNA was amplified using 1µg of RNA and the RT kit. Once the RNA was mixed with genomic DNA wipeout buffer, samples were heated at 42°C for 5 minutes. Samples were then mixed with RT buffer, RT enzyme, and amplification primers for a total volume of 20µl. Samples were heated for another 30 minutes at 42°C, 95°C for 3 minutes, and kept at 4°C. Finally, cDNA concentrations were measured using the Nanodrop and stored at -20°C until use.

qPCR was performed on the Roche LightCycler 2.0 (Roche Applied Science, Cat# 03531414001, Indianapolis, IN) using the LightCycler FastStart DNA Master SYBR Green I kit (Roche Applied Science, Cat# 12239264001, Indianapolis, IN) and LightCycler glass capillaries (Roche Applied Science, Cat# 04 929 292 001, Indianapolis, IN) for fluorescence amplification detection. Samples were prepared as indicated by Roche at half the volume (10µl). Standard curves were created for each primer pair (Appendix A.2) to calculate primer efficiency using the Lightcycler 2.0 software using cDNA from late stage hESC-derived CSs. Briefly, qPCRs were conducted as follows: samples were denatured at 95°C for 8 minutes with a temperature slope of 20 °C/s (slope used for every step unless otherwise specified), sample amplification

occurred with the following sequence, 95°C for 15 seconds, 60°C for 5 seconds, and 72°C for 20 seconds, for 40 cycles, melting curves were obtained with a subsequent cycle starting at 95°C, 70°C for 20 seconds, and a return to 95°C at a slope of 0.1°C/s, and finally samples were cooled at 40°C for 30 seconds. For each primer set, C_p values were obtained using the Lightcycler software. Using efficiency values for each primer pair, transcript expression could be calculated using the $\Delta\Delta C_p$ method. Transcript levels were normalized to GAPDH expression.

2.3.8 Immunostaining

Prior to immunostaining, cells were washed with dPBS and fixed in 4% paraformaldehyde (PFA) for 10 minutes (monolayer cells) and 20 minutes (CSs). Cells were blocked in a blocking buffer composed of 1X dPBS, 2% BSA, 2% goat serum, 50mM glycine (Bio-Rad, Cat# 161-0718, Hercules, CA), 0.01% Triton-X (Sigma-Aldrich, Cat# T8787, St. Louis, MO), and 0.005% Tween 20 (Sigma-Aldrich, Cat# P9416, St. Louis, MO). Primary antibodies used for these studies were diluted in 10% blocking buffer in the following ratios: mouse monoclonal anti- α -actinin (1:300, Sigma Aldrich, Cat# A7811, St Louis, MO), rabbit polyclonal anti-CD31 (1:150), fluorescein conjugated-lectin (1:1000), 4',6-diamidino-2-phenylindole (DAPI, 1:5,000), and To-Pro-3 iodide (1:5,000). Once stained, glass coverslips were mounted with (Dako, Cat# S3023, Carpinteria, CA) on glass slides (Surgipath Medical Industries, Cat# 00210, Richmond, Illinois) and imaged with an inverted fluorescent microscope (Leica DMI-4000B, Buffalo Grove, IL or Olympus IX71, Center Valley, PA).

2.4 Results

2.4.1 Media comparison for Long-term Culture of ECs

Figure 7 and Figure 8 detail a 3-week media test experiment that was conducted with HUVECs and the effect of different medias on their long-term viability and phenotype. Seven different medias were tested in both 100% and 50/50 EGM-2/X, where X is either 2% hEB media, 0.25% Neonatal CM media, or Neonatal CM media with no serum. For HUVEC cultures, we established the following criteria to determine the optimal media composition: 1) cell viability, 2) cobblestone morphology characteristic of ECs, and 3) expression of endothelial markers, CD31 and lectin at intercellular junctions between ECs.

Cultures were observed early on at 8 days of culture and later at 22 days of culture. In terms of viability, EGM-2 and 2% hEB only media conditions were the only conditions that demonstrated HUVEC viability at 22 days. By mixing medias with 50% EGM-2, HUVEC viability was observed in all cases.

With regards to HUVEC morphology, 50/50 EGM2/neonatal CM medium (no serum) conditions fostered confluent HUVEC cultures with the characteristic cobblestone morphology that most closely resembled EGM-2 media conditions at 22 days. A similar morphology was also observed in 50/50 EGM2/2% hEB and 50/50 EGM2/0.25% neonatal CM medium conditions but with lower cell viability. (Figure 7)

When stained with endothelial markers at D22 of culture, HUVECs in EGM2 conditions exhibit a few instances of the characteristic localization of CD31 and lectin at intracellular junctions. (Figure 8A, white arrowheads) In contrast, it was clear that media containing 0.25% neonatal CM medium did not foster HUVEC viability, which was

reflected in the paucity of nuclei (blue) and accordingly CD31 or lectin positive cells. (Figure 8C) In the case of 50/50 EGM2/Neonatal CM medium without serum, sporadic clusters of ECs expressed CD31 (green) robustly with proper organization but lectin was not detected. Finally, HUVECs treated with 50/50 EGM2/2% hEB most closely resembled HUVECs cultured in pure EGM2 (Figure 8B). ECs were positive for both CD31 and lectin with clear delineation at intracellular junctions.

Ultimately, we determined that 50/50 EGM2/2% hEB media conditions would be optimal for co-culture. One of the primary reasons behind this decision was because 2% hEB medium has been used ubiquitously in our laboratory to maintain hESC-derived CMs in the long-term with maintained contractility observed for 100+ days post-differentiation. [74] In addition, HUVEC viability, morphology, and endothelial marker expression with this media condition satisfy each of our criteria and was the only subset aside from EGM2 controls that met all three conditions. Treating HMEC-1 cells with 50/50 EGM2/2% hEB media also satisfied the defined criteria after 43 days in culture.

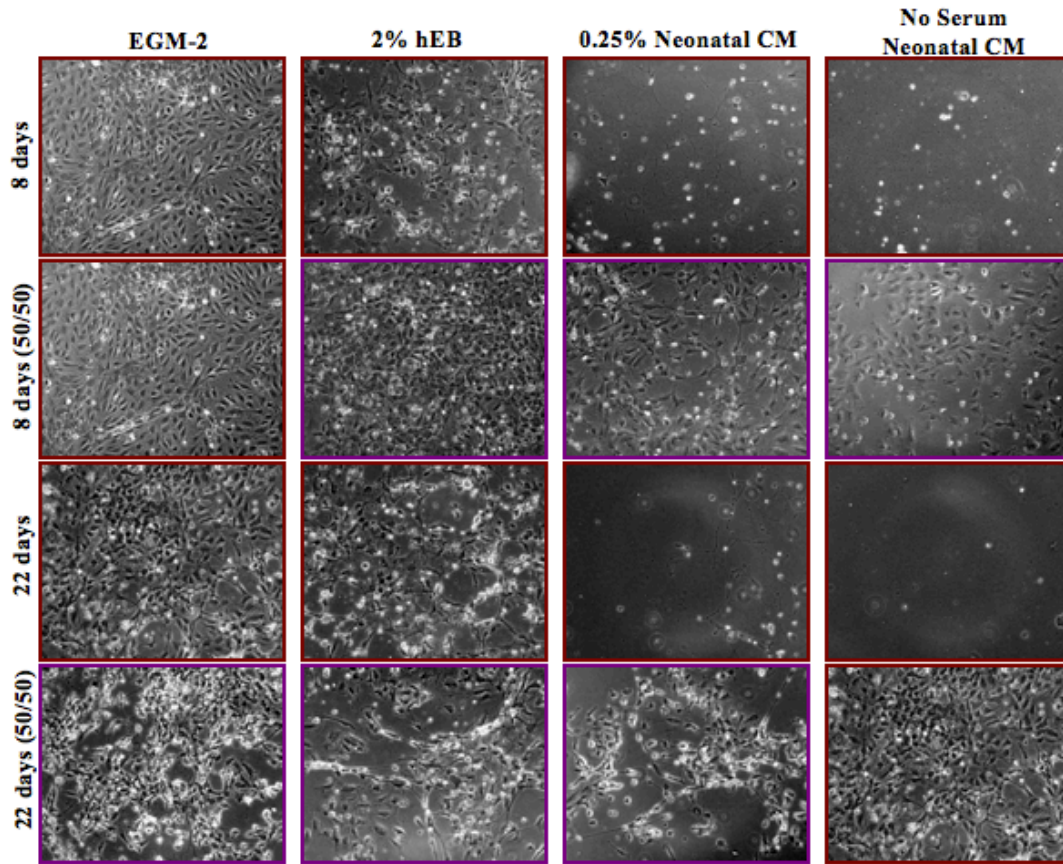


Figure 7 HUVEC media testing 8 days of culture versus 22 days of culture. Different medias were tested with HUVEC cultures: EGM-2, 2% hEB differentiation media, 0.25% Neonatal CM media, and neonatal CM media with no serum. (Rows 1 and 3) For each time point, 50/50 EGM-2 media to the four different types of media were also tested (Rows 2 and 4), 10X.

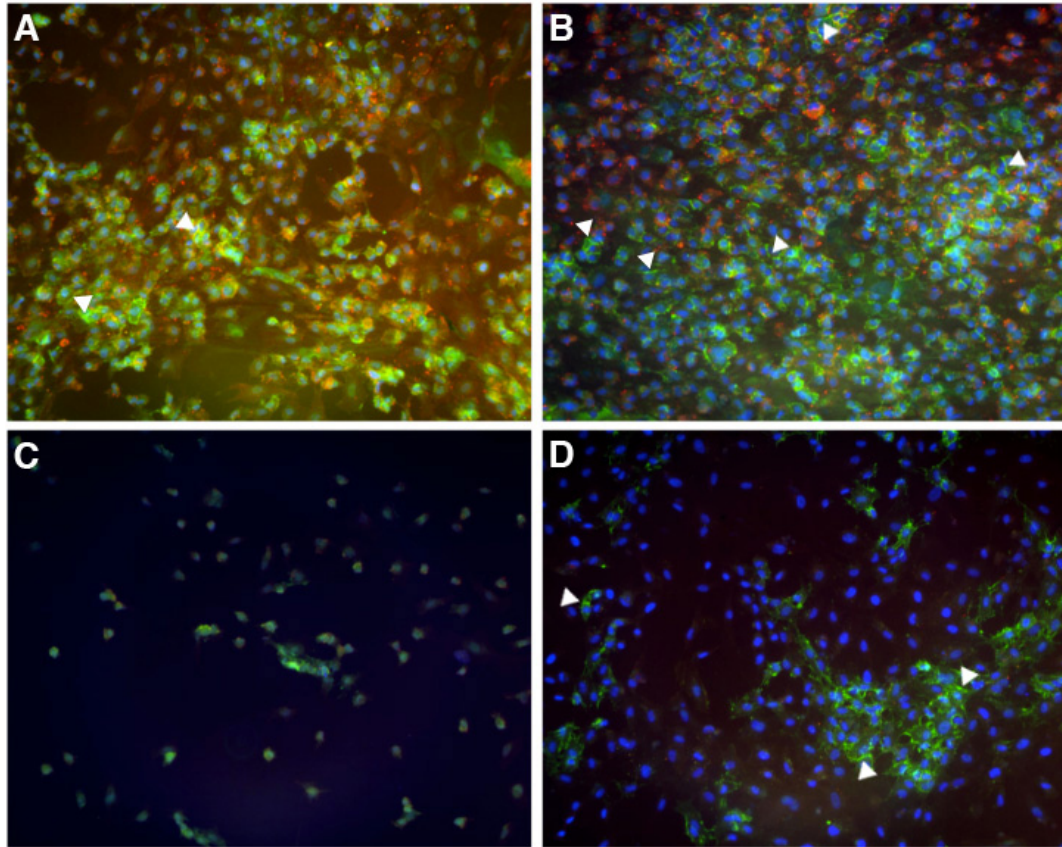


Figure 8 Immunostaining of D22 HUVEC cultures. Staining is as follows: CD31 (green), lectin (red), To-Pro-3 (blue), 10X. White arrowheads indicate representative localization of EC markers to intracellular junctions.

2.4.2 Dissociation of cardiospheres for multi-well formats

Due to the structural complications of CSs for experiments investigating microenvironment influences, we developed methods to dissociate 3D CS cultures into contractile, 2D CM monolayer cultures. Many groups, including our own, have observed that increased incidences of contractile hESC-derived EBs peak around D20 post-differentiation using traditional culture and differentiation methods with H9 cell line. [90] Using genetically modified hESC lines that render α MHC positive cells both mCherry positive and puromycin resistant, we are able to isolate CMs from EBs ($97.02 \pm 0.96\%$ purity [158]) using puromycin selection. In our CS dissociation trials, we demonstrated that dissociation of CSs into a 2D monolayer could generate contractile sheets of hESC-derived CMs, which remain contractile for long-term (30+ days) culture. In addition, we plated dissociated CSs at different densities and different well formats and showed that these CMs remain contractile and express α -actinin throughout long-term culture as well. (Figure 9)

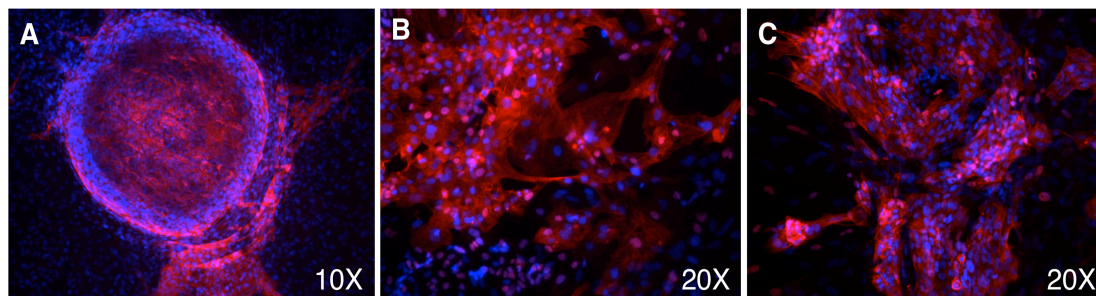


Figure 9 Dissociation of cardiosphere to a contractile CM monolayer in multi-well formats. (A) Cardiosphere (10X), (B) 24-well, 3.5×10^5 cells plated (20X), and (C) 384-well, 2×10^4 cells plated (20X). Stained with α -actinin (Red) and DAPI (Blue).

2.4.3 Co-culture of hESC-derived CMs and Endothelial Cells

2.4.3.1 Co-culture of hESC-derived CSs with HUVECs (CCE1)

HUVECs were added to D20 CSs and co-culture was maintained for 57 days. The first goal of this experiment was to test the feasibility of long-term co-culture of CSs and HUVECs. To this end, CSs persisted for the duration of the experiment and remained contractile. However, by the end of the 57-day co-culture period, absence of CD-31 expression revealed that HUVEC viability is challenged within this 57-day culture period. (Figure 10) Although it was unclear from this experiment at which point or why HUVECs disappeared, we continued to evaluate whether transient exposure of CSs to endothelial influences would affect CM maturation in terms of CS morphology, gene expression profile, and electrophysiological characteristics.

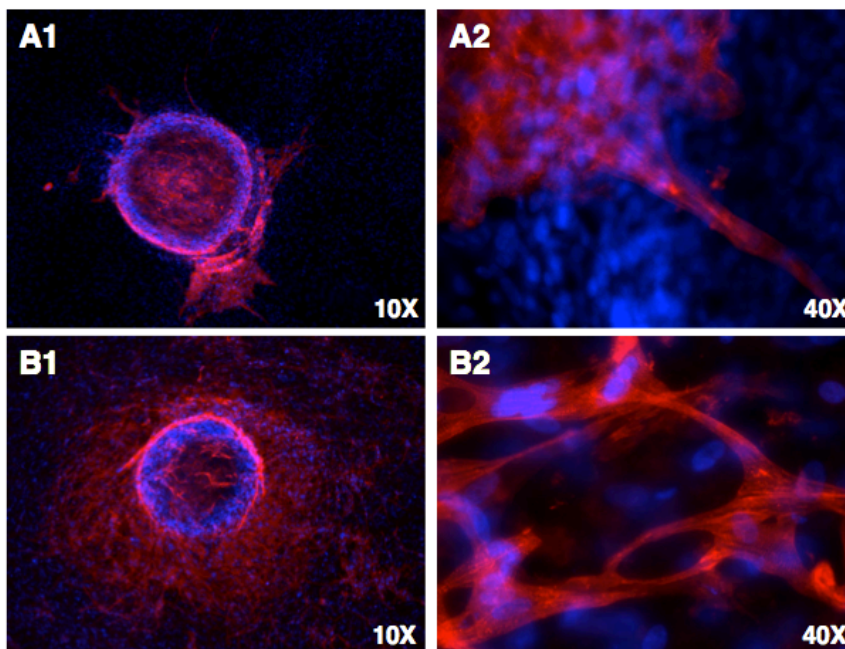


Figure 10 Immunostainings of CS-HUVEC co-culture, 57 days. CS only cultures are shown in panels (A1) and (A2). CS-HUVEC co-cultures are shown in panels (B1) and (B2). Cultures were stained with α -actinin (Red), CD-31 (green), and DAPI (blue).

CS morphology differed between CS only (Figure 10 A1 and A2) and co-cultured subsets (Figure 10 B1 and B2). In control CS only conditions, α -actinin positive CMs (shown in red) were localized primarily around the dense nuclei cluster (shown in blue) with a few fiber-like projections (Figure 10 A2) appearing to extend from the central CS to the surrounding area. In contrast, CSs that had been co-cultured with HUVECs exhibited a profuse, branching network of α -actinin-positive cells circling about twice the diameter of the central CS. These clear morphological differences suggest an EC-modulated effect.

In addition, the gene expression profile of co-cultured CSs shows enhancement of key cardiac markers of maturation. (Figure 11) Co-cultured CSs exhibit upregulation of more mature electrophysiological markers, such as the L-type Ca^{2+} channel ($\text{Ca}_v1.2$), the sodium-calcium exchanger (NCX1), the ryanodine receptor (Ryr2), several potassium channels ($\text{I}_{Kr2.1}$, $\text{I}_{Kr2.2}$), and $\text{Na}_v1.5$, which governs the fast upstroke velocity of the cardiac action potential. In addition, down-regulation of the inositol 1,4,5-trisphosphate receptor (IP3R2) [175], a Ca^{2+} handling receptor that dominates in early CM development suggests maturity as well. α MHC expression is minimally upregulated compared to controls, which might suggest either more CMs or increases in this contractile protein within existent CMs.

Finally, electrophysiological attributes of co-cultured CSs also suggest that EC influences enhance AP properties towards a more mature phenotype. (Figure 12) First, in comparing IC recording results, we show that CSs exposed to HUVEC co-culture display significantly higher MDP, APA, APD_{90} , and RR values. V_{max} values also demonstrate faster upstroke velocities in co-cultured CMs although not at statistical significance. The pharmacology experiments compared differences in beating frequency

upon exposure to a panel of drugs, which target key channels in CM development. As indicated in Figure 13, TTX and ryanodine treatment of CSs depressed beating frequency in co-cultured CMs by about 80% compared to controls. ZD7288 did not seem to have a significant effect on beating rate depression between co-cultured CSs and CS only controls.

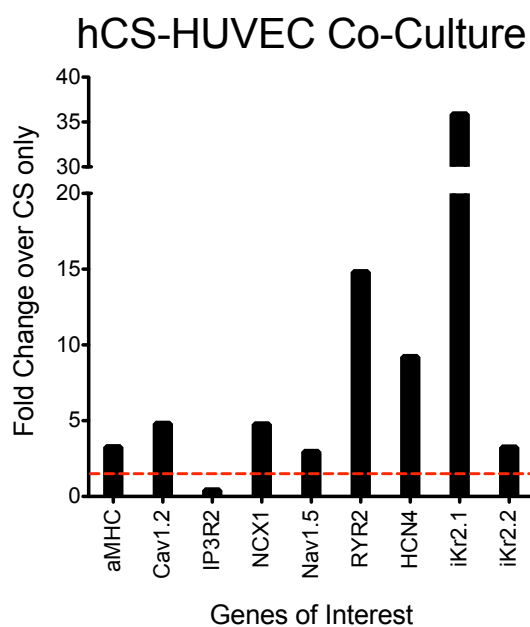


Figure 11 Gene expression profile of key cardiac markers during CM development of co-cultured CSs versus CS only controls. The panel of genes surveyed represents key cardiac markers that are active at different points of CM development. All expression values are expressed as fold change over control values (dashed red line = 1).

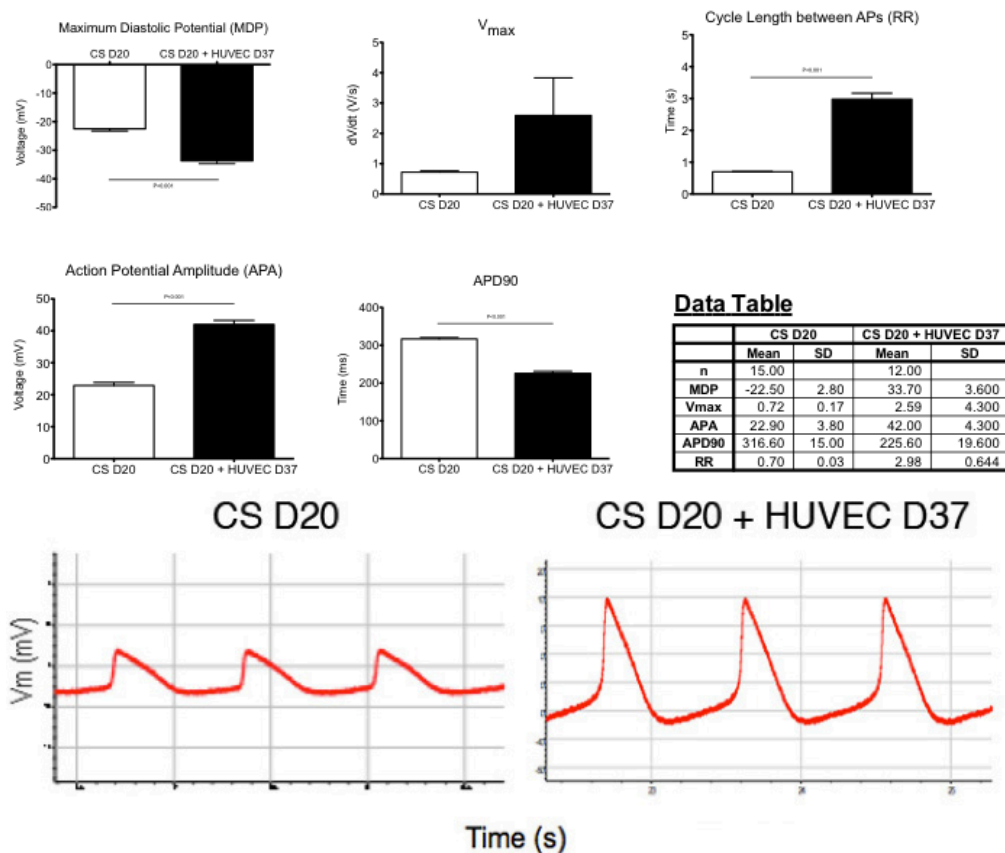


Figure 12 Electrophysiological parameters from IC recordings for co-cultured CS and CS only subsets. The parameters measured were as follows: (A) maximum diastolic potential (MDP), (B) V_{max} , (C) cycle length between APs (RR), (D) action potential amplitude (APA), and (E) action potential duration (APD90). (G) and (H) are representative tracings from each subset.

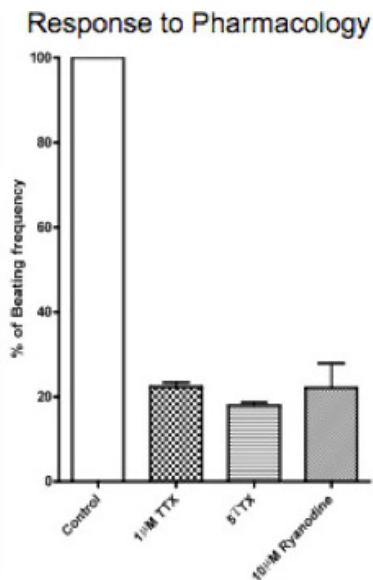


Figure 13 Pharmacology profile of co-cultured CSs versus CS only controls. Depression of beating frequency in comparison to control CS only conditions are compared with exposure to TTX (1µM, 5µM) and ryanodine (10µM).

2.4.3.2 Co-culture of dissociated hESC-derived CMs and Disparate Endothelial Sources (CCE2 and CCE3)

In CCE2 and CCE3, HUVECs and HMEC-1 cells, respectively, were co-cultured with dissociated hESC-derived CMs. From CCE1, we recognized a number of limitations due to the 3D structure of CSs (discussed further in Section 2.5.3.2) that we believed could be improved by dissociating CSs to a monolayer culture format. The goals of CCE2 and CCE3 were to compare and reproduce the developmental effects observed in CCE1 by using dissociated CMs instead of CSs. In addition, as HUVECs could not persist over long-term co-culture, we intended to 1) characterize HUVEC viability in co-culture and 2) to compare the effects of HUVECs and HMEC-1 cells on CM development as HMEC-1 cells have the advantage of long-term culture viability.

As with CCE1, dissociated CMs remained contractile for the 62-day co-culture period with HUVECs. However, in monitoring their presence at 2-week increments, HUVECs could not be detected in co-culture at each time point, as monitored through live lectin staining. We attribute the loss of HUVECs to the inability of primary cells to remain viable over long-term culture. Thus, fresh HUVECs were added every two weeks for the duration of the experiment to maintain an EC influence over the 62 days.

As mentioned, CM and EC morphology was monitored with live fluorescence imaging at each HUVEC seeding and 2 weeks afterwards. The CMs used in this experiment were both mCherry-positive and possessed GFP-positive nuclei. Live ECs could be stained with lectin and imaged concurrently. Thus, co-cultures were monitored for both CMs and ECs about every 2 weeks. From these fluorescent images, it appears that CMs did not exhibit the expected monolayer morphology but were typically clustered together in small aggregates. (Figure 14A) ECs appeared as clustered sheets but primarily associated with other ECs as well. (Figure 14B and C, yellow arrows)

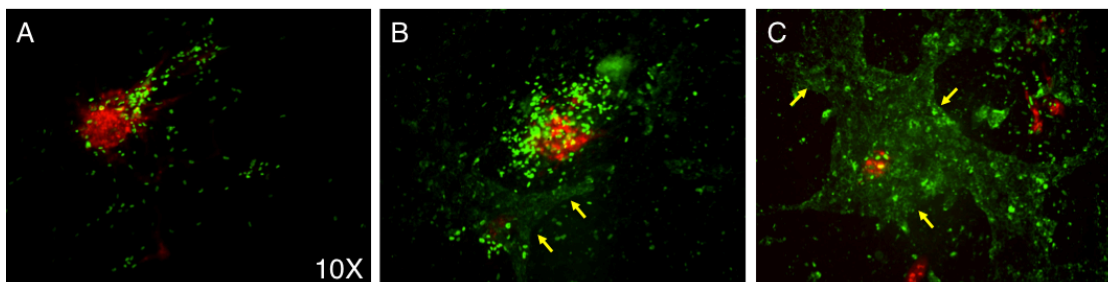


Figure 14 Live fluorescence imaging of dissociated CM:HUVEC co-culture (10X), Day 48 of co-culture. (A) CM only, (B) 1:1 HUVEC:CM co-culture, and (C) 2:1 HUVEC:CM co-culture. CMs are represented by mCherry expression (Red) and GFP-positive nuclei. HUVECs are detected by fluorescein-conjugated lectin shown in green (non-nuclear pattern). ECs are only detected in (B) and (C) as indicated by the arrows.

Similar to CCE1, co-cultured hESC-derived CMs exhibit a more mature gene expression profile than CM only controls. (Figure 15) Specifically, gene expression of α MHC, β MHC, MLC2a, and Serca2 was higher in co-cultured CMs, particularly when co-cultured in 1:1 HUVEC:CM ratios. MLC2v and PLB expression however were expressed more highly in 1:1 HUVEC:CM ratio subsets, but exhibited expression values less than controls for 2:1 HUVEC:CM ratio subsets. Gene expression levels of $\text{Na}_v1.5$, $\text{Ca}_v1.2$, and IP3R2 was higher in co-cultured CMs as well, but with insignificant differences between the different HUVEC:CM ratio subsets. Expression of NCX-1 and Cx43 were both expressed at much lower levels in co-cultured CMs than CM only controls. Although a couple discrepancies exist between the gene expression profiles for CCE1 (Figure 11) and CCE2 (Figure 15) , in particular with IP3R2 and NCX1, CMs from both experiments exhibit more mature gene expression profiles overall than CM only controls.

Functionally, we were not able to obtain IC recordings of high quality and number from these cultures. First, only one control well and two of each experimental well remained viable by 62 days. In addition, although cultures were spontaneously contracting, when pierced with sharp electrodes, spontaneous activity would cease. Thus, although a few recordings were obtained for both co-cultured (n=1) and control (n=7), sampling error and technical challenges rendered this data inconclusive.

Finally, co-culture of dissociated CMs with HMEC-1 cells revealed that the results reported from CCE1 and CCE2 are HUVEC-specific. Morphologically, CMs co-cultured with HMEC-1 cells exhibited a monolayer morphology that contrasted with the diffuse, 3D clusters observed in CCE2. In addition, when qPCR was performed with the same marker panel as CCE1, gene expression of HMEC-1 co-cultured CMs was either down-regulated or no different from controls in all cases.

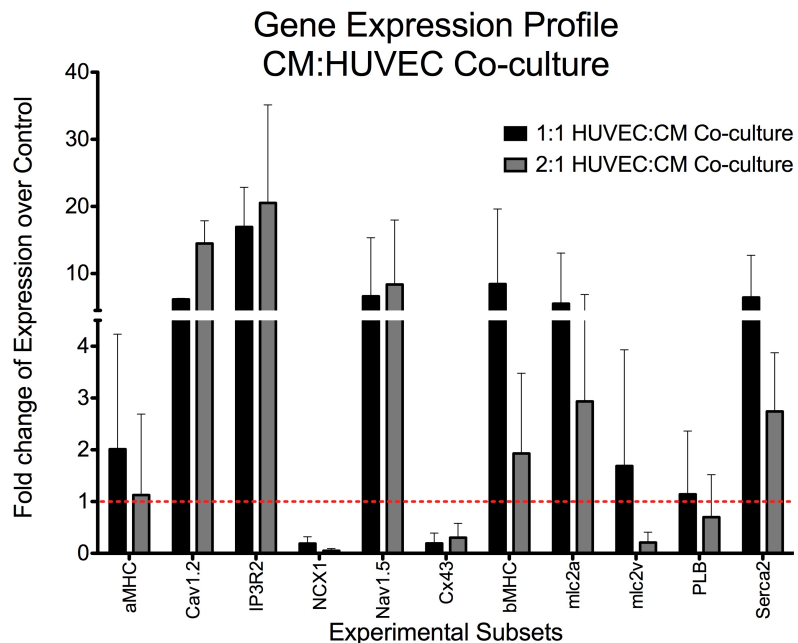


Figure 15 Gene expression profile from qPCR of key cardiac markers during CM development with HUVECs and dissociated CM co-culture versus CM only controls. Here, CMs seeded with HUVECs in a 1:1 HUVEC:CM ratio (n=2) are shown in black and CMs seeded with HUVECs in a 2:1 HUVEC:CM ratio (n=2) are shown in grey. All expression values are expressed as fold change over control values (n=1; dashed red line = 1).

2.5 Discussion

2.5.1 Media Comparison for Long-term Culture of ECs

We determined that 50/50 EGM-2/2% hEB medium would be best for co-culture conditions as this media condition maintained EC and hESC-derived CM viability for at least 22 days. One of the major reasons why we favored this media composition was because it incorporates 2% hEB, which we regularly use for maintenance of hPSC-derived CMs. In addition, this was the only media condition that satisfied all of our criteria, aside from EGM-2 controls.

The main disadvantage of HUVECs is that they are primary cells and thus cannot remain in culture for extended periods of time. From preliminary co-culture studies, we observed that the HUVEC presence, as monitored by live lectin staining, disappeared after about 2 weeks. Thus, constant addition of cells was necessary throughout the co-culture period. HMEC-1 cells provide a potential solution as they are an immortalized cell line. [176] From similar media tests as conducted with HUVECs, we determined that HMEC-1 cells remained viable even after 43 days of culture in all media conditions as evidenced by the presence of cobblestone morphology and constant nuclear mCherry expression throughout the media test.

2.5.2 Dissociation of cardiospheres for multi-well formats

Culture of hPSCs, their differentiation, and subsequent maintenance are reputed as extremely labor-intensive and costly necessities to the realization of the immense scientific and clinical potential that these cells hold. [93, 177] A repertoire of literature has now begun to focus not only on improving the efficiency of current culture methods [178, 179] but also lowering the laboratory costs associated with hPSC work [180-182]. The ability to make hPSC culture and maintenance less of a financial burden and more efficient will undoubtedly enable faster scientific progress as well as other non-clinical applications, such as large-scale, commercial drug discovery or toxicity studies. [183] In this study, we have shown that dissociation of CSs to single cell suspensions enables adaptation of these cells to multi-well formats so that cell needs are reduced by 80% with a transition from 24-well to 96-well format and by 90% with a transition from 24-well to 384-well format. Accordingly, this is advantageous for long-term experiments because a reduction in cell needs translates into a reduction in culture costs as well.

In addition to the practical advantages of CM dissociation, using hPSC-derived CMs in a monolayer format improves the ability to assay these cells from a scientific point of view as well. As mentioned, EBs and CSs are heterogeneous not only in cell composition but also in cell number, size, and matrix composition. [184-186] In addition, as they are 3D, depending on where cells are located (eg. outer surface versus center of cell mass), cells are exposed to different microenvironments that may alter their differentiated phenotype. These structural heterogeneities were identified as major limitations to CS exposure to EC stimuli, confounding results from CCE1. (Refer to Section 2.5.3.2) Dissociation of hESC-derived CMs into a 2D monolayer enhances reproducibility of experiments and enables increased surface area exposure to culture stimuli. In addition, monolayer CMs are more accessible for immunostaining, imaging, and IC recordings.

2.5.3 Co-culture of hESC-derived CMs and Endothelial Cells

2.5.3.1 Co-culture of hESC-derived CSs with HUVECs (CCE1)

Our interest in determining whether and in what capacity EC factors influence CM maturation motivated this co-culture experiment with CSs and HUVECs. As it had been determined that CSs were of high CM purity and could display a more mature phenotype when exposed to a heterogeneous population of non-cardiac cells [158], we hypothesized that this culture format would be feasible for answering our hypothesis that ECs modulate aspects of CM maturation. To this end, we were able to observe changes in CM morphology through immunostaining techniques as well as gene expression and electrophysiological differences.

With respect to CS morphology, differences were reflected on a macroscopic scale as specific attributes of individual CMs within the CS could not be easily resolved. However, the morphology that was exhibited by co-cultured CSs suggests that CM proliferation or migration was enhanced by co-culture. Potential mechanisms for this phenotype may relate to factors released by ECs that have been shown to stimulate CM proliferation [16] or potentially EC-secreted matrix proteins [187, 188] that may enhance CM migration, contractile protein expression, and/or CM proliferation from the CS to the surrounding culture area.

The gene expression and electrophysiological data seem to correspond with expectations for CM maturation in the literature. In reference to Appendix 0, the gene expression profiles exhibited in CCE1 suggest that co-cultured CSs are tending towards a more mature phenotype. We observed upregulation of key cardiac markers of maturation, namely α MHC, $Ca_v1.2$, RYR2, $Na_v1.5$, Cx45, HCN4, KCNQ1, KCNH1, $iK_r2.1$, and $iK_r2.2$, and downregulation of IP3R2 and Cx40. With both IC recording and pharmacological evaluation, the functional contributions of this gene expression profile can be elucidated.

From IC recordings, co-cultured CSs display more mature AP characteristics compared to CS only controls. Mummery et al reported that atrial fetal CMs (16 weeks) exhibit a MDP, V_{max} , APA, and APD90 values of -34.9 ± 1.6 mV, 1.2 ± 0.3 V/s, 57.2 ± 5.0 mV, and 164.9 ± 14.3 ms, respectively. Comparably, fetal ventricular CMs (16 weeks) have been reported to exhibit parameter values of -38.5 ± 1.6 mV, 8.9 ± 4.3 V/s, 69.0 ± 9.1 mV, and 370.0 ± 45.8 ms. [95] Values observed for V_{max} and APA seem to be much lower than these reported values, but co-culture appears to enhance these parameters towards more mature values as well. However, the MDP and APD90 values that were

observed for both CS only and co-cultured CS subsets are comparable with reported fetal CM values. The tendency towards a lower resting potential in developing CMs is determined in large part by the potassium gradient, which is influenced by NCX1 and inward-rectifying potassium currents. [141] Through qPCR, we observed that NCX1 expression is upregulated in co-cultured CMs (Figure 11), which may reflect the lower resting potential of co-cultured CSs. Moreover, in the developing heart, APD increases with CM maturation due to the expression and functionality of K^+ channels, which modulate AP repolarization and thus APD. [6, 141] Through qPCR, we observe that a range of K^+ channels were upregulated, in particular $iK_r2.1$, $iK_r2.2$, KCNQ1, and KCNH1, (Figure 11) which are delayed-rectifier K^+ channels. Activity of these K^+ channels governs AP repolarization and may account for the extended APD₉₀ values observed in co-cultured CSs. [189]

Pharmacological evaluations of CS-HUVEC co-cultures further reinforce our findings with qPCR. TTX treatment of co-cultured CSs caused an 80% depression of beating frequency over CM only controls, which suggests the functionality of $Na_v1.5$ channels. The difference in TTX sensitivity between co-cultured and CM only controls can be attributed to a few different phenomenon. First, increased functionality of $Na_v1.5$ in co-cultured CMs versus non-functional channels in CM only conditions could produce this pharmacological response. Contrastingly, since qPCR indicated a 3-4 fold increase in $Na_v1.5$ expression in co-cultured CMs, more functional channels could explain the discrepancy in TTX sensitivity as well. Finally, a combination of both phenomenon could also be the case. Using our current methods, we cannot resolve the exact mechanism. However, we can conclude that co-culture with HUVECs enhances the functionality and expression of $Na_v1.5$ in CMs.

Increased ryanodine sensitivity was also witnessed in these experiments with a 75-80% depression of CM beating frequency over control subsets after treatment. Ryanodine blocks the ryanodine receptors (RYR2) and thus Ca^{2+} release from intracellular Ca^{2+} stores. Again in the case of RYR2, we see around a 15-fold increase in expression of this receptor in co-cultured CMs. As expression of RYR2 does not necessarily correlate with functionality early on in CM development [91], it is unclear whether the differences observed in ryanodine sensitivity can be attributed to increased functionality of RYR2, higher expression of functional receptors, or a mixture of both phenomena. Yet, it is clear that co-cultured CSs exhibit RYR2 functionality and gene expression at much higher levels than CM only CSs.

2.5.3.2 Potential Limitations to Evaluating CSs in Biological Assays

A number of technical limitations and concerns arose in performing CCE1. First, in terms of the number of replicates, we were limited by our ability to produce CSs due to the low yield from traditional hESC culture techniques. In this experiment, only two CSs were used per condition so that one CS from each subset would be used for immunostaining and one for the electrophysiological studies and qPCR data. Although CS number is low, these CM clusters are typically composed of 10^4 - 10^6 cells/CS, which is reasonable to ensure data certainty for these particular CS characterizations. However, because CSs are heterogeneous in composition, size, and shape, more CS replicates need to be evaluated to determine whether the phenotype we observed is simply an artifact of the particular CSs we evaluated.

In addition to a paucity of replicates, CS structure and composition, as mentioned, are variable and difficult to control. Shape differences can modulate the

extent of exposure to extracellular influences, as different surface area to volume ratios could change exposure conditions for individual CMs depending on their localization within the CS. Since CS structure is a function of random formation, even with the introduction of more CS replicates, it would be unclear and impossible to determine whether differences in physiology are a function of structural heterogeneities, actual modulation from co-culture conditions, or a mixture of both. In addition, as EB formation is performed manually, operator biases may also impact the reproducibility of results.

The phenotypic heterogeneity of CSs and hESC-derived CMs is another concern. Current differentiation methods generate, at random, hESC-derived CMs that vary in developmental stage, cardiac cell type, and morphology. [90, 95, 108] Additionally, current techniques used to assay CM function (eg. electrophysiology and Ca^{2+} handling) are disadvantaged by their relatively low sample size due to the complexity of the techniques paired with manual sampling methods. In a homogeneous population, this technical limitation would not misrepresent biological phenomenon, as an average amongst 15-20 cells would provide a reasonable assessment of the entire population. However, probing < 1% of the cell content of an extremely heterogeneous population could possibly misrepresent and potentially misguide experimental observations and conclusions.

2.5.3.3 Co-culture of dissociated hESC-derived CMs and Disparate Endothelial Sources (CCE2 and CCE3)

To address our concerns with CSs, we subsequently designed experiments (CCE2 and CCE3) where dissociated CMs in monolayer culture were either co-cultured with HUVECs or HMEC-1 cells, respectively. From these studies, we demonstrated that

dissociated CMs co-cultured with HUVECs appear to exhibit a more mature gene expression profile compared to CM only controls, reinforcing our findings from CCE1. In both CCE1 and CCE2, hESC-derived CMs co-cultured with HUVECs show upregulated expression of α MHC, $Ca_v1.2$, and $Na_v1.5$ channels, markers we would expect to be more highly expressed with cardiac maturation.

IP3R2 expression levels were comparable to control in co-cultured CSs but were 15-20 fold higher in dissociated CM co-cultures over CM only controls. IP3R2, a variety of Ca^{2+} release channels on the sarcoplasmic reticulum, are typically highly expressed in very immature CMs and atrial CMs. [190] The high level of IP3R2 expression by co-cultured CMs in CCE2 may be reflective of physiological immaturity. Alternatively, as *mlc2a* levels also show a 3-8 fold upregulation in co-cultured CMs, upregulation of IP3R2 could be coincident with atrial specification in these cultures. Without more specific functional analysis, such as IC recording or immunostaining for atrial markers, conclusions could not be made.

On the other hand, NCX1, or the Na^+-Ca^{2+} exchanger, is highly expressed in CSs but downregulated in dissociated CMs as compared to CM only controls. In mature CMs, NCX1 expression can be detected, but peak expression occurs in developing CMs as NCX1 serves as the main mechanism of Ca^{2+} extrusion before intracellular Ca^{2+} stores and reuptake mechanisms (through *Serca2*) become functional. Thus, the downregulation of NCX1 paired with the 3-10 fold upregulation of *Serca2* observed in CCE2 suggest that CMs may be heading towards a more mature Ca^{2+} -handling phenotype.

In contrast, CMs co-cultured with HMEC-1 cells exhibited downregulation of every marker assayed. This discrepancy between EC sources is not entirely unexpected,

as a plethora of literature exists that compares disparate endothelial cell types and their differential phenotypes. [191, 192] Uncertain about the biological effects of HMEC-1 cells on hESC-derived CM development, we originally chose to use HMEC-1 cells because their endothelial and immortalized characteristics give them a technical advantage over primary HUVEC cultures. However, from CCE2 and CCE3, it seems that HMEC-1 influences do not induce the more mature phenotype as observed with HUVECs. Overall, these findings demonstrate that disparate endothelial sources influence changes in CM phenotype differently and that the enhancements in CM maturation observed are HUVEC-specific.

2.5.3.4 Technical Limitations of CCE2 and CCE3

Several technical limitations manifested from CCE2 and CCE3 as well. First, HUVEC viability cannot be maintained in long-term culture and as a primary cell can display considerable lot variations. In our study, only one lot of HUVECs was evaluated and thus it is unclear whether another lot would produce similar results. In addition, to address the transient viability of these primary cells, fresh HUVECs were constantly added to hESC-derived CMs every two weeks. Another challenge for these co-culture experiments was the low CM yield from hESCs as well as sampling limitations in our assay methods. With large heterogeneities in CM development, physiology, and morphology, the number of replicates or CMs sampled is crucial to definitively assess any phenotypic changes observed.

It is also important to note that the timing of co-culture initiation differed for each experiment detailed in this study. Specifically, ECs were plated on dissociated CMs at D65 for HUVEC co-culture and D35 for HMEC-1 co-culture as compared to D20 for the

CCE1. The discrepancies in the timing of EC seeding were due, in part, to variations in quality of differentiation cultures. For instance, the onset of contractile activity between different differentiation trials varied considerably. In addition, decreased cardiac differentiation efficiency and ability of CMs to regain contractility post-dissociation also appeared as symptoms. EC seeding was not performed unless contractile CMs were present. Thus, it is possible that differences in seeding timing can be attributed to the variations observed in the results. However, it has also been evidenced in the literature that if CMs are isolated from other cell sources early on in differentiation (D20), electrophysiological developments are minimal. [158] In addition, with traditional differentiation methods, even late-stage CMs exhibit very immature CM phenotypes. [91]

2.6 Conclusions

Overall, these co-culture studies demonstrated that the maturity of developing CMs, in terms of gene expression and electrophysiology, could be influenced and enhanced by endothelial sources. These findings have significant implications for developmental biology and regenerative medicine as till now little is still understood about how maturation occurs on the myocyte scale. As detailed in this chapter, we were able to develop and/or implement necessary methods and techniques to evaluate maturity at morphological, genetic, and functional levels. Through these evaluations, we observed that co-culture of HUVECs with either hESC-derived CSs or dissociated CMs influences the development of CMs towards a more mature phenotype.

Briefly, HUVEC co-cultured CMs exhibited a more mature gene expression profile than CM only controls. Upregulation of major ion channels, Ca²⁺ handling proteins, and

contractile machinery followed trends that are observed in endogenous CM development. [6, 110, 141, 159] Functional evaluation of co-cultured CM physiology further bolstered the implications of maturity from qPCR evaluation. First, we described how co-cultured CMs exhibit more mature action potential kinetics with more negative MDP, faster V_{max} , and prolonged APD90 compared to CM only controls. Pharmacological inhibition of both $Na_v1.5$ and RYR2 demonstrated channel and receptor functionality, which has been used in the field as an indicator of the maturity of Ca^{2+} handling and electrophysiological machinery. [91, 158, 193] Moreover, co-cultured CMs exhibit heightened sensitivity to inhibition of these channels, signifying a more mature phenotype. We also determined that these effects seem to be HUVEC-specific as similar changes in gene expression were not observed with HMEC-1 co-culture.

However, with co-culture of these cell types, many limitations manifested during the completion of this study, which reflected both cellular and technological limitations of this co-culture model. Although we demonstrated that EC influences can modulate CM phenotype, our ability to obtain adequate numbers of high-quality hESC-derived CMs and accessibility to technologies for evaluating the phenotype of CMs with proper sampling were limiting factors.

With evidence that endothelial influences contribute to CM maturation, this study provides novel insight to one of potentially many players that modulate cardiac development. We believe that elucidating the necessary influences that control functional cardiac maturation will spur further progress in developing hPSC-derived regenerative therapies particularly for recapitulating the functional needs that are lost with MI. Co-culture of ECs and CMs represents a good first approximation for confirming whether endothelial influences modulate CM phenotype and characterizing global changes in CM

phenotype in response to ECs. In this study, we have shown reproducibly that HUVECs can induce developmental progress in hESC-derived CMs. The next step is to dissect this interaction further by describing how this heightened developmental phenotype is mediated.

2.7 Acknowledgements

I would like to thank Dr. Vincent Chen and his post-doctoral fellows, Drs. Changsung Kim and Maryam Majdi, for their help with electrophysiological characterizations and pharmacological evaluations of cardiomyocytes; Dr. Hiroko Kitamatsuo for generating the H9 human embryonic stem cell, α MHC reporter lines with which experiments were completed; Paul Bushway and Dr. Ke Wei for their insight on human umbilical vein endothelial cell (HUVEC) and human microvascular endothelial cell (HMEC-1) culture, respectively; and Drs. Mark Mercola and Andrew McCulloch for discussion and direction.

3 Endothelial Paracrine Factors Enhance Maturation of Human Induced Pluripotent Stem Cell- derived Cardiomyocytes

3.1 Abstract

Identifying developmental regulators and characterizing how they contribute to cardiac maturation is imperative to the application of hPSC-derived CMs for regenerative therapies. In this study, we hypothesized that paracrine factors from endothelial sources could enhance aspects of CM maturation. Specifically, we treated hiPSC-derived CMs with conditioned media from two endothelial sources, human umbilical vein endothelial cells (HUVECs) and human microvascular endothelial cells (HMECs), and compared them to non-conditioned media controls and hESC-derived fibroblast conditioned media

treated CMs. To address the vast heterogeneities present with hPSC-derived CM populations, we employed a high-throughput method for evaluating Ca^{2+} transients and electrical stimulation, which enabled description of CM populations two orders of magnitude larger than traditional methods. Maturation was assessed based on a series of metrics, including Ca^{2+} transient kinetics, pacing ability, pharmacology response, and gene expression profiles. After 2 weeks of culture, HUVEC conditioned media treated CMs exhibited enhanced ability to respond to 3Hz electrical stimulation, faster Ca^{2+} transient kinetics, and functional $\text{Na}_v1.5$ channels at heightened levels over all other experimental subsets. We conclude that unique paracrine factor(s) from HUVEC sources enhance aspects of functional maturation in hiPSC-derived CMs towards a more mature phenotype.

3.2 Introduction

The mechanisms that govern CM maturation remain largely obscure. Thus far, hPSC-derived CMs have served as an instrumental in vitro model of development by elucidating important cues and uncovering key signaling molecules that govern cardiac specification. [70, 71, 73, 96-98, 194] Characterization of hPSC-derived CMs reveals their similarity to fetal CMs in physiology and morphology [78, 95, 103, 105, 195], which many groups have hypothesized may explain the inability of hPSC-derived CMs to functionally replace damaged myocardium. An emerging thrust in the field is now centered on understanding the multifarious cues, both autonomous and non-autonomous, that govern the functional maturation of developing CMs, in particular the elements that require rescue post-MI, such as CM morphology, spatial organization, and

contractile function. [78, 139, 155, 158, 196] In the previous chapter, we presented evidence that co-culture of endothelial cell sources with hESC-derived CMs promotes a more mature phenotype as assayed through both gene expression and functional assays. Yet, the mechanisms at play still remain unclear after co-culture evaluation.

Communication between neighboring cells can be mediated through contact-dependent and/or paracrine mechanisms. Moreover, within either method of communication, a myriad of signal-receptor combinations direct cell phenotype. For instance, Narmoneva et al reported that CMs co-cultured with ECs or treated with EC conditioned media exhibited significantly less signs of apoptosis or necrosis when cultured in 3D versus their CM only or fibroblast co-cultured counterparts. However, enhancement of CM spatial organization was only exhibited in direct EC-CM co-culture conditions. [164] In vivo, disruption of proper vasculogenesis prevents heart formation. In addition, endothelial-specific knock out of numerous paracrine factors, such as neuregulin, neurofibromatosis-1, and platelet-derived growth factor B, inhibits proper myocardial development in mouse models. [16]

Here, we hypothesize that ECs significantly influence aspects of CM maturation. Specifically, we characterized the effects of paracrine endothelial factors on major functional determinants of CM function, in particular Ca^{2+} handling, gene expression, and CM morphology, using a high-throughput, single-cell analysis method. With this method, we were able to characterize the Ca^{2+} handling ability of an unprecedented CM population that is 2- to 3- fold greater than traditional methods. From these studies, we were able to conclude that exposure of hPSC-derived CMs with HUVEC conditioned media enhances CM maturation in terms of Ca^{2+} handling and electrophysiological function by two weeks in culture. These results have important implications for

understanding the process of CM development as well as improving current cardiac regenerative strategies.

3.3 Methods

3.3.1 Cells

CDI iCell hiPSC-derived Cardiomyocytes

hiPSC-derived cardiomyocytes (Cellular Dynamics International (CDI), Inc., Cat# CMC-100-110-001/CMC-100-110-005, Madison, WI) were used for these experiments. CDI CMs are genetically modified so that CMs are mCherry-positive and blasticidin-resistant (regulated by an α MHC promoter). CMs are frozen down at D35 of differentiation and once thawed can be maintained indefinitely in culture. Cells were thawed and plated as indicated by CDI on 0.1% gelatin-coated 96-well, glass-bottomed plates at a density of 1.5×10^4 CMs/well. After three days of recovering in plating media (CDI, Inc., Cat# CMM-100110-001, Madison, WI), CMs were maintained in 50/50 EGM-2/2% hEB media throughout the duration of culture with media changes every other day.

Endothelial Cells

Human umbilical vein endothelial cells (HUVECs) (Lonza Walkersville, Inc., Cat# C2519A, Lot#6F3251, Walkersville, MD) and human microvascular endothelial cells (HMEC-1) (ATCC, Cat# CRL-10636, Manassas, VA) were used for co-culture studies. For experiments, HUVECs were used until passage 10 before being discarded. HMEC-1s are an endothelial cell line and thus can be used indefinitely in vitro. HUVECs and

HMEC-1s were maintained in endothelial growth medium (EGM-2; Lonza Walkersville, Inc., Walkersville, MD) and media was changed every 2 days. For passage of both endothelial cell types, confluent plates were washed with Dulbecco's phosphate buffered saline, or dPBS, (Mediatech, Inc., Cat# 21-031-CV, Manassas, VA) and treated with 0.25% trypsin-EDTA (Invitrogen, Cat# 25200, Carlsbad, CA) for 2.5 minutes. Once cells detached, cells were resuspended in fresh EGM-2 to stop trypsinization and for transfer into new tissue-culture plates.

hESC-derived Fibroblasts

hESC-derived fibroblasts from the H9 α MHC-Puro^r-Rex-Neo^r/PGK-H2B-mCherry hESC line were used to generate conditioned media. Fibroblasts were isolated from 1-3 month old cultures differentiated under traditional serum-based methods. Cultures were dissociated with 0.25% Trysin-EDTA five times to isolate fibroblasts. Once fibroblasts were isolated from differentiated hESC cultures, cells were FACS sorted for mCherry expression at passage 2 or 3. Conditioned media was obtained from fibroblasts from passage 12-15.

3.3.2 Conditioned Media

HUVEC, HMEC-1, and hESC-derived fibroblast conditioned media was collected from confluent cultures. 10 ml of EGM-2 for ECs and 2% hEB for fibroblasts were incubated with confluent cultures for 2 days. Aged media controls were generated in a similar fashion by incubating fresh media without cells for 2 days at 37°C. Media was then collected and centrifuged (Eppendorf Centrifuge 5702R, Hauppauge, NY) for 5

minutes at 3000 x g to pellet cell debris. Supernatant was then collected and stored at -20°C until use. Three media collections were obtained from each confluent plate.

3.3.3 Time course of Endothelial Paracrine Effects on CM Maturation

hiPSC-derived cardiomyocytes (Cellular Dynamics International (CDI), Cat# CMC-100-110-005, Lot# 149825, Madison, WI) were plated at 1.5×10^4 cells/well in 96-well, glass-bottomed plates (Grenier Bio-One, Cat# 655892, Monroe, NC) that were pre-coated with Matrigel (0.0625 mg/ml, BD Biosciences, Cat# 354230, San Diego, CA). The conditions tested were: 1) Control, 2) HUVEC conditioned media, 3) HMEC-1 conditioned media, and 4) hESC-derived fibroblast conditioned media. In each case, a 50/50 EGM2:2% hEB media was used. Conditioned media was generated in EGM2 and diluted by 50% with 2% hEB media. Control media conditions involve aged EGM2, which is described as EGM2 incubated for 48 hours at 37°C without cells in a 10-cm tissue culture plate.

Four time points were evaluated in this study, specifically 1-, 2-, 4-, and 8-week exposure to the different experimental conditions. Three separate plates were allocated per time point for each evaluation method of CM maturation, namely for qPCR, baseline Ca^{2+} transient measurements, and pharmacology studies. Cells used for Ca^{2+} transient measurements and pharmacology were subsequently fixed with 4% PFA for 10 minutes and stored in dPBS at 4°C until processing. qPCR samples were processed with Trizol reagent and stored at -80°C until use. Ca^{2+} transient measurements and pharmacology were loaded with Fluo4-NW and imaged on the KIC (Vala Sciences, Inc., San Diego, CA).

3.3.4 Fluo4 Loading of Cardiomyocytes for Ca²⁺ Transient Imaging

Prior to loading with Ca²⁺ sensing dyes, cultures were changed to 2% hEB media 12-24 hours before loading for all conditions. Fluo4-NW (Invitrogen, Cat# F36206, Carlsbad, CA) dye was reconstituted in 10mL of assay buffer, which is composed of 1X Hanks balanced salt solution (HBSS) (Gibco, Cat# 14025-092, Carlsbad, CA) with 20mM HEPES buffer solution (Gibco, Cat# 15630-106, Carlsbad, CA). For recordings in hiPSC-derived CMs, ¼ of the manufacturer recommended dye concentration was used. In addition, 250mM solution of probenecid (included in the kit) was made by adding 1ml of assay buffer to the vial until dissolved. 100 µl of 250mM probenecid was added to the diluted Fluo4-NW dye solution and mixed thoroughly. To label nuclei, Hoechst dye was diluted in assay buffer at 4 µl in 196 µl and was then added to the dye solution at a ratio of 1:2000 µl. 100 µl of Hoechst-dye solution was incubated per well for 20 minutes at 37°C and for an additional 20 minutes at room temperature. Cells were then washed with 200 µl of Tyrode's solution with 10mM glucose twice. Cells were recorded in 200 µl of Tyrodes solution with 10mM glucose.

3.3.5 Pharmacology

For the pharmacology studies, drugs were diluted in Tyrode's solution with 10mM glucose and incubated with the cultures for 10 minutes before KIC recordings. The following drugs and respective dilutions were used: tetrodotoxin citrate (TTX, 1µM, Tocris, Cat# 1069, Ellisville, MO), thapsigargin (TSG, 1µM, EMD-Calbiochem, Cat# 586005, Gibbstown, NJ), diltiazem (DTZ, 1µM, Sigma-Aldrich, Cat# D2521, St. Louis, MO), and ryanodine, a blocker of the RYR2 channel, (10µM, Tocris, Cat# 1329, Ellisville, MO). 0.001% DMSO (Sigma-Aldrich, Cat# D2650, St. Louis, MO) controls were also

included in the pharmacology trials since stock solutions of TSG, DTZ, and ryanodine are dissolved in DMSO. Once drugs were added, Ca^{2+} transients were recorded using the KIC and analyzed with Cytoseer compared to untreated controls.

3.3.6 Kinetic Imaging Cytometer (KIC) for High-throughput

Acquisition of Cardiomyocyte Ca^{2+} Transient Generation

KIC Instrument

The components of the KIC module include a video acquisition PC with the Windows XP operating system with control software programmed in C++ using Microsoft Visual Studio 2008 (Bellevue, WA), a NI-PCI-6251 data acquisition I/O board from National Instruments (Austin, TX), a stimulator/electrode assembly (lowered and raised using a computer-controlled Sutter Instruments (Novato, CA) micromanipulator, the MP-285), a Grass Technologies (West Warwick, RI) S48 square pulse stimulator, and the high-speed scientific-grade iXon DU-897 EMCCD camera with 16-mm pixels (Andor, South Windsor, CT).

The KIC module is placed on an IC 100/200 high content screening system (Vala Sciences, San Diego, CA) that includes: 1) an inverted epifluorescence microscope (Nikon Eclipse TE2000-U), 2) an intensity-feedback stabilized 100 W Hg arc lamp [197] 3) excitation and emission filter wheels, 4) a motorized stage with XY-axes control, and 5) a piezoelectric Z-axis control for fast, precise autofocus. A Nikon multi-image module splits the emission light paths on the IC 100 to the autofocus camera (Cohu, Poway, CA) and an Orca-ER CCD camera (Hamamatsu, Bridgewater, NJ), which was replaced by the iXon EMCCD for KIC. Cytoshop on the IC100 controlled the instrument and scanned

the plate, with KIC module timed from the IC100 epifluorescence shutter sync signal; and CyteSeer software controls the IC 200 version.

KIC Data Acquisition

Plate scanning parameters were selected and KIC automatically scanned each plate without further operator intervention. KIC acquired and stored video streams of Fluo-4 (the green channel) lasting 3-30 seconds at 33 fps simultaneously with user specified electrical stimulation frequencies ranging from 1-6Hz. Electrical stimulation and video acquisition were triggered during scanning on the prototype KIC by the open/close sensor of the arc lamp shutter on the IC100. Electrical pacing parameters were 15 volts and 5 ms duration for each stimulus. Prior to video stream acquisition, KIC auto-focused on each field using the nuclear channel of the cells. KIC scans a rectangular grid of contiguous fields of view in each well, for any density microtiter plate. One field/well was acquired over 20 to 50 seconds in each well in 96-well plates for all experiments in this report. All images were captured with a 20x 0.50 numerical aperture (NA) objective and 1x tube and relay lenses.

3.3.7 Cyteseer Analysis of Ca²⁺ Transient Imaging Data

Image analysis for time-series images obtained from the KIC was performed by CyteSeer (Vala Sciences, San Diego, CA). Automated image analysis included the following steps:

- 1) Time-averaging of the Ca²⁺ channel. The Ca²⁺ channel images were averaged over all time-slices to increase the signal-to-noise ratio for improved image

segmentation. For typical experiments with 100 to 250 time-slices, the signal-to-noise improved by a factor of roughly 10 to 15, facilitating segmentation.

- 2) Background subtraction of the nuclear and the Ca^{2+} channels. The background was defined at each pixel to be the minimum intensity of all pixels within a large user-defined radius around that pixel. These background images were subtracted from the original images. Then both images were clipped to ignore pixels outside the range between the 2nd and 98th percentile in pixel intensity.
- 3) Segmenting the cell nuclei. The nuclear image was segmented by first thresholding to find a binary mask for the nuclear regions, and then applying a watershed algorithm to separate nuclei that were touching or nearly touching.
- 4) Segmenting the cells. The Ca^{2+} image was segmented by first thresholding to find a binary mask for the cell regions, and then applying a watershed algorithm to the masked Ca^{2+} image using the nuclei as seeds.
- 5) Measuring the Ca^{2+} image intensity on each cell. For each time-slice, the average pixel intensity of the Ca^{2+} image was measured for each pixel in the entire cell mask, in the cytoplasmic mask (defined to be all pixels in the cells that are not in the nucleus) and in the nuclear mask alone.
- 6) Computing time-traces for the Ca^{2+} signal. For each cell or cellular compartment, the average pixel intensity was plotted as a function of time. The baseline of each time-trace was computed and subtracted from each function to compensate for artifacts at the very beginning and very end of some of the traces. Time-course data could subsequently be exported for each segmented cell.

Data Extraction

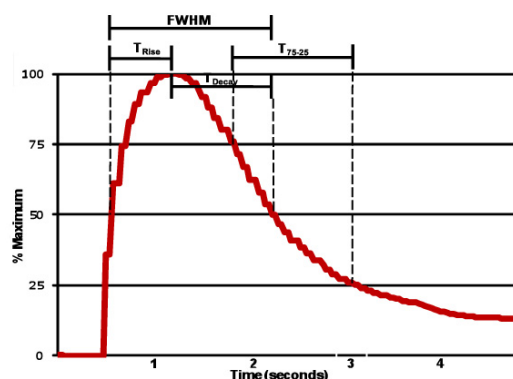


Figure 16 Diagram of Ca^{2+} transient parameters extracted by Cyteseer.

For each well, cell segmentation, nuclear segmentation, and cell ID maps were generated. Time-series data of Ca^{2+} activity as assayed by fluctuations in average pixel intensity (API) was generated for each segmented cell. In addition, we are able to obtain peak value (API), rise time from 50% rise amplitude to the peak (T_{rise} , ms), decay time from the peak to 50% decay amplitude (T_{decay} , ms), and full-width-half-maximum (FWHM, ms) values, which is the sum of T_{rise} and T_{decay} , for each individual cell from the Cyteseer software. (Figure 16) T_{rise} , T_{decay} , and FWHM values were then normalized with peak value to generate rise velocity (V_{rise} , API/ms), decay velocity (V_{decay} , API/ms), and nFWHM (ms/API).

3.3.8 Quantitative Polymerase Chain Reaction (qPCR)

Total RNA was extracted using Trizol reagent (Invitrogen, Cat# 15596-018, Carlsbad, CA) in conjunction with the protocol provided by the manufacturer for cells in a monolayer. Samples incubated in Trizol were either stored at $-80^{\circ}C$ or processed immediately. Once RNA extraction was complete, RNA was resuspended in $10\mu l$

distilled, deionized water (ddH₂O) (Mediatech, Inc., Cat# 25-055-CV, Herndon, CA). RNA concentrations were measured using the Nanodrop spectrophotometry system (Thermo Scientific, Inc., Cat# ND-1000, Wilmington, DE). cDNA was synthesized using the QuantiTect Reverse Transcriptase (RT) Kit (Qiagen, Inc., Cat# 205314, Valencia, CA). cDNA was amplified using 1 µg of RNA and the RT kit. Once the RNA was mixed with genomic DNA wipeout buffer, samples were heated at 42°C for 5 minutes. Samples were then mixed with RT buffer, RT enzyme, and amplification primers for a total volume of 20 µl. Samples were heated for another 30 minutes at 42°C, 95°C for 3 minutes, and kept at 4°C. Finally, cDNA concentrations were measured using the Nanodrop and stored at -20°C until use.

qPCR was performed on the LightCycler 480 (Roche Applied Science, Cat# 05015278001, Indianapolis, IN). Samples are prepared using extracted cDNA as indicated by the manufacturer using the LightCycler 480 SYBR Green I Master kit (Roche Applied Science, Cat# 04887352001, Indianapolis, IN) in a 96-well plate format (Roche Applied Science, Cat# 04729692001, Indianapolis, IN). Briefly, qPCRs were conducted as follows: samples were denatured at 95°C for 8 minutes with a temperature slope of 20 °C/s (slope used for every step unless otherwise specified), sample amplification occurred with the following sequence, 95°C for 15 seconds, 60°C for 5 seconds, and 72°C for 20 seconds, for 40 cycles, melting curves were obtained with a subsequent cycle starting at 95°C, 70°C for 20 seconds, and a return to 95°C at a slope of 0.1°C/s, and finally samples were cooled at 40°C for 30 seconds. Primer sequences are listed in Appendix 2. C_p values were obtained using the LightCycler 480 Multiple Plate Analysis software (Roche Applied Science, Cat# 05075122001, Indianapolis, IN).

Using efficiency values for each primer pair, transcript expression could be calculated using the $\Delta\Delta C_p$ method. Transcript levels were normalized to GAPDH expression.

3.3.9 Immunostaining

Prior to immunostaining, cells were washed with dPBS and fixed in 4% paraformaldehyde (PFA) for 10 minutes. After fixation, samples were stored in 1X dPBS at 4°C until processed. Cells were blocked in a blocking buffer composed of 1X dPBS, 2% BSA, 2% goat serum, 50mM glycine (Bio-Rad, Cat# 161-0718, Hercules, CA), 0.01% Triton-X (Sigma-Aldrich, Cat# T8787, St. Louis, MO), and 0.005% Tween 20 (Sigma-Aldrich, Cat# P9416, St. Louis, MO). Primary antibodies used for these studies were diluted in 10% blocking buffer in the following ratios: mouse monoclonal anti- α -actinin (1:300, Sigma Aldrich, Cat# A7811, St Louis, MO), rabbit polyclonal $Na_v1.5$ (1:150, Alomone Labs, Cat# ASC-005, Jerusalem, Israel), and 4',6-diamidino-2-phenylindole (DAPI, 1:5,000). Once stained, cultures were imaged with an inverted fluorescent microscope (Leica DMI-4000B, Buffalo Grove, IL or Olympus IX71, Center Valley, PA) or using the KIC system.

3.4 Results

3.4.1 High-throughput analysis of cardiac Ca^{2+} -handling parameters enables large-scale evaluation of heterogeneous hiPSC-derived CM populations

Due to the highly random and heterogeneous nature of hPSC-derived CMs, current methods used for investigating CM maturation and function suffer from low

sample size and thus potentially erroneous conclusions. We investigated the variation of hiPSC-derived CMs using the KIC high-throughput imaging instrument and Cyteseer-facilitated single-cell analysis. Using these tools, we were able to evaluate the Ca^{2+} transients of CMs at numbers at least an order of magnitude larger than traditional methods ($n=600-1060$ versus $n=6-60$). [95, 105, 115] (Figure 17)

In these particular studies, CM number remained unchanged between 1- and 2-week time points. (Figure 18) However, it is important to note that non-cardiac cell types arose with increased culture duration, although never outnumbering CMs. To characterize the functional properties of CMs, we identified CMs as only those cell segments which could generate Ca^{2+} transients either spontaneously or in response to electrical stimulation. All other cell segments, which were devoid of transient activity, were not included in subsequent analyses. (Figure 19)

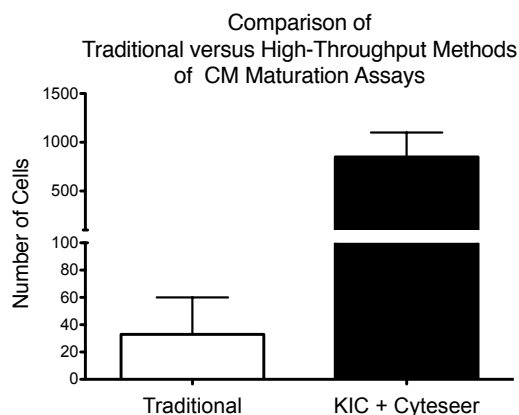


Figure 17 Comparison of population sampling capabilities between traditional versus high-throughput methods of assaying CM maturation.

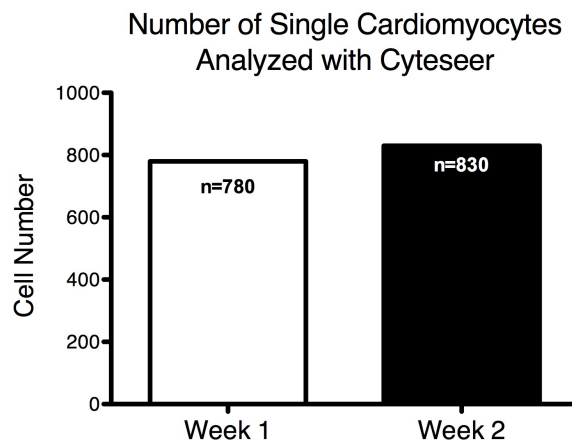


Figure 18 Number of individual CMs analyzed at week 1 (n=780) and week 2 (n=830) time points.

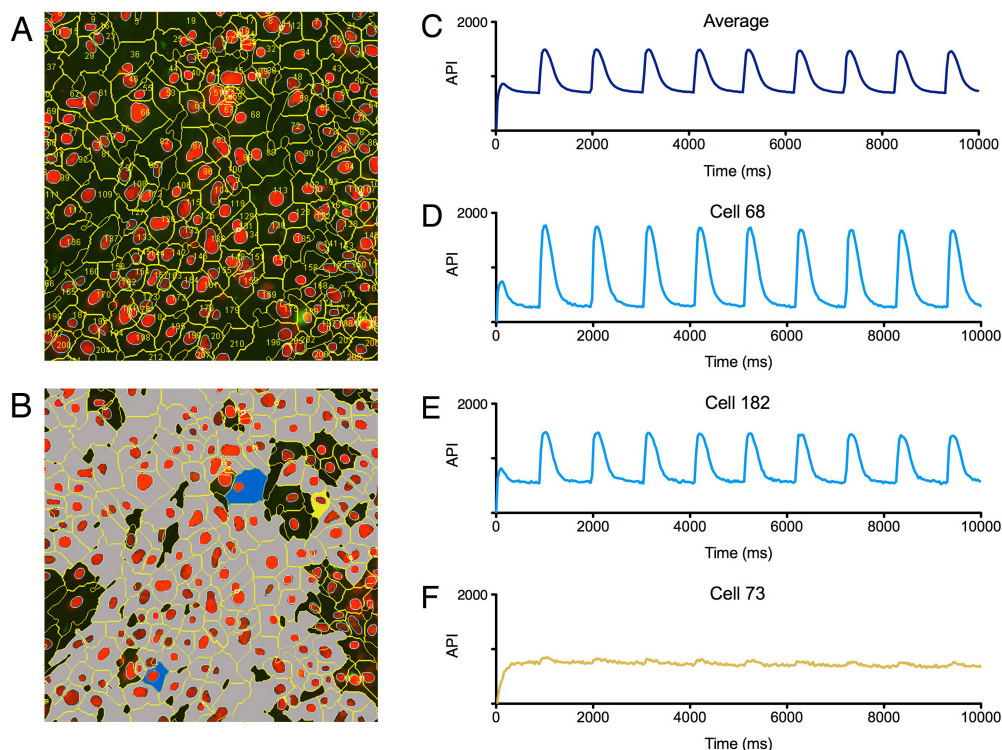


Figure 19 Cyteseer processing of representative well (D05) of baseline CMs. (A) Single cells were segmented and assigned a unique cell ID. (B) CMs were identified as cell segments that could generate spontaneous or electrically stimulated Ca^{2+} transients (grey). Cells that were unresponsive or exhibited low quality transients (noise or drifting baseline) were not included in analyses (black). (C) By week 2 of culture, CM contractions were synchronous across the entire well as evidenced by the uniform Ca^{2+} trace when time series data for each CM was averaged. (D)-(F) are Ca^{2+} traces for representative cells that were included in analyses (blue, D-E) or excluded (yellow, F).

Using this large CM sample population, we monitored changes in Ca^{2+} handling parameters for each segmented CM. For each kinetic parameter, histograms were generated for rise velocity, decay velocity, and full-width-half-maximum (nFWHM), an approximation of transient duration. As shown in Figure 20, population distributions of each kinetic parameter exhibited non-Gaussian, skewed characteristics as well as broad data ranges suggesting heterogeneous populations for each kinetic parameter. In fact, nFWHM values were lognormally distributed suggesting the multiplicative effect of multiple independent variables. [198] (Figure 20E) From one to two weeks in culture, rise and decay velocities of baseline CMs shift towards faster values and, accordingly, nFWHM values shortened. (Figure 20)

Although heterogeneities in individual kinetic parameters can be described, it is important to mention that CMs predominantly formed synchronously contractile monolayers one week after plating. CM culture morphology was monitored using mCherry expression that was preferentially expressed only in αMHC -positive cells. In addition, evaluation of Ca^{2+} flux in individual, segmented CMs revealed that transient timing was typically consistent amongst all CMs. As Cyteseer enables single cell analysis of cultures, detection of asynchronous populations was also possible but with low incidence at week 1 and disappearing by week 2 in culture.

To further quantify shifts in Ca^{2+} kinetic parameters over time, a percentile-based comparison was used. Percentile cut-offs were established based on the median value (assigned to the 50th percentile) for each kinetic parameter at Week 1. (Table 3) The percentages of CMs were then plotted for each percentile gate for both time points. Additionally, fold change of Week 2 versus Week 1 cell percentages were plotted for each percentile. (Figure 21) Peak values of fluorescence, an approximation of Ca^{2+}

transient amplitude, did not change significantly between Week 1 and Week 2. (Figure 21A) About 45% of CMs exhibit nFWHM values less than the 15th percentile than CMs at Week 1. (Figure 21B) These shorter nFWHM values are reflected in a shift towards faster rise and decay velocities, with a 3-4 fold increase of CMs (40-45% of the CM population) residing in the 90th percentile. (Figure 21C and D) Thus, culture duration alone augmented Ca^{2+} transient kinetics.

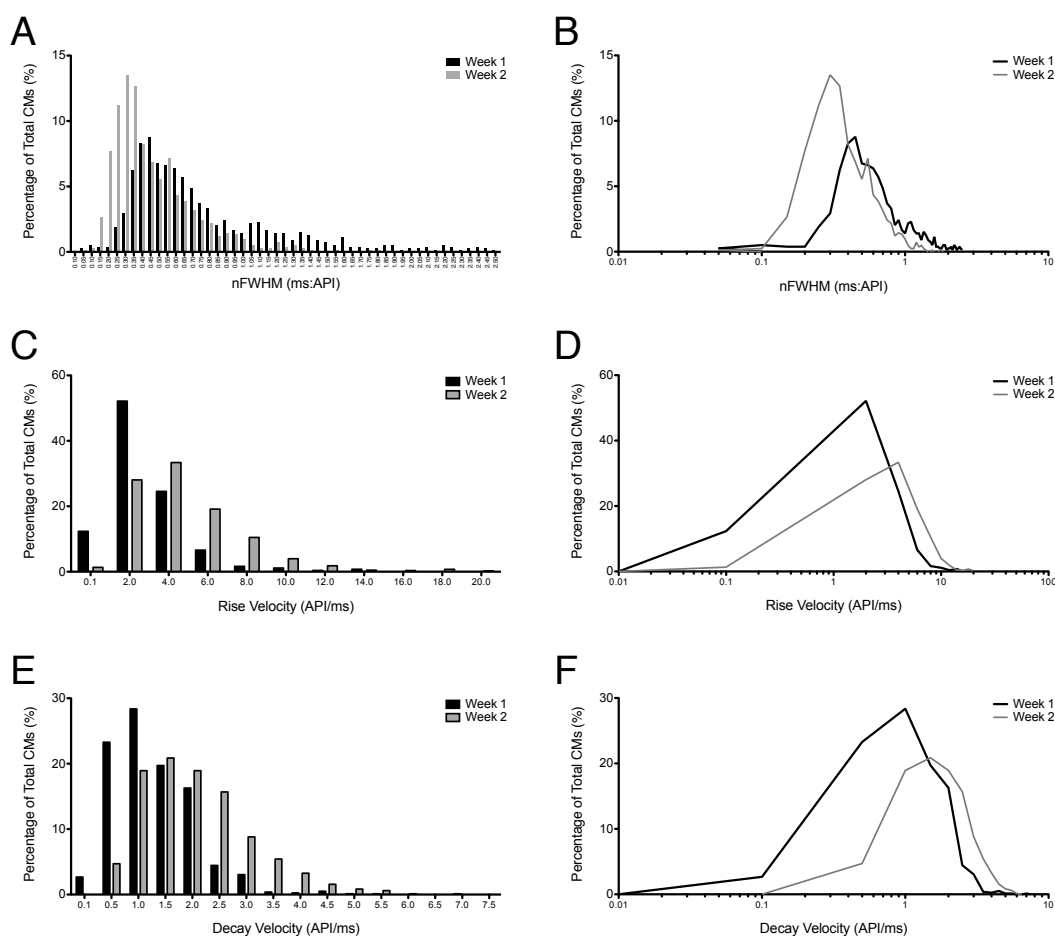


Figure 20 Frequency distributions of Ca^{2+} kinetic parameters, (A) nFWHM, (B) rise velocity, and (C) decay velocity, and lognormal transformation of each parameter, respectively (B), (D), and (F).

Table 3 Table of percentile gates based on Week 1 median values (50th percentile) for each Ca²⁺ kinetic parameter.

	5th	15th	30th	45th	60th	75th	90th	Median
Peak Value (API)	130.34	195.51	391.01	586.52	782.02	977.53	1173.04	651.69
Vrise (API/ms)	0.49	0.73	1.46	2.19	2.92	3.65	4.39	2.44
Vdecay (API/ms)	0.23	0.35	0.70	1.05	1.40	1.75	2.10	1.17
nFWHM (ms:API)	0.13	0.19	0.38	0.57	0.76	0.95	1.14	0.63

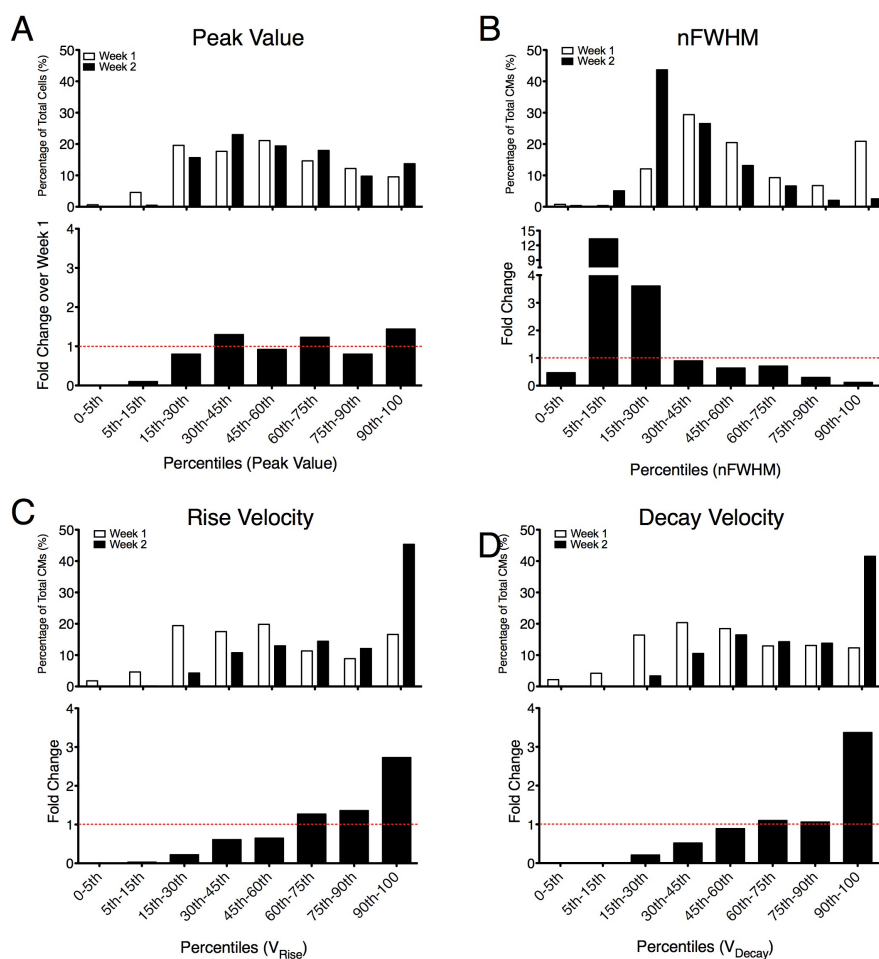


Figure 21 Time course characterization of Ca²⁺ kinetic parameters. Percentile distributions of kinetic parameters, (A) peak value (B) nFWHM (C) rise velocity, and (D) decay velocity, based on **Table 3** and corresponding fold changes of Week 2 cell percentages over Week 1 for each percentile.

3.4.2 Maturation of hiPSC-derived CMs correlates with lower nFWHM values

To determine whether the shifts in Ca^{2+} transient kinetic parameters actually translate to a more mature phenotype, CMs were also assayed for response to electrical stimulation. Mirroring the developmental increase in resting heart rate in the developing heart, hiPSC-derived CMs spontaneously contracted at 0.5Hz in the first week and at 1Hz by the second week of culture. (Figure 22A) Additionally, CMs demonstrated that they could respond to 2 and 3Hz electrical stimulations regimes. (Figure 23) However, the proportion of CMs that could respond to different pacing challenges varied, with a higher proportion of CMs able to respond at lower pacing frequencies. (Figure 22B) The varying ability of CMs to respond to electrical stimulation suggests that developmental heterogeneities exist in this large CM sample population.

Using KIC and Cyteseer analysis, we are able to directly correlate baseline Ca^{2+} kinetic parameters of an individual CM with its 3Hz pacing ability. 3Hz stimulation frequency was chosen as a metric of maturation as endogenous human heart rates are maximally limited around 3-4Hz. Here, we hypothesized that lower nFWHM values correlate with an increasing ability of these CMs to respond to 3Hz stimulation, and thus a more mature phenotype. A response was only counted if CMs could respond to all 12 stimulations. Single CMs were characterized using a percentile scale based on nFWHM values for all CMs ($n=830$). Briefly, the 50th percentile was assigned to the Week 2 median value for nFWHM and the other percentile gates were calculated accordingly. (Table 4) Once categorized, single CMs were evaluated for whether they could respond to 12 stimulations at 3Hz.

In one representative well (D05), 22.86% of a total 175 CMs responded to 3Hz pacing. (Figure 24A) Although comprising only 17% of the total CMs evaluated, 75% of CMs that could respond to 3Hz pacing exhibited nFWHM values below the 45th percentile suggesting that shorter nFWHM values translate to an increased ability to respond to 3Hz challenge. (Figure 24B) This idea was further substantiated in replicate wells where we also observed that the majority of CMs capable of 3Hz pacing exhibited nFWHM values less than the well median. Thus, shortened nFWHM values, which directly relate to faster rise velocities, decay velocities, or both, correlate with an increased ability of CMs to respond to challenging pacing regimes.

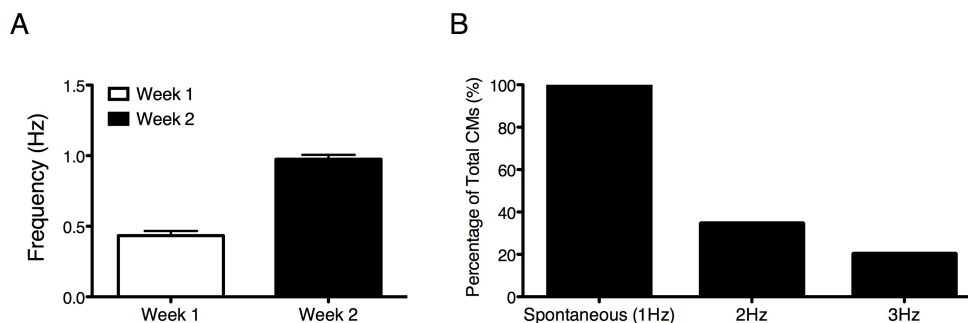


Figure 22. CMs were spontaneously contractile and could respond to electrical stimulation. (A) Spontaneous beating frequency at 1- and 2-week time points were about 0.5Hz and 1Hz, respectively. (B) Baseline CMs could respond to 2 and 3Hz electrical stimulation regimes after 2 weeks in culture (D50 of differentiation).

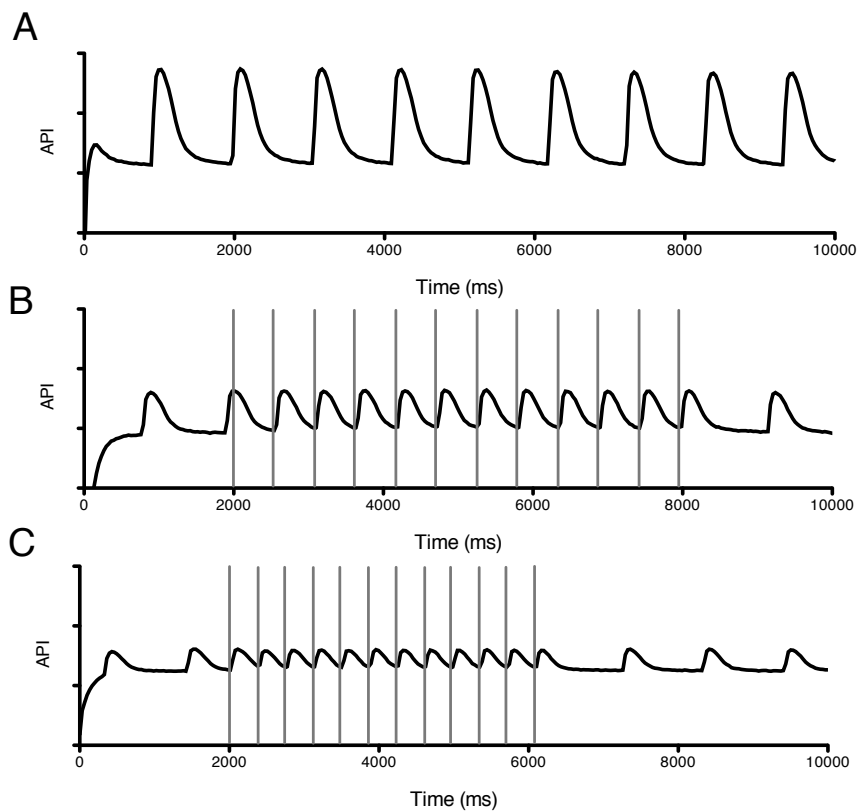


Figure 23 Pacing ability of 2-week (D50 of differentiation) hiPSC-derived CMs. (A) Spontaneous, (B) 2Hz, 12 stimulations, and (C) 3Hz, 12 stimulations.

Table 4 Table of percentile gates based on Week 2 median values (50th percentile) for each Ca²⁺ kinetic parameter.

	5th	15th	30th	45th	60th	75th	90th	Median
Peak Value (API)	136.02	204.03	408.05	612.08	816.10	1020.13	1224.15	680.08
Vrise (API/ms)	0.82	1.23	2.47	3.70	4.93	6.17	7.40	4.11
Vdecay (API/ms)	0.38	0.57	1.14	1.70	2.27	2.84	3.41	1.89
nFWHM (ms:API)	0.08	0.12	0.23	0.35	0.46	0.58	0.69	0.39

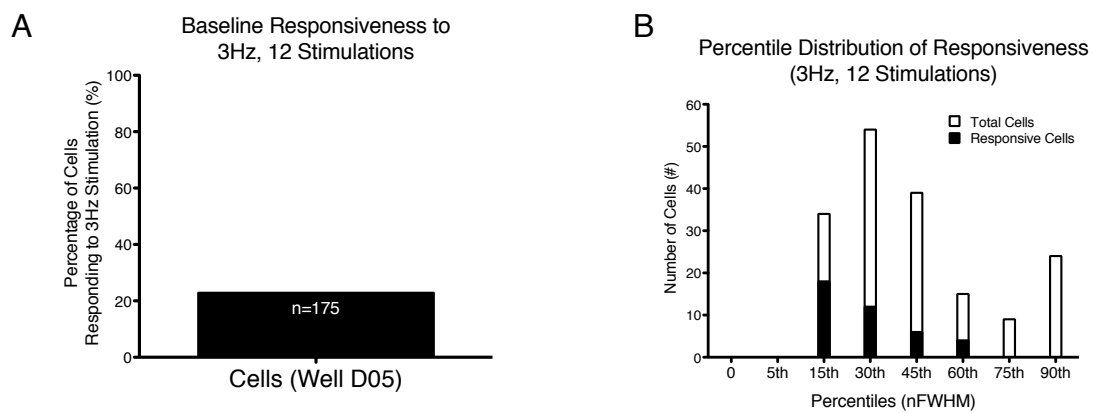


Figure 24 Correlation of 3Hz pacing responsiveness with nFWHM values suggest response to pacing signifies increased maturity can be reflected by lower nFWHM values. Data is from one representative control well (Well D05).

3.4.3 Treatment with HUVEC conditioned media enhances pacing ability of hiPSC-derived CMs.

Our main hypothesis for this study was that conditioned media from endothelial sources enhance the functional maturation of hiPSC-derived CMs. To this end, we evaluated 3Hz pacing ability of CMs treated with HUVEC, HMEC, and hESC-derived fibroblast conditioned media compared to untreated controls after 2 weeks of culture. In all subsets, a proportion of CMs could respond to all 12 stimulations. (Figure 25B-E) Specifically, 34.84% of HUVEC conditioned media treated CMs demonstrated 3Hz pacing ability as compared to 5.11%, 4.57%, and 20.14% in HMEC conditioned media, hESC-derived fibroblast conditioned media, and untreated subsets. (Figure 25A) Based on pacing ability alone, HUVEC conditioned media enhanced the functionality of hiPSC-derived CMs. This effect appeared to be HUVEC-specific as 3Hz pacing ability in CMs treated with HMEC and hESC-derived fibroblast conditioned medias was lower even than untreated controls.

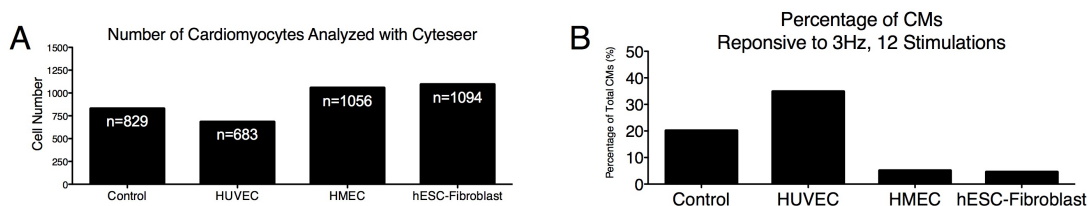


Figure 25 3Hz pacing ability of hiPSC-derived CMs was evaluated in all CMs from each subset (A). (B) A proportion of CMs from each experimental sample could respond to all 12 stimulations at 3Hz. Total CM number is listed above each bar.

3.4.4 Treatment with HUVEC conditioned media enhances Ca²⁺

transient kinetic parameters towards a more mature phenotype.

Similar to control CMs (Section 3.4.1), we observed that CMs exhibiting shorter transient durations indeed demonstrated a heightened ability to respond to 3Hz pacing in representative wells for all experimental subsets. (Figure 26) Of all the subsets, HUVEC conditioned media treated CMs were most apt to respond to 3Hz pacing. Particularly, in one representative well, 87% of HUVEC conditioned media treated CMs exhibited nFWHM values below the 45th percentile based on control nFWHM values and 74% of these CMs were able to respond to 3Hz electrical stimulation. Thus, we next characterized the kinetic parameters of all conditioned media-treated CMs versus controls at week 2.

As a population, CMs treated with HUVEC paracrine factors exhibited significantly faster rise velocities, decay velocities, and shortened nFWHM values than control CMs at the week 2 time point. Figure 25A describes the number of CMs evaluated in this study for each experimental subset. As with control CMs (Section 3.4.1), frequency distributions of each parameter were generated for conditioned media treated CMs. Mean values for each parameter are represented in Figure 27 with SEM and significance for the CM populations analyzed. Frequency distributions for individual CMs are shown in Figure 28 (A, C, E) for each parameter. With each experimental subset, populations exhibited broad distributions underscoring the heterogeneities of these cultures. Yet, despite some overlap between experimental subsets, population shifts towards significantly faster transient dynamics than all other subsets were evident with HUVEC conditioned media treatment.

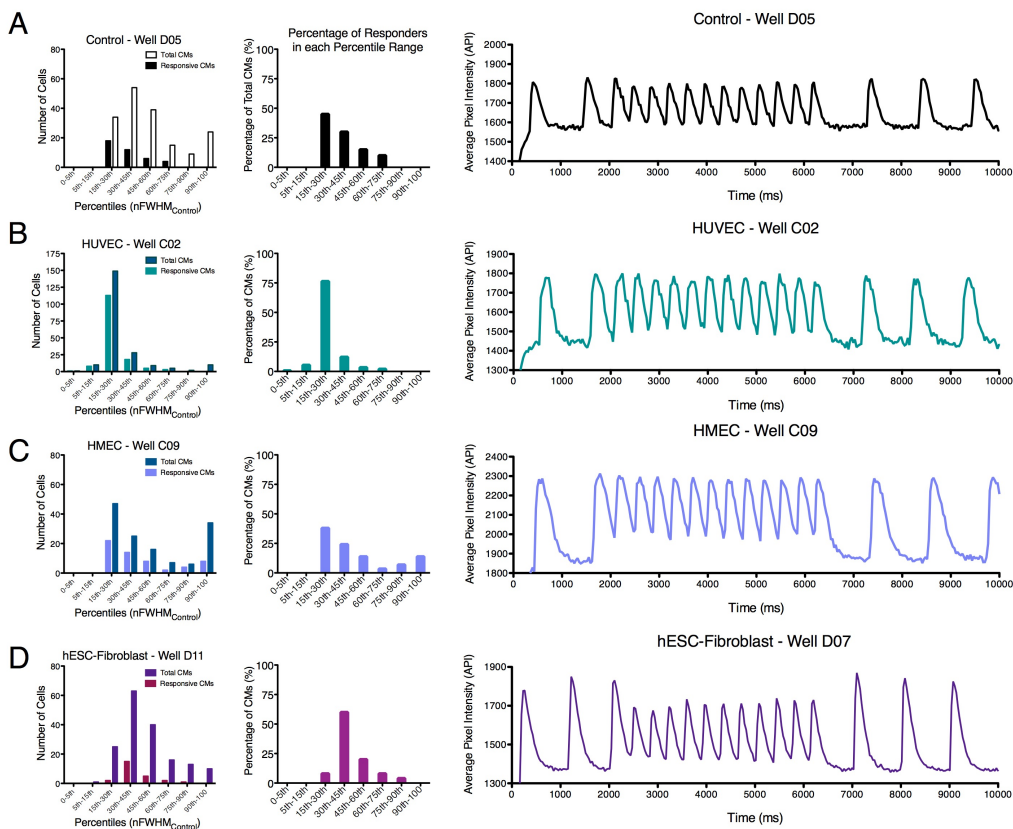


Figure 26 Correlation of CM responsiveness to 3Hz pacing and nFWHM values for each experimental subset: (A) untreated, (B) HUVEC, (C) HMEC, and (D) hESC-derived fibroblast conditioned media treated hiPSC-derived CMs after 2 weeks of culture. The first column represents the cell number of responders versus total CM number in each percentile. The second column shows the percentage of responding CMs from the total number of CMs in each percentile range. The third column gives representative traces from each well.

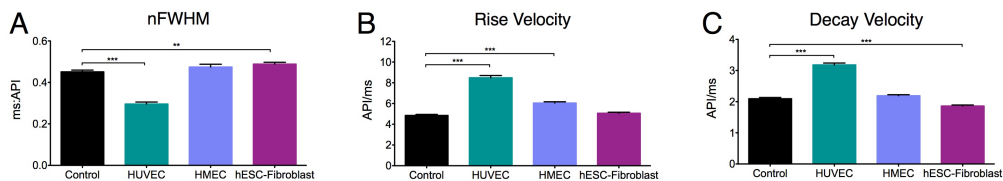


Figure 27 Mean values of Ca kinetic parameters over all CMs assayed. (SEM, ** $p < 0.01$, *** $p < 0.0001$)

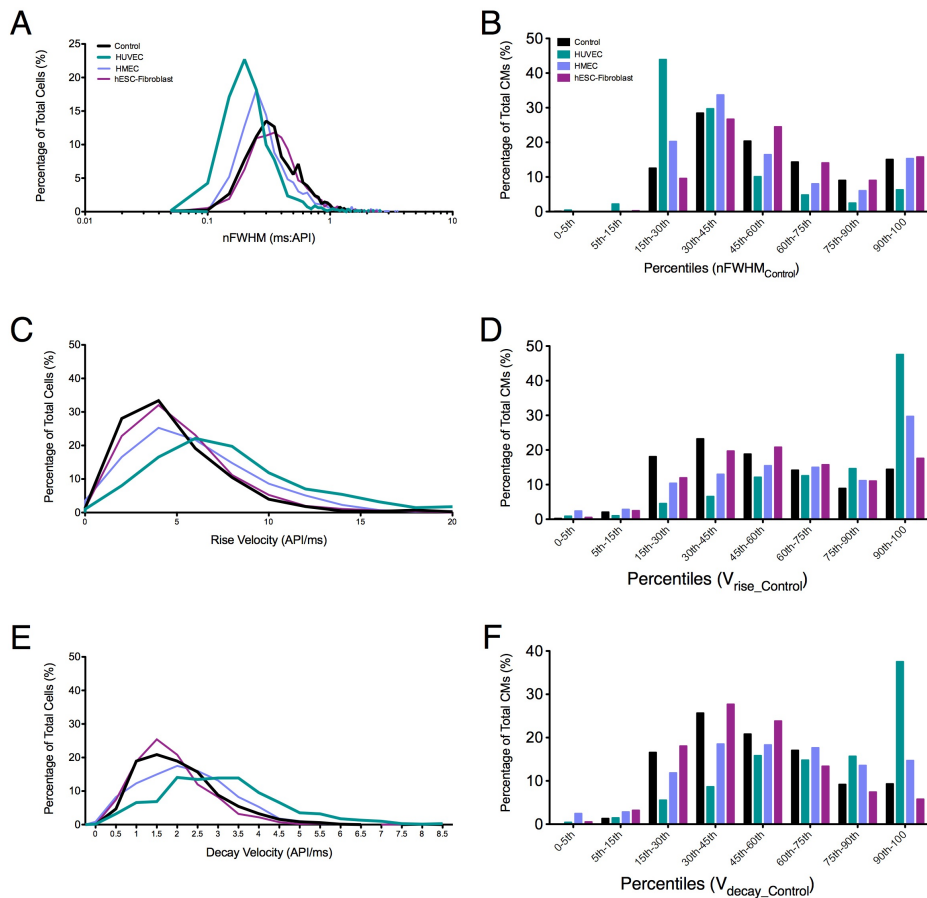


Figure 28 Evaluation of Ca^{2+} transient kinetics, nFWHM (A, B), rise velocity (C, D), and decay velocity (E, F) for conditioned media treated CMs versus untreated CMs. Both frequency distributions (A, C, E) and percentile-based (B, D, F) evaluations are represented to quantify differences between conditioned media treated and untreated samples.

To quantify the differences between conditioned media treated CMs versus untreated controls, percentile evaluation based on control parameter values was performed. (Figure 28B, D, F) For each kinetic parameter, 53% and 62% of HUVEC conditioned media treated CMs exhibited decay and rise velocities, respectively, greater than the control 75th percentile, and 47% of CMs demonstrated nFWHM values less than the control 30th percentile compared to controls. (Figure 28B) Comparatively, 26% and 42% of HMEC conditioned media treated CMs exhibited decay and rise velocities, respectively, greater than the control 75th percentile, and 20% of CMs exhibited nFWHM values less than the control 30th percentile. (Figure 28C) Finally, CMs treated with hESC-derived fibroblast conditioned media demonstrated insignificant difference from control percentile distributions, reinforcing the idea of endothelial-specific factor modulation of Ca²⁺ transient kinetics. In particular, -5.3% and 5.3% of hESC-derived fibroblast conditioned media treated CMs exhibited decay and rise velocities, respectively, greater than the control 75th percentile, and -2.8% of CMs exhibited nFWHM values less than the control 30th percentile. (Figure 28D)

3.4.5 Inhibition of the L-type Ca²⁺ channel eradicates contractile activity of hiPSC-derived CMs

To understand the underlying mechanisms governing the increases in Ca²⁺ transient kinetics, we evaluated the functionality of the major contributors to proper cardiac Ca²⁺ cycling. One such player is the transsarcolemmal L-type Ca²⁺ channel that is responsible for Ca²⁺ influx into CMs. Diltiazem treatment of CMs eradicated spontaneous Ca²⁺ transients, and accordingly contractile activity, in control and conditioned media treated hiPSC-derived CMs. (Figure 29A) The cessation of beating

due to the blockade of L-type Ca^{2+} channels could not be rescued by electrical stimulation suggesting the functionality and dependency of the Ca^{2+} transient on these channels in all experimental subsets. (Figure 29B) Expression of $\text{Ca}_v1.2$, a subunit of the L-type Ca^{2+} channel, was also confirmed in all cases with qPCR. (Figure 30)

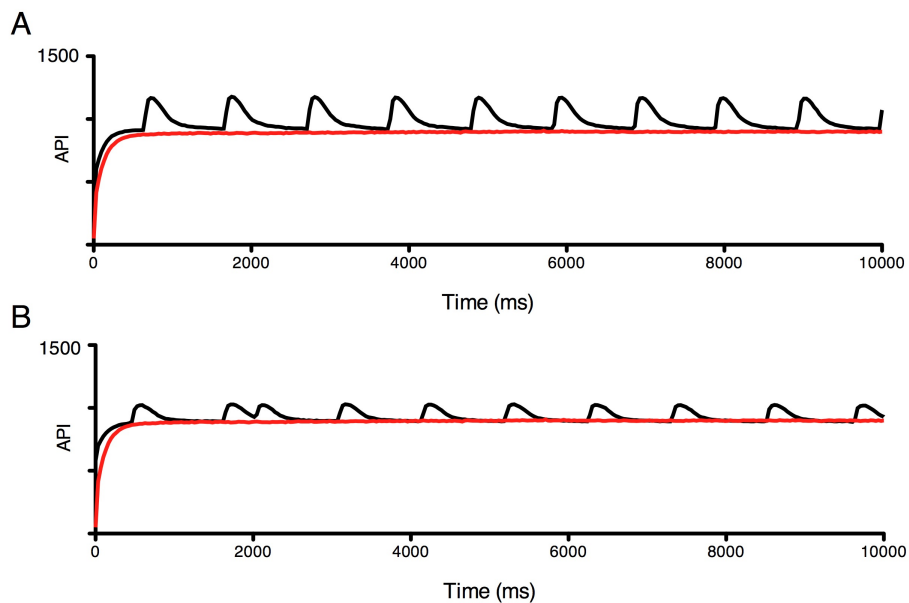


Figure 29 Representative Ca^{2+} transient tracings of diltiazem (DTZ)-treated (red) and untreated (black) hiPSC-derived CMs. DTZ inhibition of L-type Ca^{2+} channels eradicates Ca^{2+} flux and contractile activity for all conditions. (A) Stimulated (B) 1Hz, 6 stimulations.

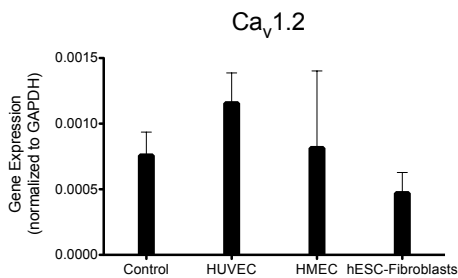


Figure 30 Expression levels of $\text{Cav}1.2$ expression normalized to GAPDH for each experimental subset after 2 weeks of culture.

3.4.6 Treatment with HUVEC conditioned media enhances $\text{Na}_v1.5$ function in hiPSC-derived CMs

To probe another potential contributor to the rise dynamics of the Ca^{2+} transient, CMs were treated with tetrodotoxin (TTX), a specific inhibitor of $\text{Na}_v1.5$ channels. With maturity, a mechanistic dependence on Na^+ -mediated, through $\text{Na}_v1.5$ channels, versus Ca^{2+} -mediated AP depolarization occurs. The concentration of TTX ($1\ \mu\text{M}$) used in this study was around the half-maximal inhibitory concentration (IC_{50}) for mature CMs. Thus, if functional $\text{Na}_v1.5$ channels were present in these developing CMs, depression of spontaneous beating frequency and rise velocity was expected. In all experimental subsets, a depression of spontaneous beating frequency was demonstrated by hiPSC-derived CMs after two weeks of culture. (Figure 32) Representative transients are also shown in Figure 31 to further illustrate the functional inhibition of $\text{Na}_v1.5$ channels. It is important to note that at earlier time points (Week 1) we did not detect changes in beating frequency or channel expression.

Although depression of beating frequency is one consequence of TTX sensitivity, this phenomenon was observed in all experimental subsets. Thus, to elucidate potential differences between subsets, we also characterized CM populations for changes in rise velocity with TTX treatment. Specifically, we expect that expression of functional $\text{Na}_v1.5$ channels would translate to a depression of rise velocity with TTX exposure.

To compare TTX-treated and untreated samples, we sorted individual rise velocity values based on the median rise velocity value of untreated control CMs. (Table 4) Again, this median value was set as the 50th percentile which was used to calculate the subsequent percentile gates used for population characterization. Figure 33 shows

the percentile distributions of each experimental subset treated with TTX versus CMs from the same subset that were not treated with TTX. A shift in the percentage of CMs towards lower percentile gates would illustrate a depression of rise velocity. From these graphs, CMs exposed to HUVEC conditioned media show the greatest shift towards slower rise velocities when treated with TTX.

To quantify these population shifts, we compared the difference in CM populations that exhibited rise velocities below the 45th percentile. (Figure 34) HUVEC conditioned media treated CMs displayed a dramatic increase from 13.2% to 92.9% (7-fold increase) of CMs exhibiting rise velocities below the 45th percentile. Therefore, effectively 79.7% of CMs treated with HUVEC conditioned media express functional Na_v1.5 channels. Control CMs treated with TTX only demonstrated a 1.1 fold increase in the percentage of CMs with rise velocities below the 45th percentile. HMEC and hESC-fibroblast conditioned media treated CMs display a 2.4 and 1.4 fold increase in CMs, respectively, below the 45th percentile. (Figure 34B)

To account for this boost in functionality, qPCR evaluation also demonstrated an increase in Na_v1.5 channel expression, albeit not achieving significance, in HUVEC conditioned media treated CMs versus controls after 2 weeks which was not seen with HMEC, hESC-derived fibroblast conditioned media treated CMs, or for any of the experimental subsets at week 1. (Figure 35) Immunostaining also confirmed expression of the fast sodium channel in CMs from all experimental subsets. (Figure 36) However, Na_v1.5 seems to be co-expressed in CMs and other cell types (mCherry-negative) as well. From fluorescence intensity alone, it seems that Na_v1.5 is more expressed in conditioned media treated conditions than the control subset. However, between the

different conditioned media subsets, significant differences in signal intensity could not be resolved.

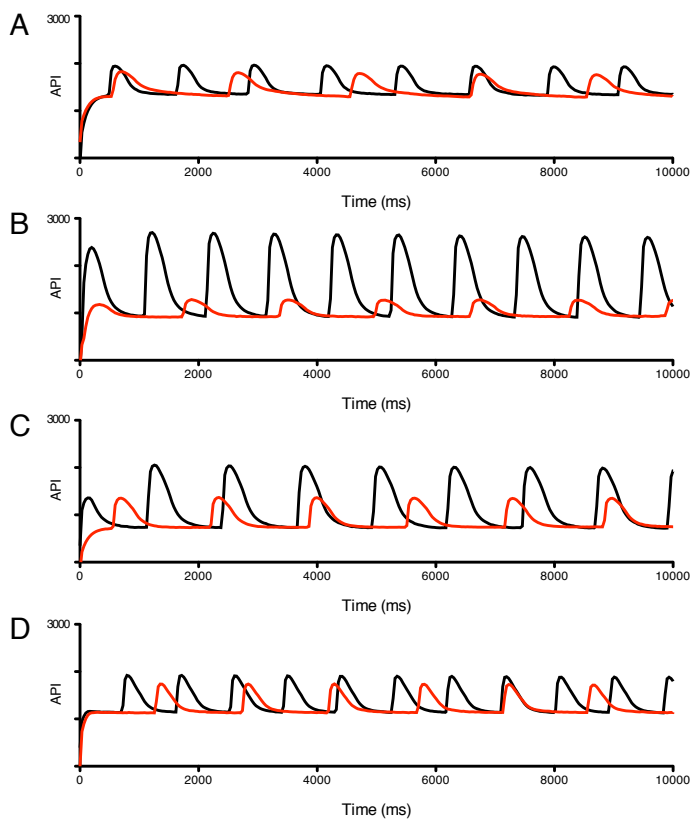


Figure 31 Representative Ca²⁺ transient traces from individual wells treated with TTX (red) versus untreated CMs (black) for (A) control CMs, (B) HUVEC, (C) HMEC, and (D) hESC-derived fibroblast conditioned media treated CMs after 2 weeks.

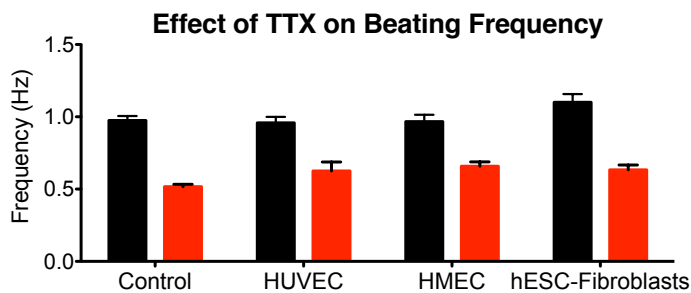


Figure 32 Effect of TTX treatment on beating frequency after 2 weeks in culture. Beating frequency is depressed with TTX treatment (red) versus untreated controls (black).

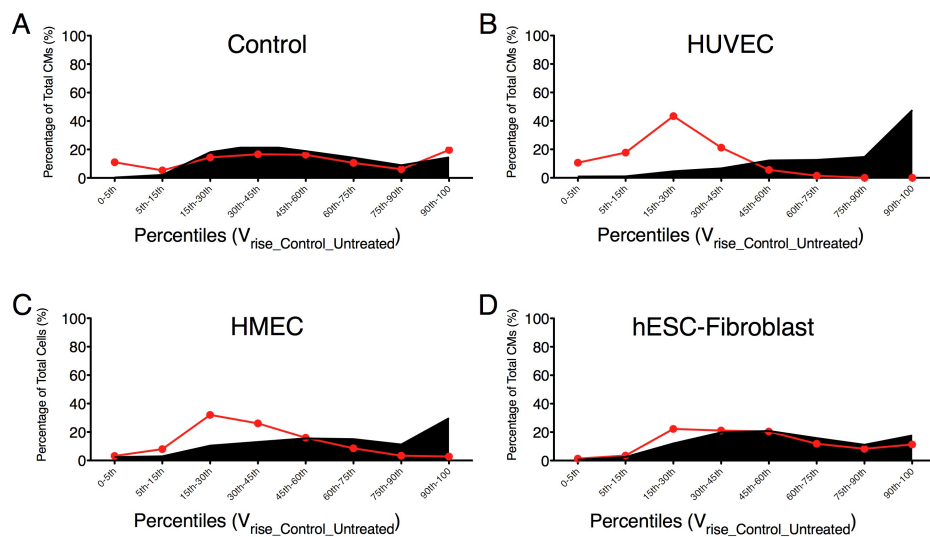


Figure 33 Percentile characterization of TTX treatment versus untreated CMs for each experimental subset, namely (A) control, (B) HUVEC, (C) HMEC, and (D) hESC-derived fibroblast conditioned media treated CMs. For each subset, overlays of percentile distributions for TTX-treated (red) and untreated (black) CMs are shown.

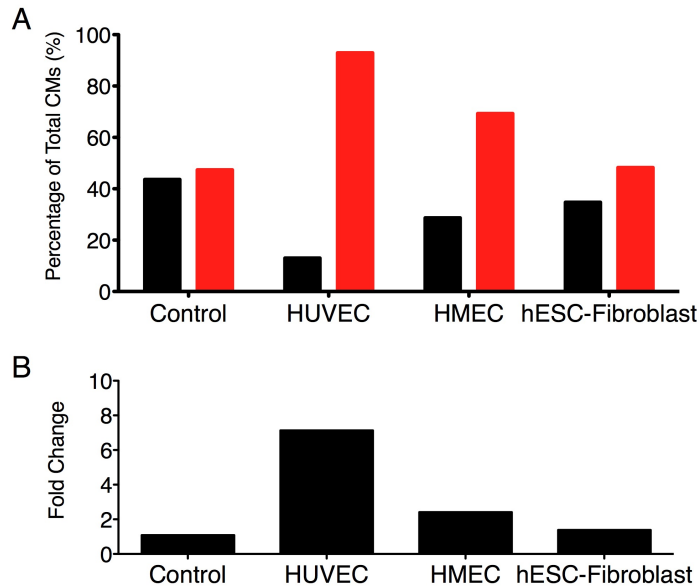


Figure 34 Characterization of CMs with rise velocities below the 45th percentile. (A) Percentage of CM population with rise velocities below the 45th percentile for untreated CMs (black) and TTX-treated (red) (B) Fold change of TTX-treated CMs with rise velocities below the 45th percentile over untreated CMs.

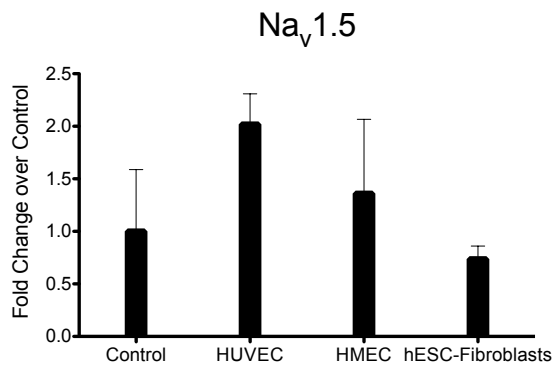


Figure 35 Fold change comparison of Nav1.5 channel expression between experimental subsets and control CMs.

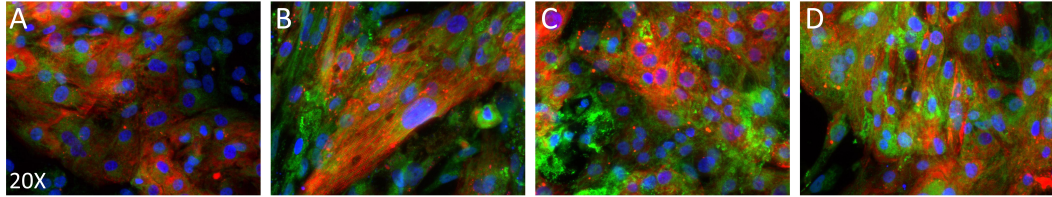


Figure 36 Immunostaining of Na_v1.5 (green) in each experimental subset (A) Control (B) HUVEC conditioned media (C) HMEC conditioned media (D) hESC-derived fibroblast conditioned media. CMs are mCherry-positive (red) and nuclei are stained with DAPI (blue), 20X.

3.4.7 Exposure to endothelial paracrine factors increases

functionality of SERCA2 in a larger proportion of CMs

The development of intracellular Ca²⁺ stores is another major hallmark of maturation and essential for proper Ca²⁺ handling in the developed CM. In particular, SERCA2 is responsible for Ca²⁺ reuptake during the relaxation phase of the Ca²⁺ cycle. For this study, we postulated that differences in SERCA2 function of HUVEC conditioned media treated hiPSC-derived CMs contributed to the increases in decay velocity observed.

To evaluate the functionality of SERCA2, we treated CMs with thapsigargin (TSG, 1 μM), an inhibitor of SR Ca²⁺-ATPase activity, and evaluated changes in Ca²⁺ transient kinetic parameters. If SERCA2 were functional, TSG treatment of CMs would depress beating frequency and decay velocity compared to 0.01% DMSO-treated CMs. TSG treatment caused a decrease in beating frequency in both control and conditioned media treated CMs suggesting that SERCA2 was functional in hiPSC-derived CMs. (Figure 38 and Figure 37)

Frequency distributions of CMs for decay velocity were created based on percentile gates derived from median decay velocity of DMSO-treated control samples. (Table 5) With TSG treatment, the frequency distributions for decay velocities

demonstrated population shifts towards slower values in all cases. (Figure 39)

Specifically, the percentage of CMs with decay velocities lower than the 45th percentile increased for every subset. (Figure 40) Interestingly, for HUVEC and HMEC conditioned media treated CMs, 4.8- and 6.9-fold respective increases occurred with TSG treatment compared to DMSO-treated CMs. Smaller increases were observed with control (2.0-fold) and hESC-derived fibroblast conditioned media treated (1.6-fold) subsets. Thus, exposure to endothelial-specific paracrine factors significantly increased the functionality of SERCA2 in developing hiPSC-derived CMs. However, it is important to note that a larger proportion of HMEC conditioned media treated CMs were sensitive to TSG treatment. Thus, it seems the contribution of SERCA2 alone may be insufficient to explain the increased ability of HUVEC conditioned media treated CMs to respond to 3Hz pacing or faster decay velocity than the other experimental counterparts.

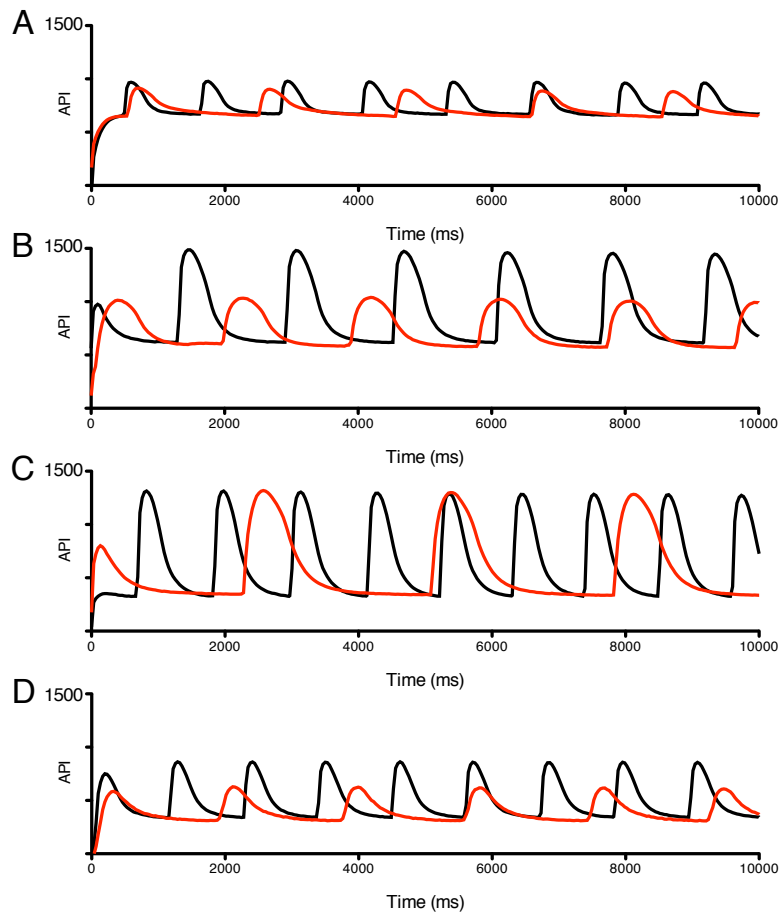


Figure 37 Representative Ca^{2+} transient traces from individual wells treated with TSG (red) versus DMSO-treated CMs (black) for (A) control CMs, (B) HUVEC, (C) HMEC, and (D) hESC-derived fibroblast conditioned media treated CMs after 2 weeks.

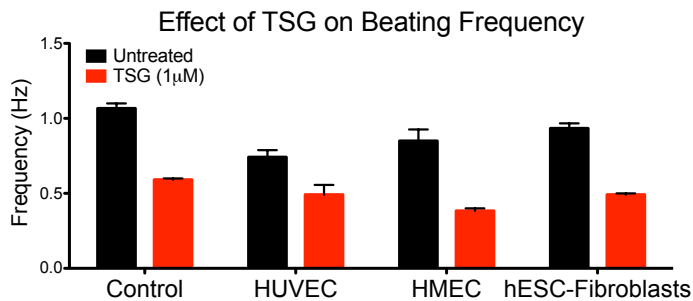


Figure 38 Effect of thapsigargin (TSG, 1 μM) on beating frequency of hiPSC-derived CMs in all experimental subsets at 2 weeks. (SEM) Beating frequency is depressed in TSG-treated (red) samples compared to untreated controls (black) in all cases.

Table 5 Table of percentile gates for decay velocity (V_{decay}) based on Week 2 median values (50th percentile) for DMSO-treated control CMs.

	5th	15th	30th	45th	60th	75th	90th	Median
Vdecay (API/ms)	0.15	0.23	0.46	0.69	0.92	1.15	1.38	0.77

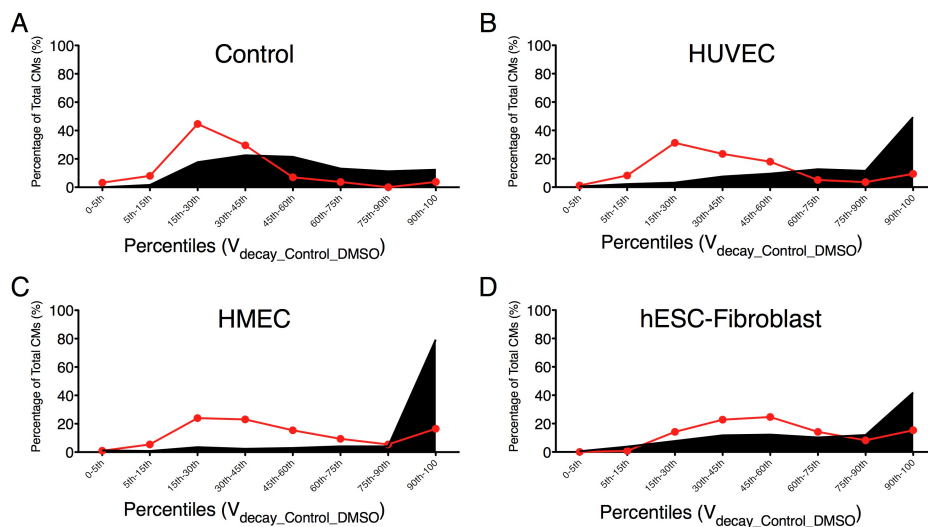


Figure 39 Percentile characterization of TSG-treated versus DMSO-treated CMs for each experimental subset, namely (A) control, (B) HUVEC, (C) HMEC, and (D) hESC-derived fibroblast conditioned media treated CMs. For each subset, overlays of percentile distributions for TSG-treated (red) and untreated (black) CMs are shown.

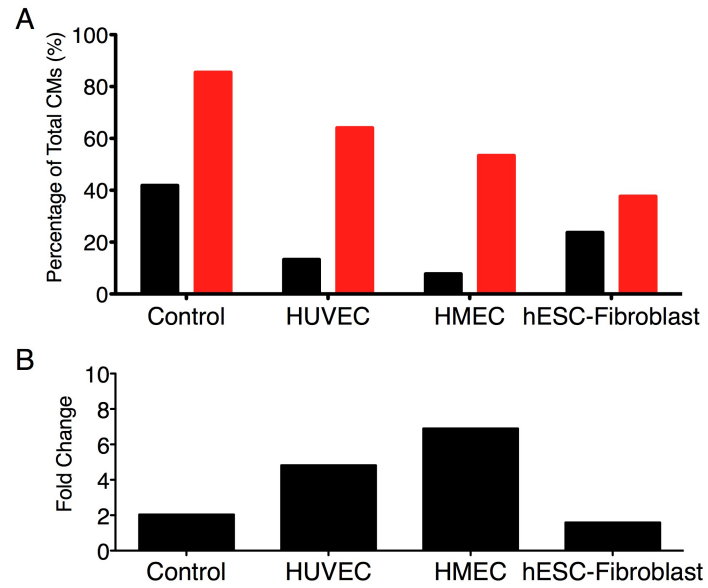


Figure 40 Characterization of CMs with decay velocities below the 45th percentile. (A) Percentage of CM population with decay velocities below the 45th percentile for untreated CMs (black) and TSG-treated (red) (B) Fold change of TSG-treated CMs with decay velocities below the 45th percentile over untreated CMs.

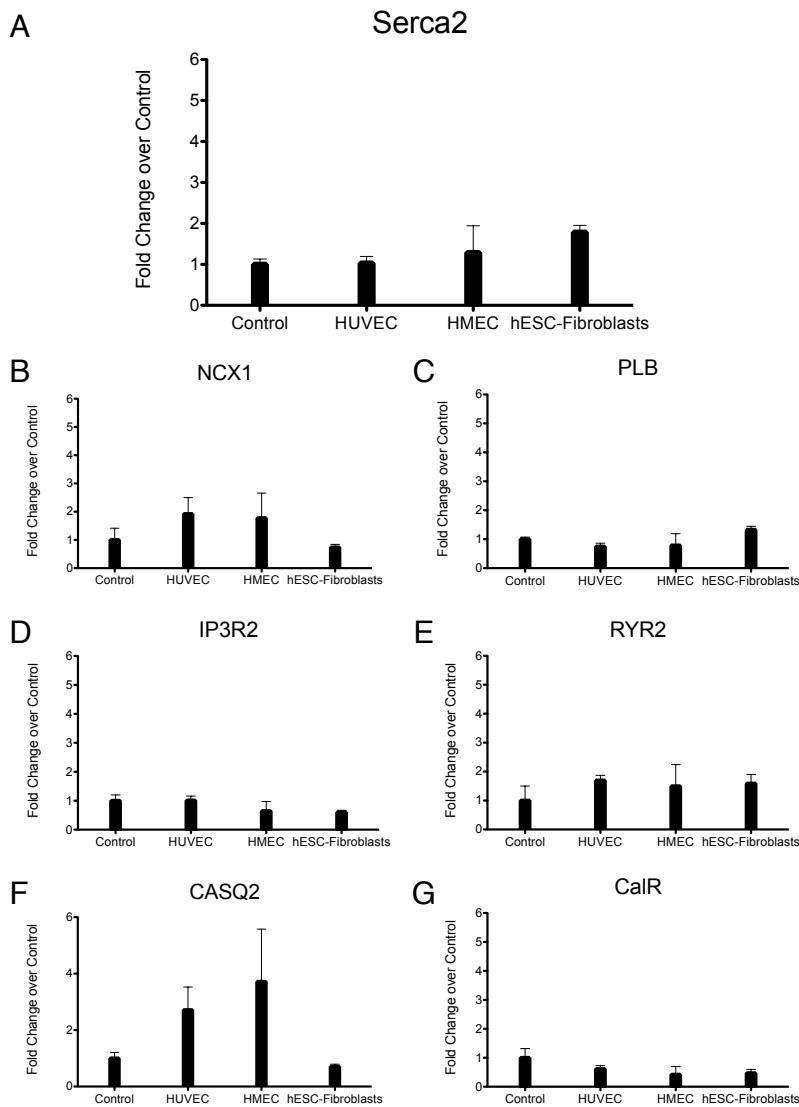


Figure 41 Fold change of Ca^{2+} -handling protein expression of conditioned media treated CMs over controls for SERCA2 (A), NCX1(B), PLB(C), IP3R2(D), RYR2(E), CASQ2(F), and CalR(G).

qPCR evaluation of SERCA2 expression reveals minimal differences in expression between control and conditioned media treated CMs. Surprisingly, SERCA2 expression is almost 2-fold higher in hESC-derived fibroblast conditioned media treated CMs despite decreased sensitivity to TSG treatment. (Figure 41A) Hence, functionality of SERCA2 does not seem to be linked to expression levels of the protein.

Because Ca^{2+} extrusion and SERCA2 function is enhanced by a variety of other Ca^{2+} -handling proteins, we also probed the expression levels of the sodium-calcium exchanger (NCX1), phospholamban (PLB), inositol 1,4,5-triphosphate (IP3R2), ryanodine receptor (RYR2), calsequestrin (CASQ2), and calreticulin (CalR). (Figure 41B-G) Upregulation of NCX1 (~2-fold), RYR2 (~1.5 to 1.7-fold), and CASQ2 (3.0 to 4.0-fold) are observed respectively in HUVEC and HMEC conditioned media treated CMs over controls though not reaching significance.

3.5 Discussion

The primary intention of this study was to elucidate potential factors that influence CM maturation for the purpose of improving current cell-based approaches to cardiac repair. Thus far, many groups have shown that hPSC-derived CMs resemble at most 100 day-old fetal CMs both electrophysiologically and in gene expression. [91, 95, 105, 115] This immaturity is one potential factor that has been hypothesized to contribute to the incapacity of hPSC-derived CMs to rescue myocardial loss after infarct is their immaturity. [23] However, it remains unclear what cues are necessary for functional maturation. We hypothesize that paracrine factors secreted from endothelial factors modulate aspects of this process. Here, we describe a novel finding that paracrine factors specifically released from HUVECs enhances the functionality of hiPSC-derived CMs towards a more mature phenotype.

3.5.1 High-throughput analysis of cardiac Ca²⁺-handling parameters enables large-scale evaluation of heterogeneous hiPSC-derived CM populations

The heterogeneous nature of CMs derived from hPSC sources has been cited extensively. [90, 91, 95, 108, 115] On the one hand, the ability of hPSCs to differentiate into a variety of CM types is advantageous as the potential to address regeneration of different cardiac constituents is possible. However, as methods to control cardiac subtype differentiation have not yet been uncovered, the ability to thoroughly characterize heterogeneous populations of hPSC-derived CMs has proven to be a major technical limitation. [91, 105, 115] In many cases, developmental conclusions are drawn from physiological evaluation of less than 5% of CMs generated. As the heterogeneities of these CM populations are poorly defined, low sampling threatens the validity of study conclusions.

In this study, we employed a high-throughput method that enables analysis of two orders of magnitude more cells without compromising single CM evaluation. Using traditional Ca²⁺ fluorescent indicators, such as Fluo4, the KIC instrument automates imaging and electrical stimulation of CMs plated in 96- and 384-well formats. From evaluation of baseline CMs at both 1- and 2-week time points, we monitored changes in transient kinetic parameters and response to electrical pacing. With Cyteseer software, we were then able to create comprehensive histograms for each functional parameter and chart changes in populations of 800-1000 CMs for each condition. Thus, for the first time, we were able to describe the physiology of a vast number of CMs.

The first goal of this study was to establish robust methods to describe the various maturation metrics of interest. A signature component of CM physiology is the ability to constantly cycle Ca^{2+} . [6] Without the ability to properly cycle Ca^{2+} , the functional relevance of hPSC-derived CMs is jeopardized as proper Ca^{2+} handling allows the heart to rhythmically contract. Accordingly, we evaluated the Ca^{2+} transient kinetics of baseline, αMHC -positive hiPSC-derived CMs. Spontaneously beating hiPSC-derived CMs generated rhythmic and synchronous Ca^{2+} transients at both 1- and 2-week time points. Using Cyteseer, we were able to extract various kinetic parameters, namely peak value, rise velocity (V_{rise}), decay velocity (V_{decay}), and transient duration (nFWHM). To describe differences between transient parameters at different time points, we created histograms of each parameter and evaluated frequency distributions based on percentiles established from the reference control. For this first study, percentiles were calculated from parameter values of baseline CMs at week 1. Using this percentile method for describing Ca^{2+} transient kinetics, we are able to assess both quantitatively and qualitatively how Ca^{2+} transient parameters change with respect to, in this case, time in culture. Overall, hiPSC-derived CMs exhibited faster transient kinetics by two weeks in culture. As cited by other groups as well, these increases in transient kinetics demonstrated that culture duration alone enhances functional maturation of hPSC-derived CMs and most likely reflects changes in the underlying Ca^{2+} -handling machinery. [158, 199, 200]

3.5.2 Maturation of hiPSC-derived CMs correlates with lower nFWHM values

The next goal of this study was to correlate changes in transient kinetics with specific features of CM physiology that suggest a more mature phenotype. In establishing our maturation metrics, we used the following criteria to determine the physiological read-outs used in this study: 1) functional relevance to the application of cell-based repair, 2) developmentally modulated, and 3) technical feasibility.

One such hallmark of maturation is the ability of CMs to respond to electrical stimulation at various rates, which reflects the ability of the heart to adapt to different output demands. In the mature myocardium, the resting heart rate is around 1Hz and can peak between 3-4Hz during exercise or challenge. Fetal and postnatal CMs exhibit a much faster resting heart rate, peaking at about 2.5 Hz in the human 2-month newborn and steadily declining to adult resting heart rates through childhood. [110, 159] Specifically, we postulated that faster Ca^{2+} transient kinetics translated to increased functional maturity as assayed by response to heightened pacing frequencies.

Hence, we chose to evaluate whether hiPSC-derived CMs could respond to 3Hz pacing. We reasoned that this stimulation frequency grazed the higher limits of contraction for both fetal and adult CMs. In addition, early stage (< D42 of differentiation or 1-week post plating) hiPSC-derived CMs cannot respond to stimulation frequencies greater than 1Hz. Therefore, 3Hz pacing could provide an effective reflection of the developmental competency of CM Ca^{2+} -handling machinery. [91, 108, 155] The power of this evaluation was increased by our ability to evaluate the same CMs at spontaneous and heightened beating frequencies. Thus, a correlation between baseline transient

kinetics and each CM's ability to respond to 3Hz stimulus could be made at the single CM level. To this end, we determined that CMs exhibiting shorter nFWHM values at resting contractile frequency were more capable of responding to 3Hz stimulation protocols when paced.

3.5.3 Treatment with HUVEC conditioned media enhances Ca^{2+} transient kinetic parameters towards a more mature phenotype.

The next goal of this study was to evaluate the overarching hypothesis that paracrine endothelial influences can enhance the functional maturation of developing hiPSC-derived CMs. Once we established the correlation between spontaneous kinetic parameters and the ability to respond to 3Hz pacing, we applied the same characterization to EC conditioned media treated hiPSC-derived CMs versus untreated and non-endothelial controls. Treatment of hiPSC-derived CMs with HUVEC conditioned media considerably enhanced the ability of CMs to respond to 3Hz pacing. This enhanced functionality was paired with overall faster Ca^{2+} transient kinetics, including shortened nFWHM values and increased rise and decay velocities. A correlation between CMs exhibiting shorter nFWHM values in each experimental subset with ability to respond to 3Hz stimulation was also established. As both response to pacing and transient kinetics reflect the functionality of the underlying Ca^{2+} -handling machinery [6, 91, 105, 115, 150, 199], we transitively postulated that CMs treated with HUVEC conditioned media would exhibit more mature expression profiles of Ca^{2+} -handling proteins as well as functionality of key modulators of the Ca^{2+} cycle. Specifically, we evaluated the effects of L-type Ca^{2+} channel, $\text{Na}_v1.5$, and SERCA2 inhibition on Ca^{2+} transient dynamic parameters.

3.5.4 Inhibition of the L-type Ca²⁺ channel eradicates contractile activity of hiPSC-derived CMs in all experimental subsets

In this study, we demonstrated that endothelial conditioned media, particularly from HUVECs, enhanced Ca²⁺ transient rise velocity. From this observation, we postulated that increased functionality of ion channels or other Ca²⁺-handling proteins that govern either Ca²⁺ influx or AP depolarization were responsible. Four potential mechanisms are most likely at play, 1) increased L-type Ca²⁺ current, 2) increased Na_v1.5 functionality, 3) dependence of the Ca²⁺ transient on intracellular Ca²⁺ stores, and/or 4) increased functionality of RYR2 for mediating Ca²⁺ release from the SR.

Here, we demonstrate diltiazem blockade of Ca²⁺ activity in all experimental subsets. Ca²⁺ influx initiates the first phase of the Ca²⁺ transient. In mature CMs, this initial influx of Ca²⁺ through L-type Ca²⁺ channels sparks the Ca²⁺-induced-Ca²⁺-release (CICR) from sarcoplasmic reticulum Ca²⁺ stores that generates enough Ca²⁺ to mediate cardiac contraction. [6] Early on in development, transsarcolemmal diffusion is the predominant source of Ca²⁺ for contraction as intracellular Ca²⁺ stores have been shown to be non-functional or underdeveloped. [91, 201, 202] With exposure of L-type Ca²⁺ channel blockers, it has been reported that spontaneous Ca²⁺ transients and contractile activity is abolished in hPSC-derived CMs. [91, 105] In this current study, we reaffirm these findings in all experimental subsets as diltiazem treatment eradicated Ca²⁺ or contractile activity in all subsets.

Upon electrical stimulation, rescue of the Ca²⁺ transient, albeit to a lesser degree, has been reported to occur in immature CMs after L-type Ca²⁺ channel blockade. [200, 203] Under these circumstances, NCX-1 has been shown as a secondary contributor to

Ca²⁺ influx. [200] In the current study, even with electrical stimulation, neither Ca²⁺ activity nor contraction was observed after diltiazem treatment. We conclude from this finding that compensatory mechanisms for voltage-mediated Ca²⁺ influx are not present in hiPSC-derived CMs and that an L-type Ca²⁺ current is responsible for transient activity in these cells.

Thus, a few mechanisms of action are potentially at play. First, L-type Ca²⁺ channels are the only mechanism of Ca²⁺ influx in these CMs so that once blocked, contractile activity could not be rescued. Second, due to non-functional SR Ca²⁺ stores and handling machinery, Ca²⁺ diffusion from NCX-1 is insufficient to either spark CICR or effectively generate transient activity. Third, in addition to the absence of functional SRs, NCX-1 is not present or non-functional. And, fourth, Na⁺ channels are inactive so that without L-type Ca²⁺ channel activity, APs are blocked as well.

In light of the inability to differentiate between experimental subsets from diltiazem blockade, we began to evaluate other potential contributors to increased rise dynamics in CMs. As mentioned, SR Ca²⁺ release is a significant contributor to the upstroke of the Ca²⁺ transient and is imperative for contraction. However, for this particular study, pharmacological evaluation of Ca²⁺ release from SR stores was not performed. Thus, using qPCR techniques, we probed the expression of both IP3R2 and RYR2, two regulators of Ca²⁺ release from the SR. (Figure 41 D, E)

In the mature myocardium, extracellular Ca²⁺ influx binds to RYR2 and stimulates Ca²⁺ release to induce contraction. IP3R2 has been shown to have a similar function but predominates in immature CMs before the SR fully matures. [175, 204] Sedan et al showed that IP3R2-mediated Ca²⁺ stores are operational in hESC-derived CMs and are responsive to endothelin-1 and angiotensin-II signaling which increase Ca²⁺ transient

kinetics and CM contraction. [205] We did detect IP3R2 expression in each experimental subset but without significant difference between populations. Moreover, an increase in IP3R2 expression occurs between 1- and 2-week time points.

RYR2 functionality in hPSC-derived CMs is disputed. Dolnikov et al demonstrated that hESC-derived CMs were insensitive to ryanodine and caffeine treatment, which suggests non-functional SR Ca^{2+} handling.[91] On the other hand, many groups have shown sensitivity of RYR2s to ryanodine inhibition and caffeine-mediated opening of the channel to demonstrate functionality of this receptor and maturity of intracellular Ca^{2+} stores in hESC-derived CMs. [105, 115, 150, 199] In this study, we detected RYR2 expression but with minimal difference in all experimental subsets. Pharmacological evaluation with agents such as ryanodine would have to be conducted to determine RYR2 functionality, as expression levels do not necessarily confer activity. [91] In the next sections, pharmacological evaluation of fast Na^+ channels and SR activity were performed to elucidate whether these elements of Ca^{2+} handling contributed to transient dynamic differences observed with HUVEC conditioned media treated CMs.

3.5.5 Treatment with HUVEC conditioned media enhances $\text{Na}_v1.5$ function in hiPSC-derived CMs

We have thus far demonstrated that L-type Ca^{2+} blockade eliminated contractile activity in all subsets and that differences in expression of $\text{Ca}_v1.2$ channel were insignificant. Thus, from diltiazem inhibition alone, we could not dissect the contribution of L-type Ca^{2+} -mediated influx to the differences observed in rise kinetics between experimental subsets. As $\text{Na}_v1.5$ channel functionality has been shown to increase in

hiPSC-derived CMs with maturation [206], extracellular influence [158], and culture duration [193], we tested the hypothesis that enhanced functionality of $\text{Na}_v1.5$ contributed to increased rise kinetics.

In this study, TTX was used to block $\text{Na}_v1.5$ in both control and conditioned media treated hiPSC-derived CMs. The fast Na^+ channel, $\text{Na}_v1.5$, mediates Na^+ influx that is not only responsible for rapid depolarization of the cardiac AP but activation of L-type Ca^{2+} channels in the mature CM. [6, 206] Contrastingly, immature CMs typically exhibit a Ca^{2+} -mediated action potential. [206] During cardiac development, increased $\text{Na}_v1.5$ expression and functionality occurs [207, 208], which paired with an absence of K^+ current has been implicated as a contributing factor to the automaticity of immature CMs. [193]

Because $\text{Na}_v1.5$ directly regulates voltage flux, TTX sensitivity was tested on spontaneous contractile activity. We observed that, first, TTX treatment depressed spontaneous beat frequency with minimal difference between experimental subsets. Accordingly, we characterized each experimental subset at a single CM level (n=683-1094) for changes in rise velocity. Through this analysis, we discovered that TTX treatment of HUVEC conditioned media subsets correlated with 1) significant median rise velocity depression (Figure 33 and Figure 34) and 2) this effect was observed in at least 79.9% of these CMs. Comparatively, decreased Ca^{2+} rise velocity was only demonstrated in 41.2%, 13.5%, and 14.0% of CMs from HMEC, hESC-derived fibroblast, and control subsets. qPCR evaluation of $\text{Na}_v1.5$ expression revealed insignificant difference between experimental subsets. However, as previously shown, presence of $\text{Na}_v1.5$ mRNA transcripts may not always confer function. [207] Ultimately,

from the significant physiological response to TTX treatment, we concluded that HUVEC-specific paracrine signaling enhanced $\text{Na}_v1.5$ function.

3.5.6 Exposure to endothelial paracrine factors increases

functionality of SERCA2 in a larger proportion of CMs

To assess the functionality and presence of SR and evaluate the mechanisms governing increased Ca^{2+} transient decay kinetics, experimental subsets were treated with thapsigargin, an inhibitor of SERCA2. In mature CMs, SERCA2 governs Ca^{2+} reuptake after a contraction event and is a major regulator of SR function. [6] In both immature CMs and in models of cardiac disease, non-functional SERCA2 contributes to decreased chronotropy, decreased inotropy, and negative force-frequency relationships. [91, 199, 209]

The presence of functional intracellular Ca^{2+} stores has been a matter of contention within hPSC-derived CM literature. Some characterizations of hESC-derived CMs have demonstrated that CMs, irregardless of differentiation period, were insensitive to SERCA2 inhibition and devoid of intracellular Ca^{2+} stores so that positive force-frequency relations or post-rest potentiation could not be demonstrated. [91, 210] Contrastingly, other groups have shown at the very least that intracellular Ca^{2+} stores are present [115, 150] and that certain subsets of hESC-derived CMs are sensitive to SERCA2 inhibition, such that application of thapsigargin translates to a reduction of beating frequency, Ca^{2+} transient amplitude, half-decay-time, upstroke velocity, and time-to-peak values. [105, 199] In each case, authors cited the discrepancies in culture methods and heterogeneities exhibited by hESC-derived CM populations as contributors to experimental inconsistencies.

First, we evaluated changes in spontaneous beating frequency with the expectation that TSG sensitivity would be reflected by an attenuation of this parameter. We observed that SERCA2 inhibition caused a depression in contractile rate in all experimental subsets. Hence, we can conclude that indeed CMs with functional SR and SERCA2 are present within each experimental subset.

To elucidate differences between experimental subsets, decay velocity values were extracted for each CM population. We found that thapsigargin treatment depressed Ca^{2+} transient kinetics in a proportion of CMs from each experimental subset. Specifically, the fold change of the percentage of CMs that exhibited decay velocities below the 45th percentile were 2.0, 4.8, 6.9, and 1.6, respectively for CMs in control, HUVEC, HMEC, and hESC-fibroblast conditioned media subsets. (Figure 40) From these evaluations, we determined that treatment of hiPSC-derived CMs with paracrine factors from both HUVECs and HMECs significantly enhanced CM sensitivity to thapsigargin over control or hESC-derived fibroblast conditioned media treated CMs; and consequently suggests that endothelial factors contribute to upregulation of SERCA2 function in a larger proportion of CMs.

However, as TSG depression of decay velocity is enhanced in HMEC conditioned media treated subsets over all other subsets, this suggests that SERCA2 functionality alone was not sufficient to confer pacing ability or increased decay velocity. As Ca^{2+} -reuptake dynamics require the concerted effort of multiple proteins, we suspected that other mechanisms in addition to SERCA2 contribute to the differences in decay dynamics observed between experimental subsets. With qPCR investigation, variance in SERCA2 expression between experimental subsets was insignificant compared to the functional effect observed with thapsigargin inhibition except in the case of hESC-

fibroblast conditioned media treated CMs which exhibit a 1.78-fold increase in expression ($p < 0.02$). (Figure 41A)

However, it seems that SERCA2 mRNA expression levels alone do not correlate well with channel functionality and that supporting Ca^{2+} -handling proteins may contribute to increased relaxation efficiency as well. [91, 115, 210] For instance, studies have shown that association with phospholamban in a unphosphorylated or phosphorylated form can either respectively depress or enhance the contractility of mature CMs. [211] Upon examination of PLB mRNA expression levels, the difference between controls and endothelial conditioned media treated CMs is essentially the same. Slightly increased expression (1.3-fold, $p < 0.07$) of hESC-derived fibroblast conditioned media treated CMs is observed, which paired with the higher SERCA2 expression levels but lower SERCA2 functionality in response to TSG treatment is a possible explanation for this observation. However, assaying for levels of phosphorylated versus unphosphorylated PLB must be performed to make definitive conclusions about PLB function.

Another important player in Ca^{2+} transient kinetics is NCX-1. Although secondary to SERCA2 in the mature heart, NCX-1 is the primary mechanism of Ca^{2+} -transient relaxation in immature CMs in vivo and in hESC-derived CM models. [200, 212, 213] Increased decay kinetics could therefore be attributed to a combination of NCX-1 and SERCA2 activity at this developmental stage. In this study, NCX-1 expression was detected in CMs from all experimental subsets. Although not significant, expression of NCX-1 in HUVEC conditioned media CMs appears to be about 2-fold ($p < 0.3$) greater than controls and almost 4-fold ($p < 0.5$) greater than hESC-derived fibroblast conditioned media treated CMs. Without evaluating functionality of NCX-1 in each experimental subset, it is unclear whether NCX-1 plays a part in enhancing transient decay kinetics.

Calreticulin (CalR) and calsequestrin (CASQ2) are also important mediators of Ca^{2+} homeostasis. We detected expression of both proteins, albeit differentially, in all experimental subsets of hiPSC-derived CMs. With development, calreticulin expression diminishes considerably after birth as sustained expression poses functionally deleterious effects, particularly with regards to cardiac conduction. [214] In this study, calreticulin expression in HUVEC conditioned media treated CMs varied insignificantly from controls so conclusions about calreticulin contribution to transient dynamics could not be made.

In mature CMs, calsequestrin becomes the principal Ca^{2+} -binding protein in the SR that increases intracellular Ca^{2+} storage capacity and helps maintain Ca^{2+} homeostasis in the cytosol. [6] In hESC-derived CMs, calsequestrin expression has not yet been documented, which partly explains the close resemblance of hESC-CMs to 100-day-old fetal CMs. [91, 115] Overexpression of CASQ2 by 1000 fold has been shown to enhance Ca^{2+} transient kinetics with increases in transient amplitude and upstroke and decay velocities. [195] However, with thapsigargin treatment, the differences in transient dynamics between CMs with overexpressed CASQ2 and control CMs were insignificant. [195]

In this study, we found that CASQ2 expression is present in all experimental subsets and in certain replicates CASQ2 expression is significantly upregulated in HUVEC and HMEC conditioned media subsets versus controls. However, in considering all replicates together, this difference does not reach significance ($p < 0.1$). Thus, it remains unclear whether CASQ2 mediates the enhanced sensitivity to thapsigargin witnessed in endothelial conditioned media subsets.

It is important to note that due to the heterogeneity of CM populations, qPCR analysis of gene expression is inherently flawed. As documented, although CMs comprise the majority of constituents in each sample, other cell types are present. (Figure 18) In addition, qPCR at the single cell level cannot be performed which limits proper expression characterization of this heterogeneous CM population. Thus, although probing for gene expression could potentially provide suggestions for mechanisms at play, physiological, pharmacological, or immunohistochemical evaluations are more reliable.

3.6 Conclusions

With the intention of capitalizing on the regenerative potential afforded by hPSC-derived CMs, we need to understand how to control functional maturation in vitro. Transplantation of heterogeneous and developmentally immature CM populations poses an arrhythmogenic risk and functional mismatch that limits the therapeutic value of these cells. [75] Extensive characterizations of hPSC-derived CMs for their functional maturity have manifested their similarity to fetal CMs, at most. [105, 115, 195, 199, 200] Thus, to increase the therapeutic efficacy and safety of hPSC-derived CM-based regenerative strategies, it is imperative to determine and characterize the necessary developmental cues to enhance functional maturation.

In this study, we have demonstrated the power of high-throughput evaluation of CM maturation. By describing the population dynamics of CMs in response to different stimuli and for various maturation metrics, we limit the possibility for erroneous conclusions due to poor sampling of this extremely heterogeneous cell population.

Moreover, using these high-throughput tools, we demonstrated our ability to correlate CM physiology with Ca^{2+} kinetic parameters at the single CM level. It is important to note that these studies were done in concert with Cyteseer software development. Thus, the kinetic parameters used to describe the transients are, at the point, an approximation of traditional kinetic values, such as dV/dt_{max} for rise velocity and $dV/dt_{\text{relaxation}}$ for decay velocity. Current efforts are being implemented to automate the calculation of these standard values through the software.

Hence, correlations between the kinetic parameters used in this study were related to the ability of CMs to respond to 3Hz electrical stimulation. We determined that faster transient kinetics correlate with increased pacing ability. In addition, through pharmacological inhibition of key Ca^{2+} -handling channels, we demonstrated that, at least in a subset of CMs, L-type Ca^{2+} , $\text{Na}_v1.5$, and SERCA2 channels are functional and that these CMs possess intracellular Ca^{2+} stores that contribute to Ca^{2+} -handling even in conytold.

With these tools, we were able to evaluate the overarching hypothesis of this study, namely the developmental influence of endothelial paracrine factors on hiPSC-derived CM functional maturation. From both electrophysiological and pharmacological evaluations, we determined that treatment of hiPSC-derived CMs with HUVEC conditioned media enhances their functional maturation over other conditioned media and control subsets. This idea was substantiated in that a significantly larger proportion of HUVEC conditioned media treated CMs displayed responsiveness to 3Hz pacing as well as faster Ca^{2+} transient kinetics.

To dissect the molecular basis for these phenotypic indicators of maturation, we evaluated the effect of L-type Ca^{2+} channel, $\text{Na}_v1.5$, and SERCA2 blockade on Ca^{2+}

dynamics of CMs in each experimental subset. With TTX inhibition, we demonstrated that HUVEC conditioned media treated CMs exhibit functionality of fast Na^+ channels in a significantly larger CM population compared to control, HMEC conditioned media, and hESC-fibroblast conditioned media subsets. This finding reflected the increased rise velocity demonstrated by HUVEC conditioned media subsets at baseline conditions and suggests that upregulation of $\text{Na}_v1.5$ is a major contributing factor to this observed difference.

Contrastingly, diltiazem inhibition of L-type Ca^{2+} channels indiscriminately abolished contractile or Ca^{2+} activity in CMs from all experimental subsets under spontaneous and electrically stimulated conditions. From this study, we concluded that Ca^{2+} influx via L-type Ca^{2+} channels is the only voltage-mediated mechanism for extracellular Ca^{2+} influx in hiPSC-derived CMs in all subsets. Thus, diltiazem blockade alone could not help us distinguish differences between Ca^{2+} influx contributions to increased rise kinetics.

Finally, SERCA2 inhibition demonstrated that both SERCA2 was functional and that SR Ca^{2+} stores are present in at least a subset of hiPSC-derived CMs. Treatment of CMs with endothelial paracrine factors from both HUVEC and HMEC sources yielded an increased number of CMs sensitive to TSG than in control or hESC-derived fibroblast conditioned media subsets. Thus, endothelial factors undoubtedly contribute to enhanced SERCA2 functionality in CMs. However, as HMEC conditioned media treated CMs display an even more pronounced thapsigargin sensitivity than HUVEC conditioned media treated samples, it seems that SERCA2 functionality alone is insufficient to confer pacing ability or increased decay kinetics of the Ca^{2+} transient.

Overall, we have demonstrated that endothelial factors, and in particular HUVEC-specific paracrine factors, enhance CM physiology and Ca^{2+} -handling machinery towards a more mature phenotype. Further evaluation of contributors to rise and decay kinetics must be conducted before exact mechanisms can be determined. Specifically, determining the contribution of RYR2-mediated Ca^{2+} release through pharmacological inhibition is instrumental. In addition, characterizing the functionality of other regulators of Ca^{2+} flux, such as CASQ2, PLB, and NCX-1, at a protein level would help elucidate the phenotypic effects observed.

3.7 Acknowledgements

I would like to thank Vala Sciences, Inc., in particular Drs. Fabio Cerignoli and Alex Savtchenko, for their help with data collection and analysis with the KIC and Cyteseer software; Dr. Vincent Chen for his counsel on pharmacological characterization of cardiomyocytes; Cellular Dynamics International, Inc. for their collaboration with iCell Cardiomyocytes; and Drs. Mark Mercola and Andrew McCulloch for discussion and direction.

Chapter 3 is in preparation for publication with authors Wei KA, Savtchenko A, Cerignoli F, McCulloch AD, Mercola M. The dissertation author is the primary investigator and author of this material.

4 Summary and Future Directions

In this work, we have shown the contributing influence of endothelial sources on hPSC-derived CM maturation in terms of CM morphology, function, and gene expression. Co-culture studies with hESC-derived CMs demonstrate the contribution of HUVEC influence on morphological differences, electrophysiological maturation, and a gene expression profile that demonstrates increased maturation. However, from these studies, we highlighted numerous technical limitations, namely the efficient production of cardiomyocytes from hPSC sources, low sampling due to method constraints, the heterogeneity of hPSC-derived CM cultures, and complications of direct EC-CM co-culture.

To address these concerns, we implemented a high-throughput method of evaluating CM function using the KIC and Cyteseer systems provided by Vala Sciences, Inc. Using this method, we were able to analyze CM populations two orders of magnitude higher than traditional methods without compromising single CM characterization. In addition, high quality, plentiful, and readily-available hiPSC-derived CMs were obtained from a commercial source (CDI, Inc.). With these advancements, we were able to evaluate the effects of endothelial paracrine factors on developing hiPSC-

derived CMs versus control and hESC-derived fibroblast conditioned media subsets in a multi-dimensional study unparalleled in the field.

Specifically, at each time point we characterized changes in baseline Ca^{2+} transient dynamic parameters for spontaneous and electrically-stimulated contractions. Through these evaluations, we determined that treatment of hiPSC-derived CMs with HUVEC-specific factors for two weeks enhances 3Hz pacing ability and increases Ca^{2+} transient dynamics over HMEC conditioned media, hESC-derived fibroblast conditioned media, or control subsets. Pharmacological evaluations enabled us to demonstrate the ability of endothelial factors to modulate the molecular mechanisms that govern Ca^{2+} flux.

With regards to the rise dynamics of the Ca^{2+} transient, we investigated the functionality of both L-type Ca^{2+} channels, which govern Ca^{2+} influx, and $\text{Na}_v1.5$ channels, that govern AP depolarization in mature CMs. Diltiazem blockade of L-type Ca^{2+} channels exposed the reliance of hiPSC-derived CMs on Ca^{2+} influx via L-type Ca^{2+} channels for contraction and transient generation in all experimental subsets. In contrast, increased tetrodotoxin (TTX) sensitivity was observed in HUVEC conditioned media treated CMs that was absent in control subsets and minimally observed in HMEC or hESC-derived fibroblast conditioned media groups. Therefore, increased dependence on $\text{Na}_v1.5$ -mediated AP depolarization seems to be a contributing factor to the faster rise velocity values observed with HUVEC conditioned media treatment.

We also examined potential contributors to the differences in decay dynamics observed with HUVEC conditioned media treatment. Thapsigargin (TSG) blockade of SERCA2 revealed the presence of SR Ca^{2+} stores and functionality of SERCA2 in a proportion of CMs in all subsets. However, endothelial factors, from HMECs and

HUVECs specifically enhanced TSG sensitivity in a larger proportion of CMs. It is clear that endothelial factors influence the functionality of key molecular determinants of Ca^{2+} handling.

Thus, in considering the next steps for this research, one avenue is to further evaluate how Ca^{2+} -handling is modulated with exposure to endothelial paracrine factors. Using whole-cell patch clamp techniques, we would like to explore more specific differences in L-type Ca^{2+} channel and current density, which could not be resolved with diltiazem blockade alone. In addition, many associated proteins are important to the function of the main players in mature cardiac Ca^{2+} handling, such as RYR2, CASQ2, PLB, NCX-1, and IP3R2. Protein-specific evaluation using western blotting techniques may be necessary to resolve differences between experimental subsets that could not be detected from mRNA transcripts alone.

From qPCR evaluation, we also detected changes in the myofibrillar content of hiPSC-derived CMs treated with endothelial factors. As endothelial cells have been implicated in releasing factors that promote both positive and negative inotropy [16], it is likely that changes in myofibrillar content and organization would also reflect the developmental state of hiPSC-derived CMs. To evaluate these differences, we have initiated collaborations to characterize single CM contractile force generation after exposure to endothelial factors.

As we have demonstrated that endothelial paracrine factors enhance maturation of hiPSC-derived CMs, characterization and identification of contributing factors and elucidating their specific mechanisms of action are other future prospects for this work. We have already initiated size fractionation studies of HUVEC conditioned media that have demonstrated varied physiological phenomenon. Evaluation of how factors from

each size fraction modulate Ca^{2+} kinetic parameters compared to unfractionated controls will be completed. Pinpointing specific factors that facilitate aspects of CM maturation are instrumental to controlling hPSC-derived CMs in vitro and tailoring them for cell-based therapeutics.

In summary, we demonstrate for the first time that specific paracrine factors that are endothelial specific modulate aspects of CM maturation. We introduce the importance of evaluating hPSC-derived CM populations using a high-throughput method in order to characterize heterogeneities that detract from conclusions drawn from traditional evaluation methods. Through the characterization of large CM populations, we show that HUVEC-specific factors enhance Ca^{2+} -handling in hiPSC-derived CMs, particularly through increased proportions of functional $\text{Na}_v1.5$. This work serves as a starting point to understand the developmental mechanisms necessary for cardiac maturation on the single myocyte level with direct implications for drug cardiotoxicity screening and cell-based myocardial repair strategies.

Appendix A Technical Tables

A.1 Table of Media Formulations

hESC (H9) Maintenance Medium	2% or 20% hEB Medium	Endothelial Differentiation Media	Neonatal CM Medium	EGM-2	HEK 293T Cells	Lentivirus Harvesting Medium
Knockout Dulbecco's modified eagle medium (Invitrogen, Cat# 10829-018, Carlsbad, CA)	Knockout Dulbecco's modified eagle medium (Invitrogen, Cat# 10829-018, Carlsbad, CA)	Dulbecco's modified eagle medium/F12 (Gibco, Cat# 1330-057, Carlsbad, CA)	Dulbecco's modified eagle medium/F12 (Gibco, Cat# 1330-057, Carlsbad, CA)	Endothelial basal medium-2 (EBM-2) (Lonza, Inc, Cat# CC3156, Walkersville, MD)	DMEM/F12 High Glucose (Hyclone, Cat# SH30081.01, Logan UT)	Ultraculture Serum-free Medium (Lonza, Cat# 12-725F, Walkersville, MD)
Penicillin (1U/ml): Streptomycin (1µg/mL) (Hyclone, Cat# SV30010, Logan, UT)	Penicillin (1U/ml): Streptomycin (1µg/mL) (Hyclone, Cat# SV30010, Logan, UT)	Glutamax (2mM) (Invitrogen, Cat# 35050-061, Carlsbad, CA)	Penicillin (1U/ml): Streptomycin (1µg/mL) (Hyclone, Cat# SV30010, Logan, UT)	EGM-2 growth factors and supplement kit (Lonza, Inc., Cat# CC3162, Walkersville, MD)	Sodium pyruvate (1mM) (Invitrogen, Cat# 11360-070, Carlsbad, CA)	L-glutamine (2mM) (Invitrogen, Cat# 11140-050, Carlsbad, CA)
L-glutamine (1mM) (Invitrogen, Cat# 11140-050, Carlsbad, CA)	L-glutamine (1mM) (Invitrogen, Cat# 11140-050, Carlsbad, CA)	N2 Supplement (1X) (Invitrogen, Cat# 17502-048, Carlsbad, CA)	Bovine serum albumin (2g/L) (Calbiochem, Cat# 12659, La Jolla, CA)		L-glutamine (1mM) (Invitrogen, Cat# 11140-050, Carlsbad, CA)	Penicillin (1U/ml): Streptomycin (1µg/mL) (Hyclone, Cat# SV30010, Logan, UT)
Non-essential amino acids (1X) (Invitrogen, Cat# 11140-050, Carlsbad, CA)	Non-essential amino acids (1X) (Invitrogen, Cat# 11140-050, Carlsbad, CA)	Basic fibroblast growth factor-2 (bFGF-2, 8ng/mL) (Sigma, Cat# F0291, St. Louis, MO)	Sodium pyruvate (3mM) (Invitrogen, Cat# 11360-070, Carlsbad, CA)		Hydrocortisone Gentamicin, Amphotericin-B Fetal bovine serum VEGF hFGF-B R ³ -IGF-1 Ascorbic acid Heparin	Penicillin (1U/ml): Streptomycin (1µg/mL) (Hyclone, Cat# SV30010, Logan, UT)
2-Mercaptoethanol (0.1mM) (Sigma, Cat# M7522, St. Louis, MO)	2-Mercaptoethanol (0.1mM) (Sigma, Cat# M7522, St. Louis, MO)	Vascular endothelial growth factor (VEGF, 50ng/ml) (NCl BRB, Cat# 01101507, Rockville, MD)	Ascorbic acid (100µM) (Sigma Aldrich, Cat# 4403, St. Louis, MO)		10% Fetal bovine serum (FBS) (Gibco, Cat# 16000-044, Carlsbad, CA)	
Sodium pyruvate (1mM) (Invitrogen, Cat# 11360-070, Carlsbad, CA)	Sodium pyruvate (1mM) (Invitrogen, Cat# 11360-070, Carlsbad, CA)		Lynoleic acid (5µg/mL) (Sigma, Cat# L1376, St. Louis, MO)			
Basic fibroblast growth factor-2 (bFGF-2, 8ng/mL) (Sigma, Cat# F0291, St. Louis, MO)	2% or 20% Fetal bovine serum (FBS) (Gibco, Cat# 16000-044, Carlsbad, CA)		Transferrin (4µg/ml) (Invitrogen, Cat# 0030124SA, Carlsbad, CA)			
Knockout serum replacement (KOSR) (Invitrogen, Cat# 108280-028, Carlsbad, CA)			0% or 0.25% FBS (Hyclone, SH30396.03, Logan, UT)			

A.2 Table of qPCR Primers.

Primer Name	Primer Sequence (F)	Primer Sequence (R)	Annealing Temperature (°C)	REF
Cardiac Contractile Proteins				
MYH7	GGCAAGACAGTGACCGTGAAG	CGTAGCGATCCTTGAGGTTGTA	60	[106]
MYH6	TCTCCGACAACGCCTATCAGTAC	GTCACCTATGGCTGCAATGCT	60	[106]
MLC2a	CAGGCCCAACGTGGTTCTT	CCATCACGATTCTGGTCGATAC	60	[106]
MLC2v	CCTTGGGCGAGTGAACGT	GGGTCCGCTCCCTTAAGTTT	60	[106]
cTnT	ATGAGCGGGAGAAGGAGCGGCAGA AC	TCAATGGCCAGCACCTTCCTCCTCT C	60	
Electrophysiological Regulators and Ca²⁺ Handling Proteins				
PLB	TCACAGCTGCCAAGGCTACC	TAGATTCTGTAGCTTTTGACGTGC	58	[215]
Serca2a	AGCGGTTACTCCAGTATTGCAG	CTGTCCATGTCACTCCACTTCC	58	[215]
CASQ2	TGCAGGGCAGAAGAGGGGCT	GGGCCACAAGCTCAAGCACGA	60	
CalR	AGGAGGGCAGCAGAAGGGGG	GACCCACTGCCCCACCCAGA	60	
RyR2	TGCAAGACTCACCGAAGATG	CCACCCAGACATTAGCAGGT	60	[158]
Cx43	TCTGAGTGCCTGAACTTGC	ACTGACAGCCACACCTTCC	60	[216]
Ca_v1.2	GAGAACAGCAAGTTTGACTTTGACA A	CGAAGGTGGAGACGGTGAA	60	[158]
Na_v1.5	CCAGACAGAGGGAGACTTGC	CTGGAGTCCACAGCTGCATA	60	[158]
NCX1	TGTGCATCTCAGCAATGTCA	TGATGCCAATGCTCTCACTC	60	[158]
iP3R2	ACTGTGTGAGAATCACAACCGGGA	TCTGGTTGACCAGCGCACATTCT	60	[158]
iK_v2.1	TGTTGGGTTTGACAGTGGAA	CCCACAGGATTTCAATTTGCT	60	[158]
iK_v2.2	AGAAGAATGGCCAGTGAAC	GCGATGACCCAGAAGATGAT	60	[158]

A.3 Table of Cardiac Markers Modulated with CM Maturation

Marker	Functional Characteristics	EWM*	REF
Cardiac Contractile Proteins			
aMHC	Alpha myosin heavy chain <ul style="list-style-type: none"> • 10% of MHC content in fetal human ventricles • Major isotype in adult human atria 	↓	[121]
bMHC	Beta myosin heavy chain <ul style="list-style-type: none"> • Major isotype in fetal and adult human ventricles • Increased expression in failing human atria and ventricles 	↑	[121]
MLC2v	Myosin light chain - ventricular <ul style="list-style-type: none"> • Major isotype in adult human ventricle 	↑	[111]
MLC2a	Myosin light chain – atrial <ul style="list-style-type: none"> • Major isotype in adult human atria • Ambiguous expression pattern in fetal ventricle 	↑	[111]
Electrophysiological Regulators and Ca²⁺ Handling Machinery			
Na_v1.5	Fast Na ⁺ Channel <ul style="list-style-type: none"> • Responsible for upstroke velocity of cardiac AP 	↑	[193, 217]
NCX1	Na ⁺ /Ca ²⁺ Exchanger <ul style="list-style-type: none"> • Extrusion of Ca²⁺ from CM cytoplasm for maintaining Ca²⁺ homeostasis 	↓	[200, 218]
iP3R2	Inositol 1,4,5-trisphosphate <ul style="list-style-type: none"> • ATP-mediated intracellular Ca²⁺ release channel 	↓	[204, 219]
RyR2	Ryanodine receptor <ul style="list-style-type: none"> • Caffeine-mediated Ca²⁺ release channel 	↑	
Ca_v1.2	L-type Ca ²⁺ Channel <ul style="list-style-type: none"> • Long-lasting Ca²⁺ channel responsible for Ca²⁺ inward current and cardiac AP plateau 	↑	[6, 220, 221]
Ca_v3.1	T-type Ca ²⁺ Channel <ul style="list-style-type: none"> • Transient Ca²⁺ channel • Contributes to cardiac automaticity and pacemaking of nodal CMs 	↓	[6, 222]
Serca2	SR-Ca ²⁺ -ATPase 2 <ul style="list-style-type: none"> • Responsible for Ca²⁺ reuptake into intracellular Ca²⁺ stores 	↑	[149, 223]
PLB	Phospholamban <ul style="list-style-type: none"> • Regulator of Serca2a activity by increasing Ca²⁺ affinity 	↑	[224]
CASQ2	Calsequestrin <ul style="list-style-type: none"> • Ca²⁺-buffering protein in intracellular Ca²⁺ stores • Maintains Ca²⁺ homeostasis 	↑	[225]
CALR	Calreticulin <ul style="list-style-type: none"> • Involved in Ca²⁺ homeostasis, protein folding, and gene expression • Essential for proper cardiac development 	↓	[226, 227]
iK_r2.1/2	Delayed-rectifier K ⁺ Channels <ul style="list-style-type: none"> • Responsible for cardiac AP plateau and repolarization 	↑	[6, 189]
Cx43	Connexin 43 <ul style="list-style-type: none"> • Dominant gap junctional protein in all working CMs – atrial or ventricular • Not expressed in nodal cells 	↑	[228]

* EWM = Changes of expression with maturation

**Appendix B Generation of a Tie2
Reporter Line for Genetic Selection
of ECs from Human Pluripotent Stem
Cells**

B.1 Rationale

As reiterated throughout this work, cardiac-endothelial interactions are pervasive and consequential to proper cardiac maturation. Inclusion of both CMs and ECs in regenerative therapy models has been shown to improve hPSC-derived CM graft retention and attenuation of pathologies associated with MI. [77, 78, 154, 155] Although encouraging, the developmental stage of CMs and ECs used in these reports have typically been mismatched with fetal like hPSC-derived CMs and mature EC sources. Interestingly, transplant of endothelial progenitor cells (EPCs) into animal models of hind limb ischemia or the ischemic heart has also shown integration of EPCs into existing vessels as well as induction of neovascularization of these oxygen-deprived tissues. [229-232] Furthermore, both ECs and EPCs have been implicated in secreting cardioprotective factors [233-235], guiding CM organization [164], and even in transdifferentiation into CMs [236]. Thus, composite cultures of ECs and CMs may not only have a pro-cardiogenic effect on developing hESC-CMs, but most likely improve transplant survival and infarct remodeling of host tissue by recruitment of new vasculature as well. We hypothesize that the interaction between CMs and ECs, potentially of the same developmental stage, is integral to the proper development of CMs. Thus, one of the major foci of this work was to develop new methods of studying the interactions between CMs and ECs in an hESC model of development.

Using genetic selection methods, we attempted to engineer a dual-selectable hESC line that would permit the isolation of ECs simultaneously with CMs so that the effect of CM-EC interactions on cardiomyogenesis could be evaluated. With cell lines prevalently used that allow puromycin selection of CMs using cardiac specific promoters

driving this drug resistance [74, 158], we applied similar design strategies to isolating ECs from hESC cultures. In the literature, ECs from hESC differentiation cultures express EC-specific markers (CD31, von Willebrand factor, VE-cadherin) as well as perform like mature HUVEC in functional assays (Dill-labeled ac-LDL uptake and matrigel tube formation assay).[237] Tie-2 was chosen as the promoter to drive EC-selection due to the high and constant expression of this receptor in both undifferentiated and differentiating hESCs as well as in mature HUVEC controls. [238] In development, Tie-2 expression has been detected in early EPCs as well as putative hemangioblasts. [239, 240] Moreover, Schlaeger et al created transgenic mice employing this Tie-2 promoter/enhancer combination driving a β -galactocidase reporter and showed uniform reporter expression throughout embryogenesis and adulthood in virtually all vascular ECs in a mouse model.[241] In human embryos, a multi-timepoint study showed that Tie-2 expression remains stable between 4 week and 8 week embryos. [242] This extensive evidence in the literature suggests the utility of this promoter as a selection tool for hPSC-derived ECs throughout differentiation and maturation stages.

B.1 Cloning of the Tie2-Selectable Lentiviral Construct

To create the EC-selectable lentiviral vectors, the previously described Sin18.WPRE lentiviral vector [74, 243] used was modified through the insertion of the Tie2, endothelial-specific, promoter and enhancer regions into existing constructs containing the drug resistance genes or fluorescent marker. The Tie2 promoter and enhancer plasmids (pSPTg.T2FpAXK, #54) were a gift from the lab of Dr. Thomas N. Sato. The Tie2 promoter fragment used is the 2.0kb fragment flanked by *HindIII* sites

including the first exon described previously. [244, 245] The minimal enhancer fragment is a 1.6 kb fragment necessary to confer Tie2 expression both in vitro and in vivo. [241]

To generate Sin18 Tie2-Puro^r-Rex-Neo^r (T2P) and Sin18 Tie2-mCherry-Rex-Neo^r (T2M) constructs (Figure 42 and Figure 43), piece-wise assembly of genetic fragments was performed. Briefly, the original Tie2-enhancer plasmid supplied by the Sato Laboratory was sequenced using existing Sp6 and T7 promoter sites in the plasmid (Eton Biosciences, San Diego, CA). Plasmid constructs were amplified in XL10 gold ultracompetent bacteria (Agilent Technologies, Inc., Cat# 200315, Santa Clara, CA). Using PCR methods, primer pair A (Table 6) was used to amplify the puro^r gene fragment from the SMPU αMHC-Puro^r-Rex-Blasticidin^r vector [74]. PCRs were performed using Phusion DNA polymerase (NEB, Inc., Cat# F-530L, Ipswich, MA) with GC buffer and 5-8% DMSO conditions with the PCR program detailed in Table 7. The amplified gene fragment was digested with both XhoI and NotI enzymes (Table 8) and inserted into the Tie2 plasmid between the NotI-XhoI sites using T4 DNA ligase (NEB, Inc., Cat# M0202L, Ipswich, MA).

After the creation of the Tie2-Puro^r gene fragment, an SgrAI site was introduced to the 3' end just upstream of the KpnI restriction enzyme site using PCR methods. A gene fragment from the XhoI restriction site to the KpnI restriction sites of the Tie2-Puro^r construct was amplified using PCR protocol B (Table 7) using unique primer pair B (Table 6). The amplified fragment was verified using PstI digestion. (Table 8) Once verified, restriction digest using both XhoI and KpnI for both the gene fragment and Tie2-Puro^r construct was performed overnight. The insert and vector were ligated for 10 minutes using T4 DNA ligase and proper clones were verified using XhoI and SgrAI digestion. (Table 8)

Using the Sin18.WPRE α MHC-GFP-Rex-Neo^r vector [74], the α MHC promoter was excised using XhoI and BamHI digestion (Table 8). This vector served as the backbone for the Tie2-Puro^r-Enhancer construct. Insertion of the Tie2-Puro^r gene fragment required a two-step protocol. First, the Tie2-Puro^r fragment was digested with Sall and BamHI (Table 8) to generate the 1619 bp 5' fragment and inserted into the Sin18.WPRE backbone replacing the XhoI-BamHI excised fragment. (Intermediate Sin18.WPRE Tie2 construct) To insert the 3' half of the Tie2-Puro fragment (BamHI-KpnI, 2803 bp), the Tie2-Puro^r construct and the intermediate Sin18.WPRE Tie2 construct were digested with BamHI and SgrAI overnight. Once fully digested, both the insertion vector (BamHI-KpnI fragment from the Tie2-Puro^r fragment) and the Sin18 backbone were ligated for 10 minutes. Successful clones were chosen after restriction digest verification. Plasmids were amplified using XL10 gold competent cells and DNA purification was performed with Marligen Maxi-prep DNA purification methods. (Marligen Bioscience, Cat# NP100009, Rockville, MD) Sequencing (Eton Biosciences, San Diego, CA) using the T7 and Sp6 primers was used to confirm proper insertion of the gene fragments. Diluted plasmids were stored at -20°C until use.

The T2M construct was made by excising the puro^r gene fragment using Sall and Ascl digestion. (Table 8) mCherry was excised from the SMPU α MHC-mCherry-Rex-Blasticidin^r construct using a Sall and Ascl digestion as well. The mCherry insert and Tie2 vector were ligated using T4 DNA ligase for 10 minutes at room temperature. Constructs were verified using restriction digest with BamHI and Ascl enzymes. Once verified, constructs were sequenced using sequencing primer pair C shown in Table 6.

In all cases, restriction enzyme digests and PCR products were run on 1% or 2% agarose gels in 1X TAE buffer with 5 μ g/ml ethidium bromide with 1kb plus ladder

(Invitrogen, Cat# 10787-026, Carlsbad, CA) Gels were imaged under UV illumination. DNA was extracted from gels using the Stratagene DNA gel extraction kit (Stratagene, Cat#400766, Santa Clara, CA).

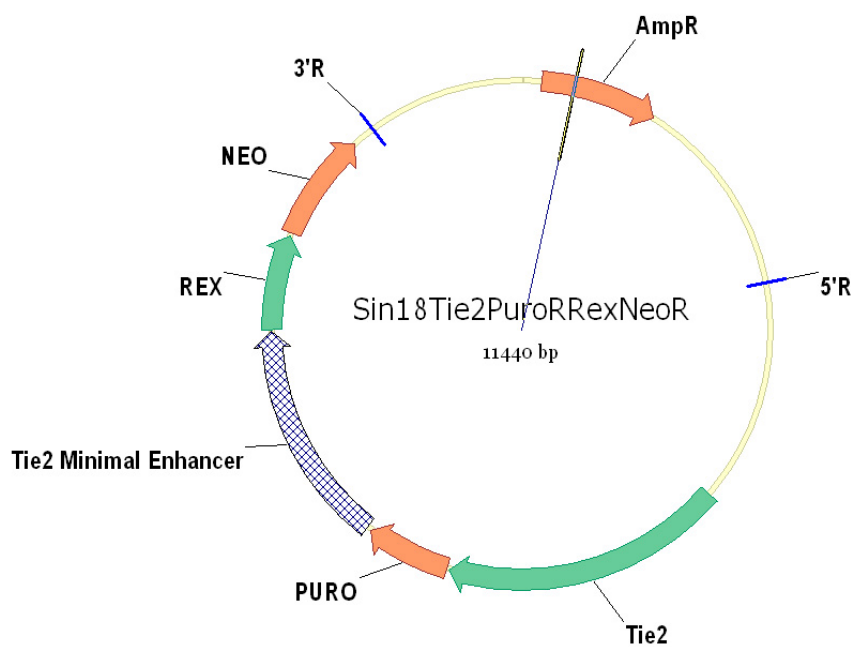


Figure 42 Plasmid map of Sin18 Tie2-Puro^r-Rex-Neo^r (T2P) construct.

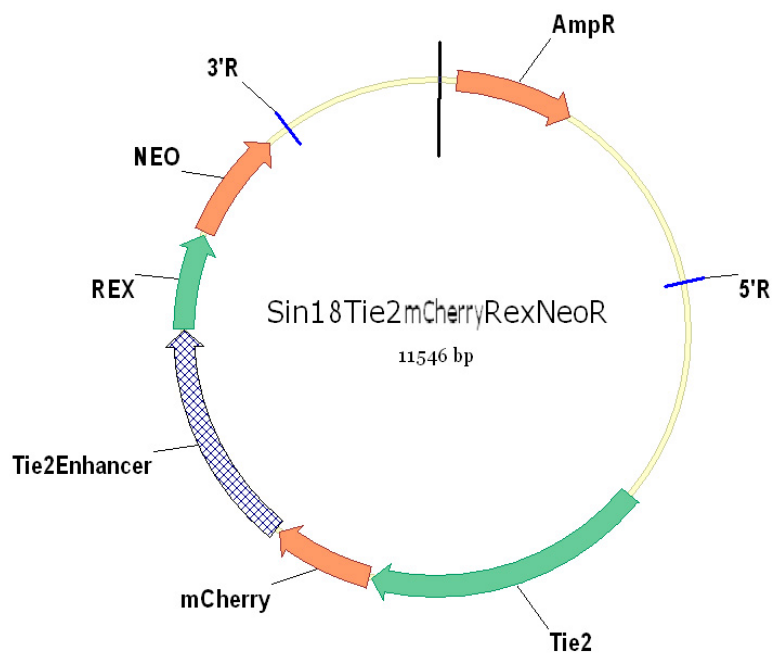


Figure 43 Plasmid map of Sin18 Tie2-mCherry-Rex-Neo^r (T2M) construct.

Table 6 PCR primers used for cloning Tie2-Puro^r-Rex-Neo^r construct.

Name	Forward Primer	Reverse Primer
Primer pair A	CTAAGCGGCCGCGTCTCGACTGATCAAAAACCGG	ATCTCGAGTTATCGGGAGGAATCGGTGG
Primer pair B	GATAACTCGAGGTCCAGTATGGCTT	CAGGTACCCACCGGTGATTATTGTTTTAC TTGGGAGGCTGG

Table 7 PCR programs for cloning Tie2-Puro^r-Rex-Neo^r construct.

Reaction Step	Program A		Program B	
	T (°C)	Time	T (°C)	Time
Initial	98°C	2 min	95°C	2 min
	5 Cycles		30 cycles	
Denature	95°C	30 sec	95°C	30 sec
Annealing	62°C	30 sec	63°C	30 sec
Extension	72°C	20 sec	72°C	4 min
	13 Cycles		End Cycles	
Denature	95°C	30 sec		
Annealing	60°C	30 sec		
Extension	72°C	20 sec		
	End Cycles			
Final Extension	72°C	5 min	72°C	10 min
End	4°C	∞	4°C	∞

Table 8 Table of Restriction Enzymes used from New England Biosciences, Inc. (Ipswich, MA).

Restriction Enzyme	Product #	Use
Ascl	R0558	Tie2-mCherry construction
BamHI	R0136	Insertion of Tie2-Puro ^r into Sin18 vector (Step 1); Insertion of Tie2-Puro ^r into Sin18 vector (Step 2);
KpnI	R0142	Insertion of SgrAI RE site at 3' end of Tie2-Puro ^r construct
NotI	R0189	Tie2-Puro ^r construction
PstI	R0140	Validate XhoI-KpnI fragment of Tie2-Puro ^r construct
Sall	R0138	Insertion of Tie2-Puro ^r into Sin18 vector (Step 1); Tie2-mCherry construction
SgrAI	R0603	Insertion of Tie2-Puro ^r into Sin18 vector (Step 2)
XhoI	R0146	Tie2-Puro ^r construction

B.2 Methods

B.2.1 Cells

H9 Human Embryonic Stem Cells (hESCs)

Wild-type H9 hESCs (WiCell Research Institute, Cat# WA09, Madison, WI) were used to make the EC-selectable cell lines. In addition, H9 hESCs genetically modified with a double-selection cassette, α MHC-puromycin^r-Rex-blasticidin^r, that renders pluripotent cells blasticidin-resistant and α MHC-positive CMs puromycin-resistant, were used to enable cardiac and EC-simultaneous selection from hESC cultures.

Undifferentiated H9 cells were cultured on Matrigel (0.0625 mg/ml, BD Biosciences, Cat# 354230, San Diego, CA)-coated 6-well plates on an irradiated mouse embryonic feeder (MEF) layer (E13.5 CD-1 mice). The medium used to maintain pluripotency was termed hESC media and is referenced in Appendix 1.

To purify hESC cultures for only pluripotent cells, the case of genetically modified cell lines, 4-6 day-old cultures were treated with 5 μ g/ml of blasticidin (Invitrogen, Cat# R21001, Carlsbad, CA) for 24 hours. Cultures were also monitored daily for differentiation contaminations. Manual dissection of differentiated areas in hESC cultures was performed using 1cc U-100 insulin syringe needles (Becton Dickinson and Company, Cat# 329420, Franklin Lakes, NJ) with a dissection microscope under sterile conditions.

H9 hESCs, both wild-type and genetically modified, were passaged every 7 days. Briefly, hESCs were dissociated with 1mg/ml of collagenase IV (Invitrogen, Cat# 17104-019, Carlsbad, CA) treatment for 5 minutes at 37°C. Fresh hESC medium was added to

collagenase-treated samples to stop enzyme activity. Using a pipet tip, hESC cultures were then scored in a grid-like pattern and dislodged from the tissue culture plate. Dislodged hESCs were then plated on fresh confluent MEF feeder layers and matrigel-coated tissue culture plates.

Embryoid body (EB) differentiation was initiated using serum-based hESC cardiac differentiation protocols. [93] Briefly, undifferentiated H9 hESCs were dissociated using collagenase IV (Invitrogen, Cat# 17104-019, Carlsbad, CA) and mechanical dispersion under 20% serum conditions. (Media is referenced in Appendix 1) Upon EB formation, media conditions were switched from hESC media to 20% hEB media (Appendix 1). EBs were formed once cells were cultured in suspension on ultra low-attachment 6-well plates (Corning, Inc., Cat# 3471, Corning, NY) for 6 days. After EB formation, EBs were plated on 0.1% gelatin-coated (Stem Cell Technologies, Cat# 07903, Vancouver, BC) tissue-culture plates.

Endothelial Cells

Human umbilical vein endothelial cells (HUVECs) (Lonza Walkersville, Inc., Cat# C2519A, Lot#6F3251, Walkersville, MD) were used to test functionality of the EC-selectable constructs. For experiments, HUVECs were used experimentally until passage 10 before discarded. HUVECs were maintained in endothelial growth medium (EGM-2; Lonza Walkersville, Inc., Walkersville, MD) and media was changed every 2 days. For passage of both endothelial cell types, confluent plates were washed with Dulbecco's phosphate buffered saline, or dPBS, (Mediatech, Inc., Cat# 21-031-CV, Manassas, VA) and treated with 0.25% trypsin-EDTA (Invitrogen, Cat# 25200, Carlsbad,

CA) for 2.5 minutes. Once cells detached, cells were resuspended in fresh EGM-2 to stop trypsinization and for transfer into new tissue-culture plates.

L-Cell Fibroblast Cells

L-cell fibroblasts (ATCC, Cat# CRL-2648, Manassas, VA) were used in co-culture experiments as a control comparison for EC-CM co-cultures. L-cells are cultured using 10% fetal bovine serum (Hyclone, Cat# SH30070.03, Logan, UT) in Dulbecco's modified eagle medium/F12 (Gibco, Cat# 1330-057, Carlsbad, CA) with penicillin (100U/ml)/streptomycin (100µg/ml) (Hyclone, Cat# SV30010, Logan, UT) and 20mM L-glutamine (Gibco, Cat# 25030, Carlsbad, CA).

B.2.2 Lentivirus Production and Infection of hESCs

Sin18.WPRE-based lentiviral production in human epithelial kidney 293T cells (Passage < 20) was performed as previously described. [74] Briefly, 293T cells were seeded on 0.1% gelatin-coated (Stem Cell Technologies, Cat#07903, Vancouver, BC) 15-cm tissue culture dishes 24 hours before transfection. Once cells reached 70% confluency, transient infection was performed. Three plasmids encoding the transfer vector with expression construct, the packaging plasmid pCMVΔR8.74, and the VSV-G envelope protein expression plasmid pMD.G were mixed in a ratio of 3:2:1 in dH₂O to 45% of the final volume. 2.5M CaCl₂ solution was added drop-wise to the viral components for a final concentration of 0.125M CaCl₂. 2X Hank's balanced salt solution (HBSS, pH7.03) was subsequently added drop-wise to the mixture (1X HBSS) while vortexing constantly to mix the solution. Once mixed, the transfection solution was immediately added gently and dropwise to 293T cells. Cells were incubated for 14-16

hours at 37°C at which time media was replaced with viral harvesting medium. Virus was collected daily for four days post transfection in fresh harvesting medium, vacuum-filtered through a 0.22µm filter (Corning, Inc., Cat# 430320, Corning, NY), and stored at 4°C.

To concentrate the collected virus, ultracentrifugation of the viral supernatant was performed. Samples were pipetted into ultracentrifuge tubes (Beckman Coulter, Cat# 344061, Brea, CA) and ultracentrifuged in a swinging bucket rotor (Beckman Coulter, Model SW28, Brea, CA) at 21,000RPM for 2 hours at 4°C. The supernatant was discarded immediately and viral pellets were resuspended in ~200-500µl of dPBS with 0.1%BSA by constant shaking at 200 RPM for 1 hour at 4°C. The resultant concentrated virus was aliquoted and stored at -80°C until use.

For viral infection of hESCs, one confluent well of a 6-well tissue culture plate of hESCs was dissociated with 1mg/ml of collagenase IV as if being passaged. Cell clumps were collected and allowed to sediment in a 50ml conical tube (5 minutes) and supernatant was aspirated. Cell clumps were washed twice with dPBS repeating the sedimentation process with each washing. Upon the final washing, dPBS was aspirated and cells were resuspended in 1ml of culture medium and allowed to sediment. 500µl of the supernatant was discarded and a mixture of 400µl fresh medium with 8µg/ml of polybrene (Millipore, Inc., Cat# TR-1003-G, Billerica, MA) and 100µl of freshly thawed virus was added to the cells in suspension. hESCs were incubated with the virus at 37°C for 4-6 hours with agitation every hour. After this incubation period, hESCs were plated on confluent MEF feeders on Matrigel-coated plates. 1ml of fresh hESC media was added to the infected wells 24 hours later and all virus particles were removed 36 hours post-infection. Neomycin or blasticidin treatment of cultures was initiated 4 days

after infection at a half-dosage to purify cultures for infected cells only. Full dosages of antibiotics were used by day 6 post-infection as commonly done before hESC passage or EB differentiation.

B.2.3 Fluorescence Activated Cell Sorting (FACS)

FACS was performed by the Sanford-Burnham Flow Cytometry Shared Resources facility using the FACSVantageSE DiVa (BD Biosciences, San Jose). In particular, we sorted for mCherry-positive and KDR (VEGFR2)-positive cells in differentiating T2M lines. Cells were first dissociated with Accutase (Millipore, Cat# SCR005, Billerica, MA) for 15 minutes at room temperature with constant agitation. Cells were then stained with phycoerythrin or allophycocyanin-conjugated KDR antibodies (R&D Systems, Cat# FAB357P or FAB357A, Minneapolis, MN) per the manufacturer protocol. Cells were blocked in PBS with 5% FBS and 0.5% BSA for 1 hour.

B.2.4 Quantitative Polymerase Chain Reaction (qPCR)

Total RNA was extracted using Trizol reagent (Invitrogen, Cat# 15596-018, Carlsbad, CA) in conjunction with the protocol provided by the manufacturer for cells in a monolayer. Samples incubated in Trizol were either stored at -80C or processed immediately. Once RNA extraction was complete, RNA was resuspended in 10 μ l distilled, deionized water (ddH₂O) (Mediatech, Inc., Cat# 25-055-CV, Herndon, CA). RNA concentrations were measured using the Nanodrop spectrophotometry system (Thermo Scientific, Inc., Cat# ND-1000, Wilmington, DE). cDNA was synthesized using the QuantiTect Reverse Transcriptase (RT) Kit (Qiagen, Inc., Cat# 205314, Valencia, CA).

cDNA was amplified using 1 µg of RNA and the RT kit. Once the RNA was mixed with genomic DNA wipeout buffer, samples were heated at 42°C for 5 minutes. Samples were then mixed with RT buffer, RT enzyme, and amplification primers for a total volume of 20 µl. Samples were heated for another 30 minutes at 42°C, 95°C for 3 minutes, and kept at 4°C. Finally, cDNA concentrations were measured using the Nanodrop and stored at -20°C until use.

qPCR was performed on the Roche LightCycler 2.0 (Roche Applied Science, Cat# 03531414001, Indianapolis, IN) using the LightCycler FastStart DNA Master SYBR Green I kit (Roche Applied Science, Cat# 12239264001, Indianapolis, IN) and LightCycler glass capillaries (Roche Applied Science, Cat# 04 929 292 001, Indianapolis, IN) for fluorescence amplification detection. Samples were prepared as indicated by Roche at half the volume (10 µl). Standard curves were created for each primer pair to calculate primer efficiency using the Lightcycler 2.0 software using cDNA from late stage hESC-derived CSs. Briefly, qPCRs were conducted as follows: samples were denatured at 95°C for 8 minutes with a temperature slope of 20 °C/s (slope used for every step unless otherwise specified), sample amplification occurred with the following sequence, 95°C for 15 seconds, 60°C for 5 seconds, and 72°C for 20 seconds, for 40 cycles, melting curves were obtained with a subsequent cycle starting at 95°C, 70°C for 20 seconds, and a return to 95°C at a slope of 0.1°C/s, and finally samples were cooled at 40°C for 30 seconds. Primer sequences are listed in Appendix 2. C_p values were obtained using the Lightcycler software. Using efficiency values for each primer pair, transcript expression could be calculated using the $\Delta\Delta C_p$ method. Transcript levels were normalized to GAPDH expression.

B.2.5 Immunostaining

Prior to immunostaining, cells were washed with dPBS and fixed in 4% paraformaldehyde (PFA) for 10 minutes. Cells were blocked in a blocking buffer composed of 1X dPBS, 2% BSA, 2% goat serum, 50mM glycine (Bio-Rad, Cat# 161-0718, Hercules, CA), 0.01% Triton-X (Sigma-Aldrich, Cat# T8787, St. Louis, MO), and 0.005% Tween 20 (Sigma-Aldrich, Cat# P9416, St. Louis, MO). Primary antibodies used for these studies were diluted in 10% blocking buffer in the following ratios: anti-RFP (MBL, LTD., Cat# PM005, Nagoya, Japan), lectin (1/1000; Vector Laboratories, Cat# RL-1062/FL-1061, Burlingame, CA), and α -actinin(1:300, Sigma Aldrich, Cat# A7811, St Louis, MO).

B.3 Tie2 Construct Validation

Prior to virus production, we verified the functionality of the two Sin18.WPRE lentiviral constructs were generated in this study, T2P and T2M, using transient transfections in Tie2-expressing endothelial cells (HUVECs).

B.3.1 Validation of T2P Construct in HUVECs

To verify construct function in the T2P construct, transient transfection of HUVECs were conducted using Lipofectamine LTR with PLUS reagent (Invitrogen, Cat# 15338-100, Carlsbad,CA) per the manufacturer's recommendation for HUVEC transfection. 200 ng of plasmid DNA were used in each well of a 96-well plate with cell densities of 8,000 cells/well. Transfections were tested at 4- and 8-hour transfection periods. Puromycin treatment was initiated 24 hours post-transfection at 4 different

concentrations: 0, 0.125, 0.250, and 0.350 $\mu\text{g/ml}$ for 24 hours. Cells were imaged 24 hours after puromycin removal.

Result: We found that T2P transfection of HUVECs conferred a low level of puromycin resistance at 0.25 $\mu\text{g/ml}$ of puromycin treatment not observed in control conditions.

(Figure 44, red boxes) This suggests the functionality of the Tie2 promoter and puromycin resistance reporter in functional endothelial cells.

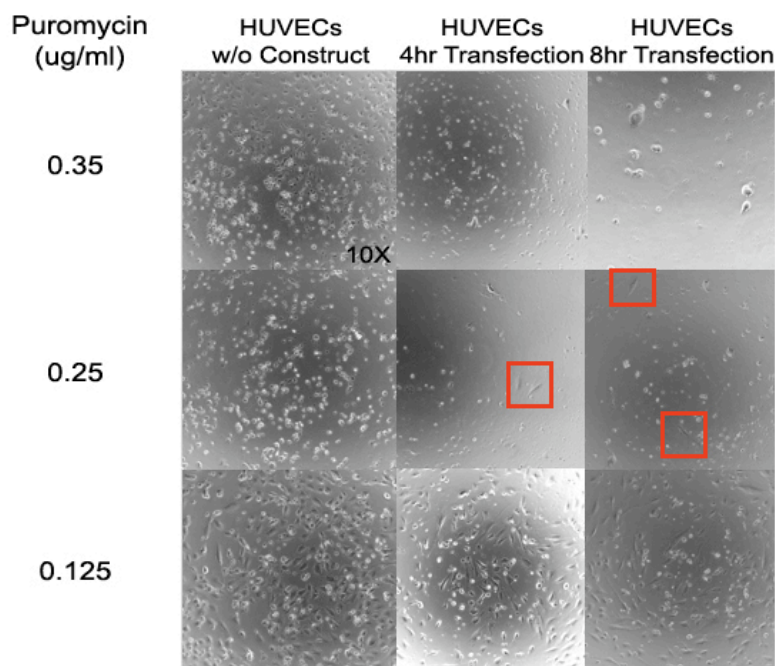


Figure 44 Lipofectamine transfection of T2P construct into HUVECs with 4 hour and 8 hour transfection protocols. Cultures were then exposed to puromycin for 48 hours at 0.35, 0.25, and 0.125 $\mu\text{g/ml}$ concentrations. Red squares outline the viable cells. (x10 magnification).

B.3.2 Validation of T2M Construct in HUVECs

To validate T2M functionality, both HUVECs and L-cells were transfected with 100 ng of construct for 4-8 hours. Cells were plated in 96-well format and seeded at a density of 8,000 cells/well. Again, a plasmid with ubiquitously expressed

phosphoglycerate kinase, hPGK, promoter driving GFP expression was also transfected to gauge transfection efficiency. Cells were assayed immediately after a 4-hour transfection period using fluorescence microscopy.

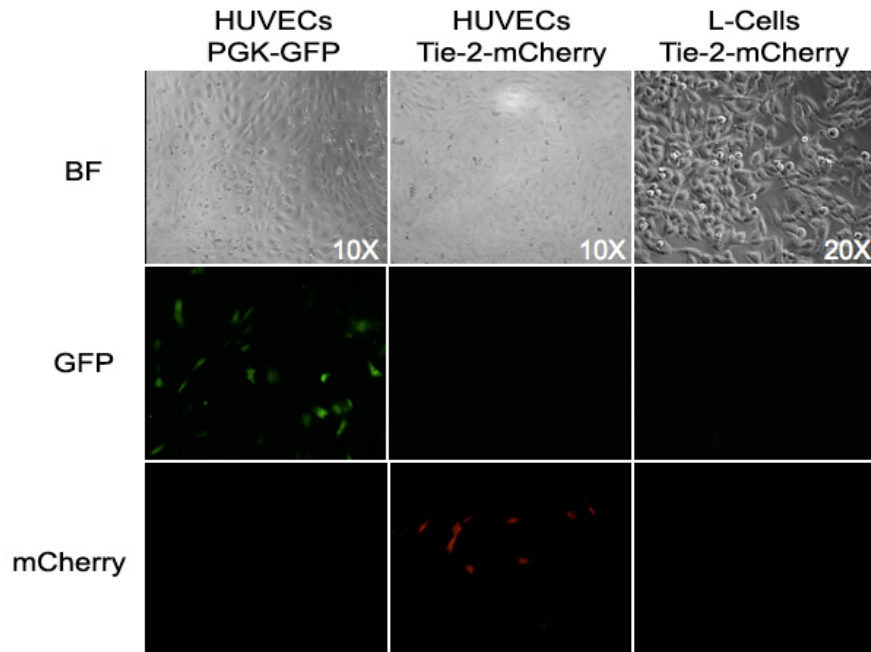


Figure 45 Lipofectamine transfection of T2M construct into HUVECs using a 4 hour transfection protocol. Phosphoglycerate kinase (PGK) is expressed at basal levels in all cells and used as a transfection control. mCherry expression is only seen in the HUVEC transfections signifying the functionality of the construct.

Result: We found that with T2M transfection into HUVECs and L-cell fibroblasts demonstrated mCherry expression in HUVECs but not in L-cells. This demonstrates that the Tie2-mCherry reporter is functional in cell types that express Tie2.

B.3.3 Validation of Tie2 Constructs in hESCs

Rex-1 driven Neomycin Resistance

After validation of the functionality of these constructs through transient transfection experiments, virus employing each of these constructs was generated as

described in Section B.2.2. The viruses were then used to infect undifferentiated wild-type H9 hESCs. Constructs were purified for infected hESCs using G418 selection of undifferentiated colonies as the plasmid contains the Rex-Neo^r selection cassette. G418-resistant hESC colonies were continually purified and passaged to isolate only infected cells.

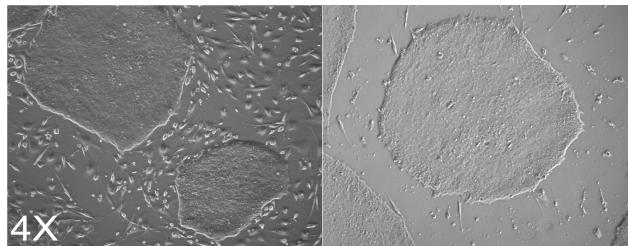


Figure 46 Neomycin selection of T2P-infected H9 hESCs. A) hESC colonies on mouse embryonic fibroblast feeder layer, pre-neomycin exposure. B) Cultures were exposed to a half dose of typically 0.2856 ug/ml of neomycin for 4 days. Elimination of non-neomycin resistant fibroblast feeders shows the resistance of the hESC colonies. (x4)

Result: G418 selection eradicated uninfected MEF feeder layers. Intact hESC colonies remained after 4 days of G418 exposure confirming successful viral infection and Rex-Neo^r functionality.

Tie2 driven mCherry Expression and Puromycin Resistance

hESCs were subsequently differentiated using traditional serum methods. [93] First, differentiated hESCs were stained with lectin to visualize ECs in differentiating cultures. (Figure 47) Additionally, in T2M-modified hESCs, cells were probed for mCherry expression under fluorescence microscopy. (Figure 48) T2P-modified hESCs were treated with 1mg/ml of puromycin for 24 hours and processed for PCR changes in EC markers, Tie2 and CD31. (Figure 49 and Figure 50) Timing of drug selection and EC

activity was determined to match the development of ECs in hESC cultures, with Tie2 expression detected from D1-D13 of differentiation. [237]

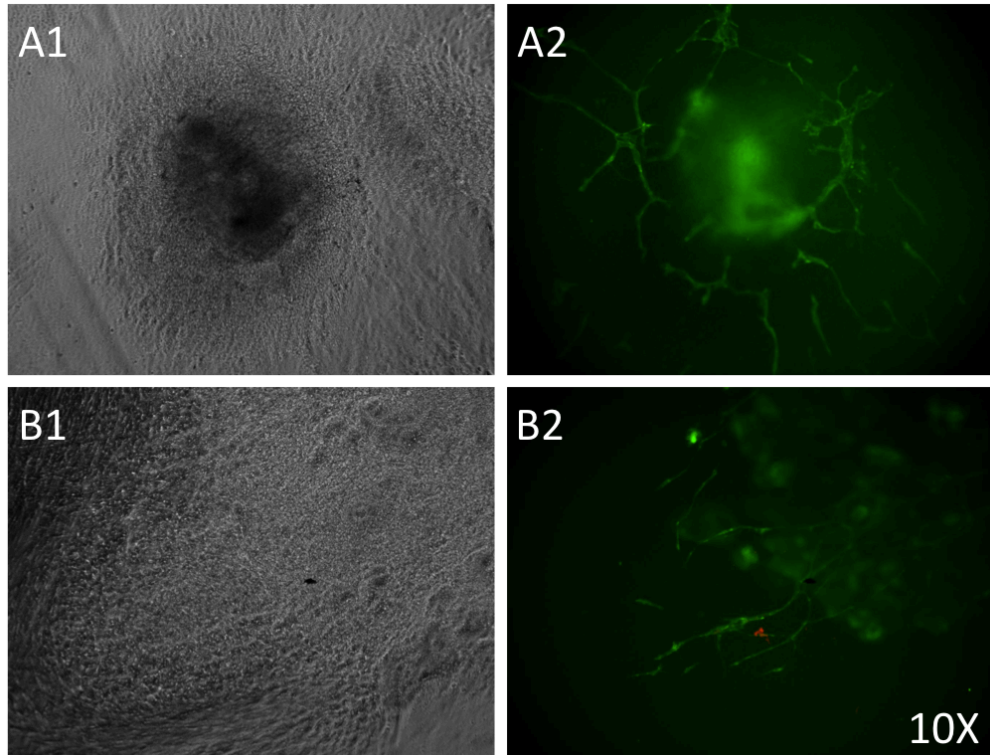


Figure 47 D17 hEB differentiation cultures of both (A) T2M and (B) T2P hESC lines, 10X. Bright field (A1 and B1) panels demonstrate the morphology of hEB cultures. Fluorescent imaging of differentiation cultures (A2 and B2) shows networks of lectin-stained ECs (green) but no cellular mCherry expression (red). Both cell lines exhibit EC differentiation.

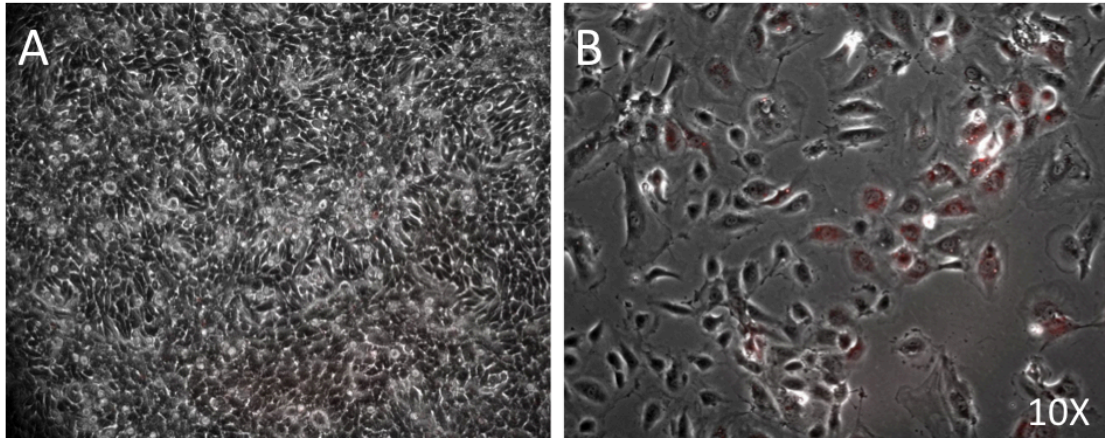


Figure 48 Evaluation of T2M functional specificity in HUVECs 7 days post-infection, 10X. L-cells (A) infected with the T2M construct do not express mCherry, whereas HUVECs (B) show expression of mCherry (red) in some of the cells. This evaluation shows that the T2M construct is not only functional, but also endothelial-specific to cells that express Tie2.

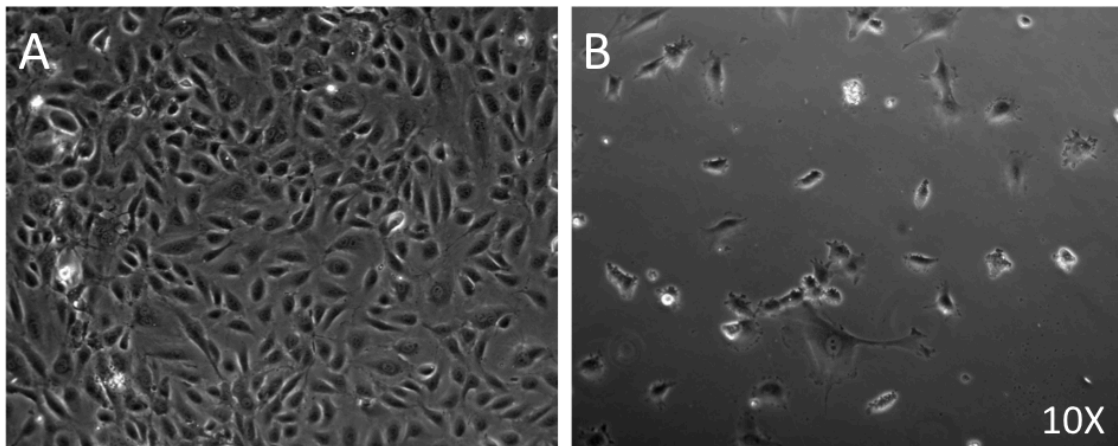


Figure 49 Evaluation of puromycin sensitivity in T2P-infected HUVECs, 10X. A comparison of untreated (A) and 24-hour puromycin-treated T2P-infected HUVECs shows that the construct can confer puromycin sensitivity in mature ECs.

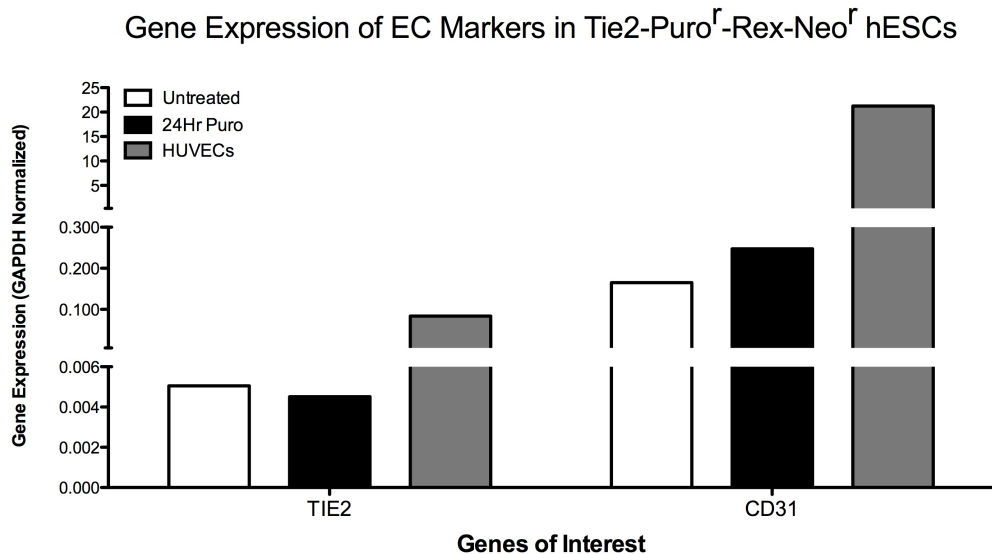


Figure 50 Gene expression of Tie2 and CD31 normalized to GAPDH in D25, T2P EB differentiation cultures. T2P-modified hESCs were differentiated to D25 to ensure an EC presence (confirmed with lectin staining). Untreated (white), 24-hour puromycin (1mg/ml) treated (black), and HUVEC controls (grey) EB cultures were processed for qPCR and probed for expression of EC markers.

Result: We did not detect mCherry expression in any of the differentiating cultures

despite evidence of EC differentiation and mRNA expression of Tie2 and CD31.

Additionally, treatment with puromycin did not seem to enrich for ECs as treated and untreated samples exhibited relatively similar gene expression profiles or complete cell death. FACS of differentiated T2M hESCs at different developmental stages (D4 or D17) for mCherry-positive cells was unsuccessful because of the inability to detect mCherry signal. Although it is important to note that at both time points, small fractions of KDR+ cells were detected, suggesting the presence of EC progenitors.[70, 98]

Infection of HUVECs with both T2P and T2M constructs demonstrated functionality of the constructs, which was not observed in non-endothelial cell types. We also noted that expression of Tie2 was much lower in EB differentiation cultures than in

HUVEC controls. Thus, we hypothesized that upregulation of Tie2 expression would be required for EC selection to occur.

B.4 Tie2 Upregulation Trials

B.4.1 Endothelial Differentiation Conditions

Rationale: Although traditional serum-based differentiation conditions did spur EC differentiation and the formation of putative vascular networks (Figure 47), we hypothesized that specific EC differentiation conditions may upregulate Tie2 expression and thus puromycin resistance and mCherry expression.

Methods: Endothelial differentiation was initiated with EB formation. Instead of standard 20% hEB differentiation media, an endothelial differentiation media was used. (Appendix 1) After 7 days of suspension culture, EBs were plated on 10 $\mu\text{g/ml}$ type I collagen (Sigma, Cat# C3867, St. Louis, MO) diluted in dPBS. ECs were assayed around D21 of culture.

Results: We compared EC conditions versus traditional serum-based differentiation methods. First, we examined differences in lectin expression in differentiated cultures in both T2M and T2P cell lines. Although in the T2M cultures (D25), EC networks appeared denser with EC differentiation conditions, mCherry expression was not detected. (Figure 51) PCR of T2P cultures also revealed that Tie2 expression was similar in both untreated and 24-hour treated samples. (Figure 52) Thus, Tie2 expression and hESC-derived ECs were not enriched even with endothelial differentiation protocols.

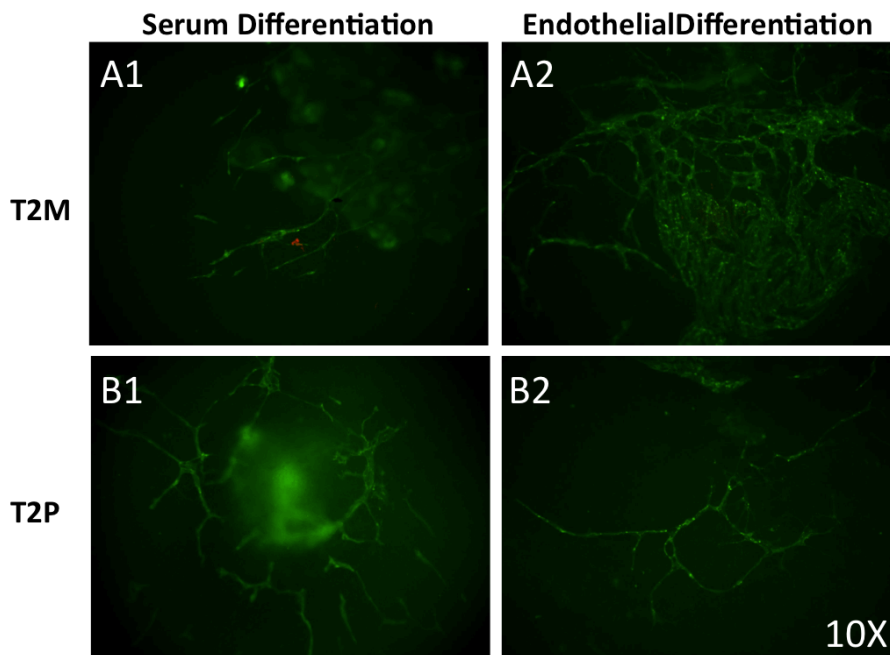


Figure 51 Comparison of traditional versus endothelial differentiation conditions, 10X. (A1) and (B1) depict T2M and T2P hESCs, respectively, differentiated with serum conditions. (A2) and (B2) depict T2M and T2P hESCs, respectively, differentiated with EC conditions. All cultures were stained with lectin (green) and evaluated for mCherry expression (red). mCherry could not be resolved.

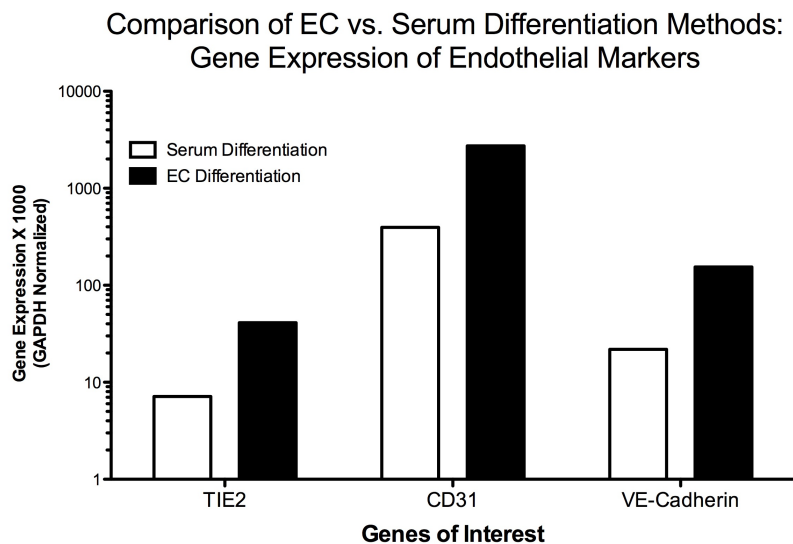


Figure 52 Gene expression profile of T2P hESCs differentiated in both traditional serum (white) and endothelial (black) differentiation protocols. Gene expression of endothelial markers, although upregulated in EC differentiation conditions, did not confer mCherry expression or puromycin resistance. α MHC expression was also tested

B.4.2 Shear Experiments

Rational: It has been shown previously, that shear stress upregulates Tie2 expression in ECs. [246] To induce Tie2 expression, EC-selectable hESCs were cultured under shear conditions using a perfusion shear system.

Methods: The flow experiments were performed using a rectangular flow channel described previously [247] with minor modifications so that multiple channels could be perfused simultaneously. All flow components were autoclaved for sterility. On D36 of differentiation, EBs derived from the Tie2-mCherry hESC line were dissociated using 0.25% trypsin and plated at confluence on 38 mm x 76 mm glass slides coated with 10 μ g/ml type I collagen. Once dissociated EBs were allowed to attach for 24 hours, cell-coated slides were assembled into the flow channel. The system was tightly sealed using a silicon gasket and a vacuum line. Perfusion experiments were performed in a cell-culture incubator under constant 95%O₂ and 5% CO₂ conditions at 37°C. Shear stress applied to the cells in the flow channel was 12 dynes/cm² to induce Tie2 expression. [246] After no shear, 48-, or 72-hour shear exposure, cells were either processed for immunostaining or qPCR analyses.

Results: mCherry expression could not be detected in either 48- or 72-hour shear exposure conditions. (Figure 54) PCR analysis of gene expression between static and shear stressed D37, T2M EB differentiation cultures show that 48-hours of shear stress cause a downregulation of EC markers with about similar expression levels in 72-hour shear conditions compared to static controls. (Figure 53)

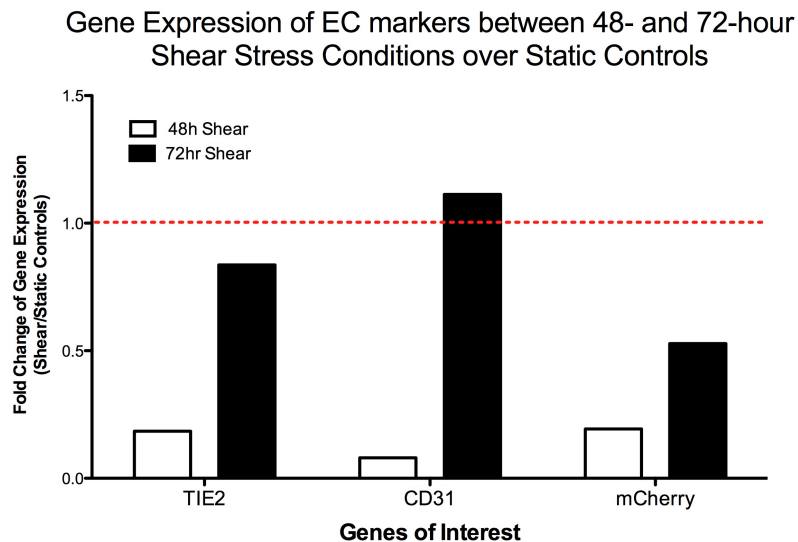


Figure 53 Gene expression of EC markers for D35, T2M differentiation cultures subjected to 48- and 72-hour shear stress. Fold change of expression over static controls is shown for Tie2, CD31, and mCherry expression.

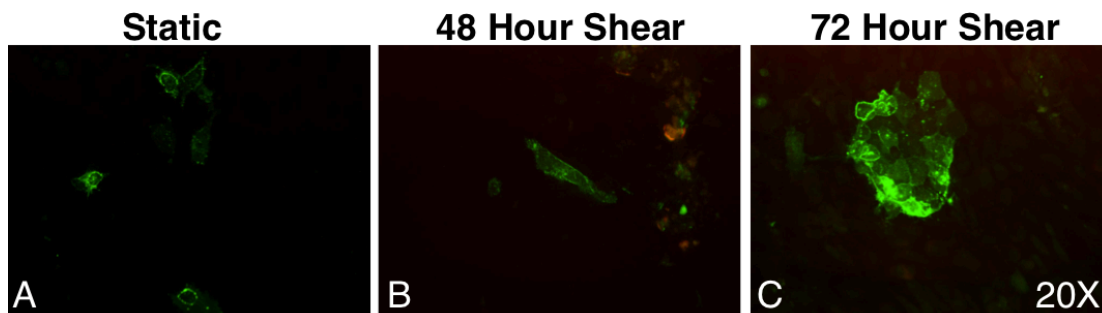


Figure 54 mCherry expression in D37 T2M differentiation cultures in static (A), 48-hour shear (B), and 72-hour shear (C) conditions, 20X. ECs were stained with lectin (green). mCherry expression (red) could not be detected in the cells. Non-specific red signal was detected in (B), but the same expression pattern was seen in all other channels as well.

B.4.3 Hypoxia Experiments

Rationale: 1% hypoxia conditions have been shown to induce upregulation of Tie2 after 24-hour exposure in a variety of endothelial cell types. [191, 192] Upon reoxygenation, the upregulation is reversible. Although the magnitude of increased expression differs

depending on the type of EC studied, we tested this method of upregulating Tie2 in hESC-derived ECs in order to assay the function of our Tie2 reporter lines.

Methods: Hypoxia experiments were performed on EBs formed from the Tie2-mCherry cell line using the Ex Vivo Hypoxia Chamber system (BioSpherix, Inc., XVivo System, Lacona, NY). EBs were cultured in endothelial cell inducing media conditions for 14 or 15 days upon which EBs were introduced to 1% O₂ hypoxia conditions for 24- or 48-hours. Control samples were cultured at normoxia (5% CO₂, 95% O₂ at 37°C). All samples were fixed on D16 of differentiation immediately at the time point specified. One sample was maintained for an additional 24 hours at normoxia (reoxygenation). Samples were analyzed with qPCR for EC markers (Tie2 and CD31), mCherry expression, and Glut1, a gene known to be upregulated in response to hypoxia, and fluorescence microscopy.

Results: With qPCR, we did not observe upregulation of Tie2, or any of the markers assayed. Glut1, positive controls, however, were upregulated in response to hypoxia at both 24- and 48-hour exposure. (Figure 55) Accordingly, we also did not observe mCherry expression at any time point.

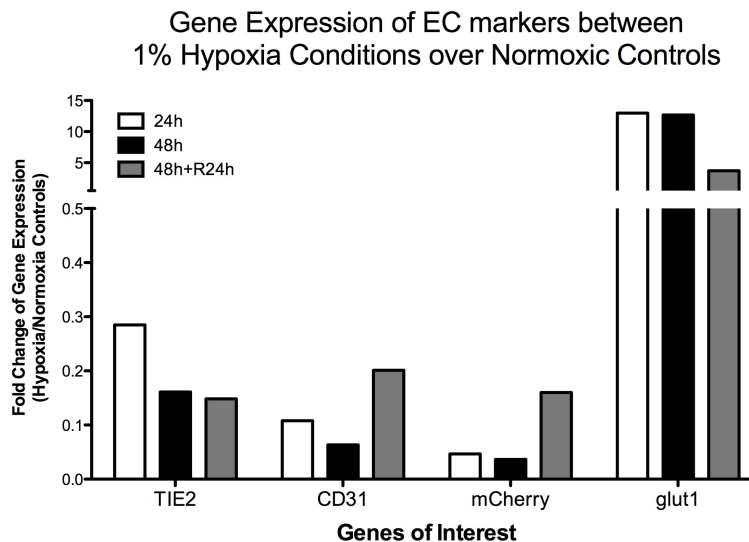


Figure 55 Gene expression of T2M hESC differentiation cultures (D17) in response to 1% hypoxia conditions. Cultures were dissociated and exposed to 24- and 48-hour hypoxic conditions. Samples were fixed and processed immediately at each time point. One sample was then returned to normoxic conditions for 24 hours. No upregulation of EC markers or reporter genes were observed, except in the expression of the positive control, Glut1.

B.4.4 FoxC2/Etv2 Induction of Tie2 Expression

Rationale: It has been demonstrated that FoxC2 and Etv2 together enhance expression of vascular genes. Co-expression of both factors induces ectopic endothelial-specific gene expression in developing *Xenopus* embryos. In addition, this group detected the presence of Fox:Ets motifs in the enhancer regions of many vascular genes, including Tie2. By transfecting constructs that induce ubiquitous expression of both factors along with endothelial-specific promoter/reporter constructs, such as Tie2-lacZ, the combined action of FoxC2 and Etv2 robustly activates reporter activity (~30 fold, Tie2). [248] Thus, we used the same FoxC2 and Etv2 expression vectors to upregulate expression of Tie2 in differentiating T2M hESC-derived cultures in order to assay functionality of our reporter constructs in hESC-derived ECs.

Methods: Transient transfection with FoxC2 and Etv2 factors were conducted in non-endothelial L-cell fibroblasts. It has been shown previously that co-transfection of FoxC2 and Etv2 factors can upregulate endothelial marker expression and, in particular, Tie2. [248] Lentiviral plasmids (pLenti6 backbone; Invitrogen, Cat# V496-10, Carlsbad, CA) with a PGK promoter driving either FoxC2 or Etv2 expression from the lab database were used. The conditions outlined in Table 9 were evaluated.

Table 9 Table of transfection conditions for FoxC2/Etv2 upregulation of Tie2 expression.

	Condition	Cells Tested	Legend
1	T2M_X_X	L-Cell Fibroblasts	X=Empty PGK vector
2	X_F_E	L-Cell Fibroblasts	P=PGK-GFP
3	T2M_P_X	L-Cell Fibroblasts	F=pLenti FoxC2
4	T2M_F_X	L-Cell Fibroblasts	E=pLenti Etv2
5	T2M_X_E	L-Cell Fibroblasts	
6	T2M_F_E	L-Cell Fibroblasts	
7	No transfection	L-Cell Fibroblasts	
8	T2M_X_X	HUVECs	
9	T2M_P_X	HUVECs	
10	No transfection	HUVECs	

Transfections were performed in triplicate and conducted as recommended by the manufacturer. Briefly, cells were plated in 48-well format at 20,000 cells per well. In each case, 100ng of each plasmid (300 ng DNA total) was diluted in OptiMEM I Reduced Serum media (Invitrogen, Cat# 11058-021, Carlsbad, CA). Samples were incubated with PLUS reagent (0.2 μ l/well) for 15 minutes at room temperature and then further diluted with Lipofectamine LTX (0.6 μ l/well) and incubated for 25 minutes. Transfection agents were then added to the cells and incubated for 4-8 hours at 37°C. After transfection, wells were imaged with fluorescence microscopy to detect GFP expression to detect the transfection efficiency. Cells were also monitored for mCherry expression. ImageJ was used to quantify fluorescence intensity of the transfected cells.

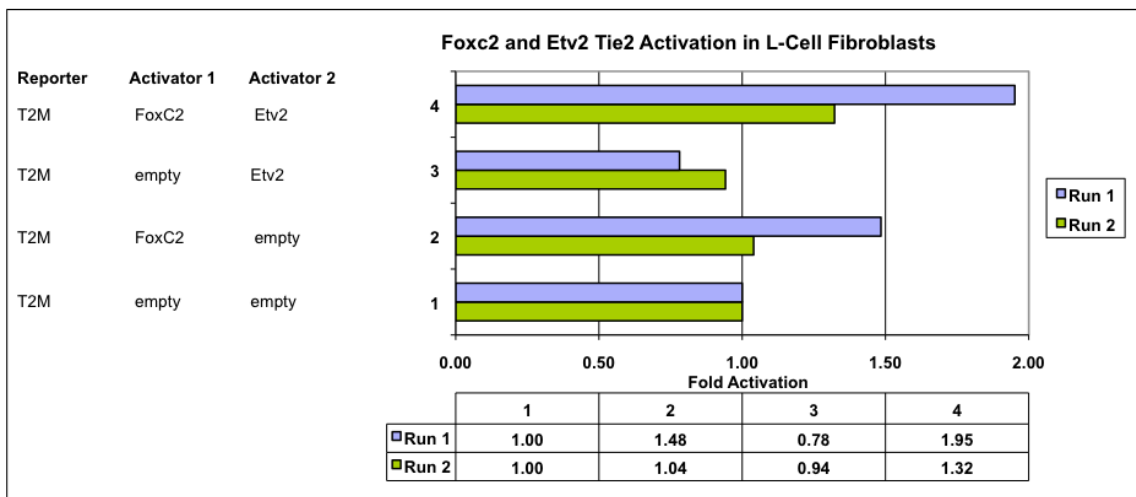


Figure 56 Activation of T2M reporter with FoxC2/Etv2 co-expression in transfected L-Cell fibroblasts. Coexpression of FoxC2 and Etv2 factors enhances the activation of the T2M reporter when transfected in non-endothelial L-Cell fibroblasts by almost 2-fold.

Results: In this transfection experiment, we demonstrated that co-expression of FoxC2 and Etv2 in L-Cell fibroblasts can enhance T2M reporter activity as assayed through mCherry expression. (Figure 56) This suggests the utility of our construct. However, the level of enhancement observed in our reporter assay pales in comparison to the 30-fold activation observed in the work presented by De Val et al. [248] We attempted to transfect KDR+, FACS-sorted cells with FoxC2 and Etv2 factors, but due to contamination of cultures post-FACS and low yield in sorting experiments, we did not pursue this avenue further.

B.4.5 Teratoma Formation

Rationale: Teratoma formation is a widely used method to test the pluripotency of putative stem cells. When pluripotent cells are injected into immune-compromised mice, they can form teratomas, which are tumors composed of cells derived from all three embryonic germ layers. [93] Although we were able to demonstrate endothelial

specification from both T2P and T2M hESC lines after differentiation, it was unclear whether the failure of reporter activity related to the immaturity of the ECs, and thus low levels of Tie2 expression, that were formed. As we demonstrated that reporter activity could be detected in more mature endothelial cell sources (HUVECs), we hypothesized that the developmental stage of ECs in hESC differentiation cultures may not be sufficient to activate Tie2 reporter activity. Thus, we decided to use the teratoma as a vehicle to generate more mature, functional vasculature from T2M-modified hESCs in order to induce reporter activity.

Methods: For transplantation, animals were anesthetized by isoflurane liquid (Baxter, Inc., Cat# NDC 10019-773-60, Deerfield, IL) by inhalation (.015 - .017 ml/gram body weight IP). The level of anesthesia was monitored by the tail pinch response.

Supplementary anesthetic doses were given as required. Surgical sites and shave sites were scrubbed with Nolvasan (Pfizer, Inc., Cat# 300253, New York, NY). A straight longitudinal 1cm incision was made in the skin left lateral to the spine between the ribs and pelvis. A shorter incision was made in the muscle approximately 0.5cm lower than the last rib. Through the incision, the kidney was transferred extracorporeally for the procedure while constantly kept moist with sterile Ringers solution. Under the dissecting microscope, a 1-2mm incision was made in the kidney capsule. A heat-sealed, drawn and blunted glass capillary was used to create a pocket between the capsule and the kidney. A sterile transfer pipette (Hamilton Company, Reno, NV) was used to transfer 10-20 μ l of densely packed hESC-derived EBs from the Tie2-mCherry-Rex-Neo^r line into the kidney capsule. The kidney was subsequently repositioned into the abdominal cavity. The abdominal wall was sutured and clamped with wound clips. Animals were monitored for tumor growth over a 6-10-week period for teratoma formation to occur. Upon tumor

formation, animals were sacrificed and the teratoma was removed. Teratomas were fixed in 4% PFA overnight with constant agitation at 4°C. Kidney and tumor tissue were then dehydrated and embedded in paraffin blocks. Blocks were sectioned at 5µm thickness and mounted on glass slides for histological haemotoxilin-eosin staining and immunostaining for Tie2 and mCherry expression.

Results: We could not detect mCherry expression in the teratomas. As most teratoma vasculature is derived from the murine host, hESC differentiation to ECs would in any event be rare.

B.5 Conclusions

In these studies, we were able to generate T2M and T2P lentiviral constructs and create hESC cell lines genetically-modified with both of these constructs. Despite the endothelial-specific functionality of these constructs in HUVECs, we could not confer the same functionality in hESC-derived ECs. Attempts to upregulate Tie2 expression in our hESC differentiation cultures also did not bolster the expression of reporters.

The reasons for why these cell lines could not confer reporter activity are multifarious. First, we did not establish clonal hESC lines. Therefore, it has been suggested that expansion of mixed populations can reduce the percentages of expressing cells due to reasons such as transgene silencing and non-integrated provirus. [74] In addition, expression levels of the transgene could be varied in different hESCs due to differences in number and locations of virus integration sites. Second, our lack of understanding of EC development and biology may have significantly hampered the design and development of these hESC lines. Third, to construct the T2M and T2P

constructs, we implemented the 2.0kb Tie2 promoter with the minimal 1.7 kb enhancer fragment instead of the 10kb full enhancer. [241] This choice may be one reason for why Tie2 promoter activity, which has already been documented as low in ESC-derived ECs, was undetectable. Although in in vitro studies, using the minimal enhancer fragment did not reduce tie2 reporter activity in transfected bovine aortic endothelial cells (BAECs), Schlaeger et al suggested that regulatory elements outside of this minimal enhancer fragment but within the 10kb full enhancer may be necessary for uniform expression of reporter activity in the Tie2-Lacz-modified murine adult vasculature. This group also discussed the sensitivity of the minimal fragment to its integration sites in terms of reporter activity.

Because the initial goal of these experiments was to study CM-EC interactions on CM maturation, our endeavors with creating, validating, and understanding this biological co-culture tool deviated from the objectives of the dissertation. Thus, we were not able to fully develop the functionality of these EC-selectable hESC lines and refocused our efforts on the original hypotheses of the dissertation.

B.6 Acknowledgements

I would like to thank Drs. Maria Barcova and Hiroko Kita-Matsuo for their counsel on cloning strategies and PCR techniques; Dr. Jeff Lindquist for his advice on endothelial differentiation of H9 hESCs; Yoav Altman for his counsel and help with FACS; Dr. Shu Chien and his lab members, Dr. Julie Li and Phu Pham, for their help and expertise with the shear stress studies; Dr. Natalia Kan for her help with the teratoma studies; and Drs. Mark Mercola and Andrew McCulloch for discussion and direction.

References

1. Rosamond, W., et al., *Heart Disease and Stroke Statistics--2007 Update: A Report From the American Heart Association Statistics Committee and Stroke Statistics Subcommittee*. *Circulation*, 2007. **115**(5): p. e69-171.
2. Zimmermann, W.-H., et al., *Engineered heart tissue grafts improve systolic and diastolic function in infarcted rat hearts*. *Nature Medicine*, 2006. **12**(4): p. 452-458.
3. Laflamme, M.A., et al., *Formation of Human Myocardium in the Rat Heart from Human Embryonic Stem Cells*. *American Journal of Pathology*, 2005. **167**(3): p. 663-671.
4. Chien, K.R., I.J. Domian, and K.K. Parker, *Cardiogenesis and the Complex Biology of Regenerative Cardiovascular Medicine*. *Science*, 2008. **322**(5907): p. 1494-1497.
5. Vunjak-Novakovic, G., et al., *Challenges in Cardiac Tissue Engineering*. *Tissue Engineering: Part B*, 2010. **16**(2).
6. Katz, A.M., *Physiology of the Heart*. Third ed. 2001, Philadelphia: Lippincott Williams & Wilkins. 718.
7. Bennett, V. and J. Healy, *Being there: cellular targeting of voltage-gated sodium channels in the heart*. *The Journal of Cell Biology*, 2008. **180**(1): p. 13-15.
8. Oyamada, M., et al., *The Expression, Phosphorylation, and Localization of Connexin 43 and Gap-Junctional Intercellular Communication during the Establishment of a Synchronized Contraction of Cultured Neonatal Rat Cardiac Myocytes*. *Experimental Cell Research*, 1994. **212**(2): p. 351-358.
9. Hirschy, A., et al., *Establishment of cardiac cytoarchitecture in the developing mouse heart*. *Developmental Biology*, 2006. **289**(2): p. 430-441.

10. Parker, K.K., et al., *Myofibrillar Architecture in Engineered Cardiac Myocytes*. Circulation Research, 2008. **103**(4): p. 340-342.
11. Gopalan, S.M., et al., *Anisotropic stretch-induced hypertrophy in neonatal ventricular myocytes micropatterned on deformable elastomers*. Biotechnology and Bioengineering, 2003. **81**(5): p. 578-587.
12. LeGrice, I.J., et al., *Laminar structure of the heart: ventricular myocyte arrangement and connective tissue architecture in the dog*. American Journal of Physiology - Heart and Circulatory Physiology, 1995. **269**(2): p. H571-H582.
13. Cukierman, E., et al., *Taking Cell-Matrix Adhesions to the Third Dimension*. Science, 2001. **294**(5547): p. 1708-1712.
14. Banerjee, I., et al., *Determination of cell types and numbers during cardiac development in the neonatal and adult rat and mouse*. American Journal of Physiology - Heart and Circulatory Physiology, 2007. **293**(3): p. H1883-H1891.
15. Banerjee, I., et al., *Dynamic Interactions between Myocytes, Fibroblasts, and Extracellular Matrix*. Annals of the New York Academy of Sciences, 2006. **1080**(Interactive and Integrative Cardiology): p. 76-84.
16. Hsieh, P.C.H., et al., *Endothelial-Cardiomyocyte Interactions in Cardiac Development and Repair*. Annual Review of Physiology, 2006. **68**(1): p. 51-66.
17. Souders, C.A., S.L.K. Bowers, and T.A. Baudino, *Cardiac Fibroblast: The renaissance cell*. Circulation Research, 2009. **105**(12): p. 1164-1176.
18. Yamazaki, T., et al., *Interaction of cardiac myocytes and non-myocytes in mechanical stress-induced hypertrophy*. Herz, 1995. **20**(2): p. 109-117.
19. Brutsaert, D.L., *Cardiac Endothelial-Myocardial Signaling: Its Role in Cardiac Growth, Contractile Performance, and Rhythmicity*. Physiological Reviews, 2003. **83**(1): p. 59-115.
20. Hunziker, R., *Fact Sheet: Regenerative Medicine*. 2010, National Institutes of Biomedical Imaging and Bioengineering (NIBIB).
21. *Principles of Regenerative Medicine*. 3 ed, ed. A. Atala, et al. 2008: Academic Press. 1472.
22. Palsson, B. and S. Bhatia, *Tissue Engineering*. 2004, Saddle River, NJ: Pearson Prentice Hall.
23. Vunjak-Novakovic, G., et al., *Bioengineering Heart Muscle: A Paradigm for Regenerative Medicine*. Annual Review of Biomedical Engineering, 2011. **13**(1).
24. Bergmann, O., et al., *Evidence for Cardiomyocyte Renewal in Humans*. Science, 2009. **324**(5923): p. 98-102.

25. Carvalho, A. and A. de Carvalho, *Heart regeneration: past, present, and future*. World Journal of Cardiology, 2010. **2**: p. 107-111.
26. Murry, C.E., L.J. Field, and P. Menasche, *Cell-Based Cardiac Repair: Reflections at the 10-Year Point*. Circulation, 2005. **112**(20): p. 3174-3183.
27. Murry, C.E., H. Reinecke, and L.M. Pabon, *Regeneration Gaps: Observations on Stem Cells and Cardiac Repair*. Journal of the American College of Cardiology, 2006. **47**(9): p. 1777-1785.
28. Harrison, M., A. Anyanwu, and S.P. Pinney, *The Management of Stage D Heart Failure*. Mount Sinai Journal of Medicine: A Journal of Translational and Personalized Medicine, 2009. **76**(4): p. 404-414.
29. Wolfe RA, R.E., Merion RM, *Trends in organ donation and transplantation in the United States, 1998-2008*. American Journal of Transplantation, 2010. **10**(4 part 2): p. 961-972.
30. Laflamme, M.A. and C.E. Murry, *Heart regeneration*. Nature, 2011. **473**(7347): p. 326-335.
31. Menasche, P., *Cardiac cell therapy: Lessons from clinical trials*. Journal of Molecular and Cellular Cardiology, 2011. **50**(2): p. 258-265.
32. van Laake, L.W., et al., *Human embryonic stem cell-derived cardiomyocytes survive and mature in the mouse heart and transiently improve function after myocardial infarction*. Stem Cell Research, 2007. **1**(1): p. 9-24.
33. Orlic, D., et al., *Bone marrow cells regenerate infarcted myocardium*. Nature, 2001. **410**(6829): p. 701-705.
34. Orlic, D., *BM stem cells and cardiac repair: where do we stand in 2004?* Cytotherapy, 2005. **7**(1): p. 3-15.
35. Laflamme, M.A., et al., *Cardiomyocytes derived from human embryonic stem cells in pro-survival factors enhance function of infarcted rat hearts*. Nature Biotechnology, 2007. **25**(9): p. 1015-1024.
36. Reffelmann, T. and R.A. Kloner, *Cellular cardiomyoplasty, cardiomyocytes, skeletal myoblasts, or stem cells for regenerating myocardium and treatment of heart failure?* Cardiovascular Research, 2003. **58**(2): p. 358-368.
37. Muller-Ehmsen, J., et al., *Rebuilding a Damaged Heart: Long-Term Survival of Transplanted Neonatal Rat Cardiomyocytes After Myocardial Infarction and Effect on Cardiac Function*. Circulation, 2002. **105**(14): p. 1720-1726.
38. Roell, W., et al., *Cellular Cardiomyoplasty Improves Survival After Myocardial Injury*. Circulation, 2002. **105**(20): p. 2435-2441.

39. Sakai, T., et al., *Fetal Cell Transplantation: A Comparison of Three Cell Types*. Journal of Thoracic Cardiovascular Surgery, 1999. **118**(4): p. 715-725.
40. van Laake, L.W., et al., *Improvement of mouse cardiac function by hESC-derived cardiomyocytes correlates with vascularity but not graft size*. Stem Cell Research, 2009. **3**(2-3): p. 106-112.
41. Fujii, T., et al., *Cell transplantation to prevent heart failure: a comparison of cell types*. Annals of Thoracic Surgery, 2003. **76**(6): p. 2062-2070.
42. Lunde, K., et al., *Intracoronary Injection of Mononuclear Bone Marrow Cells in Acute Myocardial Infarction*. New England Journal of Medicine, 2006. **355**(12): p. 1199-1209.
43. Fernandez-Aviles, F., et al., *Experimental and Clinical Regenerative Capability of Human Bone Marrow Cells After Myocardial Infarction*. Circulation Research, 2004. **95**(7): p. 742-748.
44. Sans-Ruiz, R., et al., *Phases I-III Clinical Trials Using Adult Stem Cells*. Stem Cells International, 2010. **2010**(579142).
45. Forte, E., et al., *Cardiac Cell Therapy: The Next (Re)Generation*. Stem Cell Reviews and Reports, 2011: p. 1-13.
46. Farahmand, P., et al., *Skeletal Myoblasts Preserve Remote Matrix Architecture and Global Function When Implanted Early or Late After Coronary Ligation Into Infarcted or Remote Myocardium*. Circulation, 2008. **118**(14_suppl_1): p. S130-137.
47. Leor, J. and S. Cohen, *Myocardial Tissue Engineering: Creating a Muscle Patch for a Wounded Heart*. Annals of the New York Academy of Sciences, 2004. **1015**(1): p. 312-319.
48. Radisic, M., et al., *High-density seeding of myocyte cells for cardiac tissue engineering*. Biotechnology and Bioengineering, 2003. **82**(4): p. 403-414.
49. Radisic, M., et al., *Medium perfusion enables engineering of compact and contractile cardiac tissue*. American Journal of Physiology - Heart and Circulatory Physiology, 2004. **286**(2): p. H507-H516.
50. Maidhof, R., et al., *Perfusion seeding of channeled elastomeric scaffolds with myocytes and endothelial cells for cardiac tissue engineering*. Biotechnology Progress, 2010. **26**(2): p. 565-572.
51. Dvir, T., et al., *A Novel Perfusion Bioreactor Providing a Homogenous Milieu for Tissue Regeneration*. Tissue Engineering, 2006. **12**(10): p. 2843-2852.
52. Stevens, K.R., et al., *Scaffold-Free Human Cardiac Tissue Patch Created from Embryonic Stem Cells*. Tissue Engineering Part A, 2009. **15**(6): p. 1211-1222.

53. Eschenhagen, T., et al., *Three-dimensional reconstitution of embryonic cardiomyocytes in a collagen matrix: a new heart muscle model system*. The FASEB Journal, 1997. **11**(8): p. 683-694.
54. Shimizu, T., et al., *Cell sheet engineering for myocardial tissue reconstruction*. Biomaterials, 2003. **24**(13): p. 2309-2316.
55. Li, R.-K., et al., *Survival and Function of Bioengineered Cardiac Grafts*. Circulation, 1999. **100**(90002): p. II-63-69.
56. Ozawa, T., et al., *Optimal Biomaterial for Creation of Autologous Cardiac Grafts*. Circulation, 2002. **106**(90121): p. I-176-182.
57. Dar, A., et al., *Optimization of cardiac cell seeding and distribution in 3D porous alginate scaffolds*. Biotechnology and Bioengineering, 2002. **80**(3): p. 305-312.
58. Ott, H.C., et al., *Perfusion-decellularized matrix: using nature's platform to engineer a bioartificial heart*. Nature Medicine, 2008. **14**(2): p. 213-221.
59. Zimmermann, W.H., et al., *Tissue Engineering of a Differentiated Cardiac Muscle Construct*. Circulation Research, 2002. **90**(2): p. 223-230.
60. Simpson, D.G., et al., *Regulation of Cardiac Myocyte Protein Turnover and Myofibrillar Structure In Vitro by Specific Directions of Stretch*. Circulation Research, 1999. **85**(10): p. e59-69.
61. Khademhosseini, A., et al., *Microfluidic patterning for fabrication of contractile cardiac organoids*. Biomedical Microdevices, 2007. **9**(2): p. 149-157.
62. Zwi-Dantsis, L., et al., *Scalable Production of Cardiomyocytes Derived from c-Myc Free Induced Pluripotent Stem Cells*. Tissue Engineering Part A, 2011. **17**(7-8): p. 1027-1037.
63. Zandstra, P.W., et al., *Scalable Production of Embryonic Stem Cell-Derived Cardiomyocytes*. Tissue Engineering, 2003. **9**(4): p. 767-778.
64. Niebruegge, S., et al., *Cardiomyocyte Production in Mass Suspension Culture: Embryonic Stem Cells as a Source for Great Amounts of Functional Cardiomyocytes*. Tissue Engineering Part A, 2008. **14**(10): p. 1591-1601.
65. Miyagawa, S., et al., *Tissue cardiomyoplasty using bioengineered contractile cardiomyocyte sheets to repair damaged myocardium: Their integration with recipient myocardium*. Transplantation, 2005. **80**(11): p. 1586-1595.
66. Hamdi, H., et al., *Cell Delivery: Intramyocardial Injections or Epicardial Deposition? A Head-to-Head Comparison*. The Annals of Thoracic Surgery, 2009. **87**(4): p. 1196-1203.

67. Zimmermann, W.H., *Embryonic and embryonic-like stem cells in heart muscle engineering*. Journal of Molecular and Cellular Cardiology, 2011. **50**(2): p. 320-326.
68. Rubart, M. and L.J. Field, *Cardiac Repair by embryonic stem-derived cells*. Handbook of Experimental Pharmacology, 2006. **174**: p. 73-100.
69. Huber, I., et al., *Identification and selection of cardiomyocytes during human embryonic stem cell differentiation*. The FASEB Journal, 2007. **21**(10): p. 2551-2563.
70. Kattman, S.J., et al., *Stage-Specific Optimization of Activin/Nodal and BMP Signaling Promotes Cardiac Differentiation of Mouse and Human Pluripotent Stem Cell Lines*. Cell Stem Cell, 2011. **8**(2): p. 228-240.
71. Mignone, J.L., et al., *Cardiogenesis From Human Embryonic Stem Cells- Mechanisms and Applications*. Circulation Journal, 2010. **74**(12): p. 2517-2526.
72. McDevitt, T.C., M.A. Laflamme, and C.E. Murry, *Proliferation of cardiomyocytes derived from human embryonic stem cells is mediated via the IGF/PI 3-kinase/Akt signaling pathway*. Journal of Molecular and Cellular Cardiology, 2005. **39**(6): p. 865-873.
73. Sargent, C.Y., G.Y. Berguig, and T.C. McDevitt, *Cardiomyogenic Differentiation of Embryoid Bodies Is Promoted by Rotary Orbital Suspension Culture*. Tissue Engineering Part A, 2009. **15**(2): p. 331-342.
74. Kita-Matsuo, H., et al., *Lentiviral Vectors and Protocols for Creation of Stable hESC Lines for Fluorescent Tracking and Drug Resistance Selection of Cardiomyocytes*. PLoS ONE, 2009. **4**(4): p. e5046.
75. Kehat, I., et al., *Electromechanical integration of cardiomyocytes derived from human embryonic stem cells*. Nature Biotechnology, 2004. **22**(10): p. 1282-1289.
76. Dai, W., et al., *Survival and maturation of human embryonic stem cell-derived cardiomyocytes in rat hearts*. Journal of Molecular and Cellular Cardiology, 2007. **43**(4): p. 504-516.
77. Sekine, H., et al., *Endothelial Cell Coculture Within Tissue-Engineered Cardiomyocyte Sheets Enhances Neovascularization and Improves Cardiac Function of Ischemic Hearts*. Circulation, 2008. **118**(14_suppl_1): p. S145-152.
78. Tulloch, N.L., et al., *Growth of Engineered Human Myocardium With Mechanical Loading and Vascular Coculture*. Circ Res, 2011: p. Circulation Research.110.237206.
79. Klug, M., et al., *Genetically selected cardiomyocytes from differentiating embryonic stem cells form stable intracardiac grafts*. Journal of Clinical Investigations, 1996. **98**(1): p. 216-24.

80. Reinecke, H., et al., *Survival, Integration, and Differentiation of Cardiomyocyte Grafts : A Study in Normal and Injured Rat Hearts*. *Circulation*, 1999. **100**(2): p. 193-202.
81. Thomson, J.A., et al., *Embryonic Stem Cell Lines Derived from Human Blastocysts*. *Science*, 1998. **282**(5391): p. 1145-1147.
82. Park, I.-H., et al., *Reprogramming of human somatic cells to pluripotency with defined factors*. *Nature*, 2008. **451**(7175): p. 141-146.
83. Takahashi, K., et al., *Induction of pluripotent stem cells from fibroblast cultures*. *Nature Protocols*, 2007. **2**(12): p. 3081-3089.
84. Takahashi, K. and S. Yamanaka, *Induction of Pluripotent Stem Cells from Mouse Embryonic and Adult Fibroblast Cultures by Defined Factors*. *Cell*, 2006. **126**(4): p. 663-676.
85. Yu, J., et al., *Induced Pluripotent Stem Cell Lines Derived from Human Somatic Cells*. *Science*, 2007. **318**(5858): p. 1917-1920.
86. Gilbert, S.F., *Developmental Biology*. 8 ed. 2006, Sunderland: Sinauer Associates Inc.
87. Tam, P.P.L. and R.R. Behringer, *Mouse gastrulation: the formation of a mammalian body plan*. *Mechanisms of Development*, 1997. **68**(1-2): p. 3-25.
88. Mikawa, T., *Determination of heart cell lineages.*, in *Cell Lineage and Fate Determination*, S.A. Moody, Editor. 1999, Academic Press: San Diego. p. 451-462.
89. Harvey, R.P., *Patterning the vertebrate heart*. *Nature Reviews Genetics*, 2002. **3**(7): p. 544-556.
90. Kehat, I., et al., *Human embryonic stem cells can differentiate into myocytes with structural and functional properties of cardiomyocytes*. *Journal of Clinical Investigations*, 2001. **108**(3): p. 407-14.
91. Dolnikov, K., et al., *Functional Properties of Human Embryonic Stem Cell–Derived Cardiomyocytes: Intracellular Ca²⁺ Handling and the Role of Sarcoplasmic Reticulum in the Contraction*. *Stem Cells*, 2006. **24**(2): p. 236-245.
92. Willems, E., P. Bushway, and M. Mercola, *Natural and Synthetic Regulators of Embryonic Stem Cell Cardiogenesis*. *Pediatric Cardiology*, 2009. **30**(5): p. 635-642.
93. Loring, J., P. Schwartz, and R. Wesselschmidt, eds. *Human Stem Cell Manual: A Laboratory Guide*. 2006, Elsevier Inc.
94. Reubinoff, B.E., et al., *Embryonic stem cell lines from human blastocysts: somatic differentiation in vitro*. *Nature Biotechnology*, 2000. **18**(4): p. 399-404.

95. Mummery, C., et al., *Differentiation of Human Embryonic Stem Cells to Cardiomyocytes: Role of Coculture With Visceral Endoderm-Like Cells*. *Circulation*, 2003. **107**(21): p. 2733-2740.
96. Ménard, C., et al., *Cardiac specification of embryonic stem cells*. *Journal of Cellular Biochemistry*, 2004. **93**(4): p. 681-687.
97. Samuel, L.J. and B.V. Latinkifá, *Early Activation of FGF and Nodal Pathways Mediates Cardiac Specification Independently of Wnt/Beta-Catenin Signaling*. *PLoS ONE*, 2009. **4**(10): p. e7650.
98. Yang, L., et al., *Human cardiovascular progenitor cells develop from a KDR+ embryonic-stem-cell-derived population*. *Nature*, 2008. **453**(7194): p. 524-528.
99. Engler, A.J., et al., *Matrix Elasticity Directs Stem Cell Lineage Specification*. *Cell*, 2006. **126**(4): p. 677-689.
100. Reilly, G.C. and A.J. Engler, *Intrinsic extracellular matrix properties regulate stem cell differentiation*. *Journal of Biomechanics*, 2010. **43**(1): p. 55-62.
101. Tay, C.Y., et al., *Micropatterned matrix directs differentiation of human mesenchymal stem cells towards myocardial lineage*. *Experimental Cell Research*, 2010. **316**(7): p. 1159-1168.
102. Kitajima, S., et al., *MesP1 and MesP2 are essential for the development of cardiac mesoderm*. *Development*, 2000. **127**(15): p. 3215-3226.
103. Fijnvandraat, A.C., et al., *Cardiomyocytes derived from embryonic stem cells resemble cardiomyocytes of the embryonic heart tube*. *Cardiovascular Research*, 2003. **58**(2): p. 399-409.
104. Dolnikov, K., et al., *Functional Properties of Human Embryonic Stem Cell-Derived Cardiomyocytes*. *Annals of the New York Academy of Sciences*, 2005. **1047**(1): p. 66-75.
105. Zhu, W.-Z., L.F. Santana, and M.A. Laflamme, *Local Control of Excitation-Contraction Coupling in Human Embryonic Stem Cell-Derived Cardiomyocytes*. *PLoS ONE*, 2009. **4**(4): p. e5407.
106. Zwi, L., et al., *Cardiomyocyte Differentiation of Human Induced Pluripotent Stem Cells*. *Circulation*, 2009. **120**(15): p. 1513-1523.
107. Xu, C., et al., *Characterization and Enrichment of Cardiomyocytes Derived From Human Embryonic Stem Cells*. *Circulation Research*, 2002. **91**(6): p. 501-508.
108. He, J.-Q., et al., *Human Embryonic Stem Cells Develop Into Multiple Types of Cardiac Myocytes: Action Potential Characterization*. *Circulation Research*, 2003. **93**(1): p. 32-39.

109. Kolossov, E., et al., *Engraftment of engineered ES cell-derived cardiomyocytes but not BM cells restores contractile function to the infarcted myocardium*. *Journal of Experimental Medicine*, 2006. **203**(10): p. 2315-2327.
110. Hew, K.W. and K.A. Keller, *Postnatal anatomical and functional development of the heart: A species comparison*. *Birth Defects Research Part B: Developmental and Reproductive Toxicology*, 2003. **68**(4): p. 309-320.
111. Anderson, P.A.W., *Maturation and Cardiac Contractility*. *Cardiology Clinics*, 1989. **7**(2): p. 209-25.
112. Eisenstein, R. and G. Wied, *Myocardial DNA and protein in maturing and hypertrophied human hearts*. *Proclamations of the Society of Experimental Biology and Medicine*, 1970. **133**(1): p. 176-9.
113. Rakusan, K., N. Cicutti, and M. Flanagan, *Changes in the microvascular network during cardiac growth, development, and aging*. *Cellular and Molecular Biology Research*, 1994. **40**(2): p. 117-22.
114. Kehat, I., et al., *High-Resolution Electrophysiological Assessment of Human Embryonic Stem Cell-Derived Cardiomyocytes: A Novel In Vitro Model for the Study of Conduction*. *Circulation Research*, 2002. **91**(8): p. 659-661.
115. Liu, J., et al., *Functional Sarcoplasmic Reticulum for Calcium Handling of Human Embryonic Stem Cell-Derived Cardiomyocytes: Insights for Driven Maturation*. *Stem Cells*, 2007. **25**(12): p. 3038-3044.
116. Muhl, C., W. Dassen, and H. Kuipers, *Cardiac remodelling: concentric versus eccentric hypertrophy in strength and endurance athletes*. *Netherlands Heart Journal*, 2008. **16**(4): p. 129-133.
117. Fisher, D. and J. Towbin, *Maturation of the heart*. *Clinical Perinatology*, 1988. **15**(3): p. 421-46.
118. Gerdes, A.M. and J.M. Capasso, *Structural remodeling and mechanical dysfunction of cardiac myocytes in heart failure*. *Journal of Molecular and Cellular Cardiology*, 1995. **27**(3): p. 849-856.
119. Bray, M.-A., S.P. Sheehy, and K.K. Parker, *Sarcomere alignment is regulated by myocyte shape*. *Cell Motility and the Cytoskeleton*, 2008. **65**(8): p. 641-651.
120. Snir, M., et al., *Assessment of the ultrastructural and proliferative properties of human embryonic stem cell-derived cardiomyocytes*. *American Journal of Physiology - Heart and Circulatory Physiology*, 2003. **285**(6): p. H2355-H2363.
121. Reiser, P.J., et al., *Human cardiac myosin heavy chain isoforms in fetal and failing adult atria and ventricles*. *American Journal of Physiology - Heart and Circulatory Physiology*, 2001. **280**(4): p. H1814-H1820.

122. Cui, L., et al., *Structural differentiation, proliferation, and association of human embryonic stem cell-derived cardiomyocytes in vitro and in their extracardiac tissues*. Journal of Structural Biology, 2007. **158**(3): p. 307-317.
123. Cao, F., et al., *Transcriptional and Functional Profiling of Human Embryonic Stem Cell-Derived Cardiomyocytes*. PLoS ONE, 2008. **3**(10): p. e3474.
124. Levick, J.R., *Introduction to Cardiovascular Physiology*. Fourth Edition ed. 2003, London: Arnold.
125. Simpson, D.G., et al., *Mechanical regulation of cardiac myocyte protein turnover and myofibrillar structure*. American Journal of Physiology - Cell Physiology, 1996. **270**(4): p. C1075-1087.
126. Battista, S., et al., *The effect of matrix composition of 3D constructs on embryonic stem cell differentiation*. Biomaterials, 2005. **26**(31): p. 6194-6207.
127. Akhyari, P., et al., *Mechanical Stretch Regimen Enhances the Formation of Bioengineered Autologous Cardiac Muscle Grafts*. Circulation, 2002. **106**(90121): p. 1371--142.
128. MacKenna, D.A., et al., *Extracellular Signal-regulated Kinase and c-Jun NH2-terminal Kinase Activation by Mechanical Stretch Is Integrin-dependent and Matrix-specific in Rat Cardiac Fibroblasts*. Journal of Clinical Investigation, 1998. **101**(2): p. 301-310.
129. Sadoshima, J. and S. Izumo, *The cellular and molecular response of cardiac myocytes to mechanical stress*. Annual Review of Physiology, 1997. **59**(1): p. 551-571.
130. Simpson, D., et al., *Mechanical regulation of cardiac myofibrillar structure*. Annals of the New York Academy of Sciences, 1995. **752**: p. 131-140.
131. Zimmermann, W.-H., et al., *Cardiac Grafting of Engineered Heart Tissue in Syngenic Rats*. Circulation, 2002. **106**(90121): p. 1511--157.
132. Zimmermann, W.-H., I. Melnychenko, and T. Eschenhagen, *Engineered heart tissue for regeneration of diseased hearts*. Biomaterials, 2004. **25**(9): p. 1639.
133. Blankesteyn, W., et al., *Dynamics of cardiac wound healing following myocardial infarction: observations in genetically altered mice*. Acta Physiologica Scandinavica, 2001. **173**(1): p. 75-82.
134. Berry, M.F., et al., *Mesenchymal stem cell injection after myocardial infarction improves myocardial compliance*. American Journal of Physiology - Heart and Circulatory Physiology, 2006. **290**(6): p. H2196-2203.
135. Jacot, J.G., J.C. Martin, and D.L. Hunt, *Mechanobiology of cardiomyocyte development*. Journal of Biomechanics, 2010. **43**(1): p. 93-98.

136. Marijjanowski, M.M.H., et al., *The neonatal heart has a relatively high content of total collagen and type I collagen, a condition that may explain the less compliant state.* Journal of the American College of Cardiology, 1994. **23**(5): p. 1204-1208.
137. Thompson, R.P., et al., *Collagen syntehsis in the developing chick heart.* Texas Reports on Biology and Medicine, 1979. **39**: p. 305-319.
138. Jacot, J.G., A.D. McCulloch, and J.H. Omens, *Substrate Stiffness Affects the Functional Maturation of Neonatal Rat Ventricular Myocytes.* Biophysical Journal, 2008: p. biophysj.107.124545.
139. Engler, A.J., et al., *Embryonic cardiomyocytes beat best on a matrix with heart-like elasticity: scar-like rigidity inhibits beating.* Journal of Cell Science, 2008. **121**(22): p. 3794-3802.
140. de Boer, T.P., et al., *Human cardiomyocyte progenitor cell-derived cardiomyocytes display a matured electrical phenotype.* Journal of Molecular and Cellular Cardiology, 2010. **48**(1): p. 254-260.
141. Mahony, L., *Cardiac membrane structure and function*, in *Development of Cardiovascular Systems*, W.W. Burggren and B.B. Keller, Editors. 1997, Cambridge University Press: Cambridge.
142. Wahler, G.M., et al., *Time course of postnatal changes in rat heart action potential and in transient outward current is different.* American Journal of Physiology - Heart and Circulatory Physiology, 1994. **267**(3): p. H1157-H1166.
143. Wetzel, G.T. and T.S. Klitzner, *Developmental cardiac electrophysiology recent advances in cellular physiology.* Cardiovascular Research, 1996. **31**(suppl1): p. E52-E60.
144. Carmeliet, E., *Intracellular Ca²⁺ concentration and rate adaptation of the cardiac action potential.* Cell Calcium, 2004. **35**(6): p. 557-573.
145. Ravens, U. and E. Wettwer, *Electrophysiological aspects of changes in heart rate.* Basic Research in Cardiology, 1998. **93**(0): p. s060-s065.
146. Itzhaki, I., et al., *Calcium Handling in Embryonic Stem Cell-Derived Cardiac Myocytes.* Annals of the New York Academy of Sciences, 2006. **1080**(1): p. 207-215.
147. Gomez, J.P., D. Potreau, and G. Raymond, *Intracellular calcium transients from newborn rat cardiomyocytes in primary culture.* Cell Calcium, 1994. **15**(4): p. 265-275.
148. Huang, J., L. Hove-Madsen, and G.F. Tibbits, *Na⁺/Ca²⁺ exchange activity in neonatal rabbit ventricular myocytes.* American Journal of Physiology - Cell Physiology, 2005. **288**(1): p. C195-C203.

149. Pegg, W. and M. Michalak, *Differentiation of sarcoplasmic reticulum during cardiac myogenesis*. American Journal of Physiology - Heart and Circulatory Physiology, 1987. **252**(1): p. H22-H31.
150. Satin, J., et al., *Calcium Handling in Human Embryonic Stem Cell-Derived Cardiomyocytes*. Stem Cells, 2008. **26**(8): p. 1961-1972.
151. Pillekamp, F., et al., *Physiological Differences Between Transplanted and Host Tissue Cause Functional Decoupling after in vitro Transplantation of Human Embryonic Stem Cell-Derived Cardiomyocytes*. Cellular Physiology and Biochemistry, 2009. **23**(1-3): p. 065-074.
152. Caspi, O., et al., *Transplantation of Human Embryonic Stem Cell-Derived Cardiomyocytes Improves Myocardial Performance in Infarcted Rat Hearts*. Journal of the American College of Cardiology, 2007. **50**(19): p. 1884-1893.
153. Cai, J., et al., *Transplantation of embryonic stem cell-derived cardiomyocytes improves cardiac function in infarcted rat hearts*. Cytotherapy, 2007. **9**(3): p. 283-291.
154. Caspi, O., et al., *Tissue Engineering of Vascularized Cardiac Muscle From Human Embryonic Stem Cells*. Circulation Research, 2007. **100**(2): p. 263-272.
155. Stevens, K.R., et al., *Physiological function and transplantation of scaffold-free and vascularized human cardiac muscle tissue*. Proceedings of the National Academy of Sciences, 2009. **106**(39): p. 16568-16573.
156. Allegrucci, C. and L.E. Young, *Differences between human embryonic stem cell lines*. Human Reproduction Update, 2007. **13**(2): p. 103-120.
157. Murry, C.E. and G. Keller, *Differentiation of Embryonic Stem Cells to Clinically Relevant Populations: Lessons from Embryonic Development*. Cell, 2008. **132**(4): p. 661-680.
158. Kim, C., et al., *Non-Cardiomyocytes Influence the Electrophysiological Maturation of Human Embryonic Stem Cell-Derived Cardiomyocytes During Differentiation*. Stem Cells and Development, 2010. **19**(6): p. 783-795.
159. Rakusan, K., *Postnatal development of the heart*. Hearts and Heart-like Organs, ed. G.H. Bourne. Vol. 1. 1980, New York: Academic Press, Inc.
160. Lough, J. and Y. Sugi, *Endoderm and heart development*. Developmental Dynamics, 2000. **217**(4): p. 327-342.
161. Marchionni, M.A., *neu tack on neuregulin*. Nature, 1995. **378**(6555): p. 334-335.
162. Lee, K.-F., et al., *Requirement for neuregulin receptor erbB2 in neural and cardiac development*. Nature, 1995. **378**(6555): p. 394-398.

163. Zhao, Y.-y., et al., *Neuregulins Promote Survival and Growth of Cardiac Myocytes*. Journal of Biological Chemistry, 1998. **273**(17): p. 10261-10269.
164. Narmoneva, D.A., et al., *Endothelial Cells Promote Cardiac Myocyte Survival and Spatial Reorganization: Implications for Cardiac Regeneration*. Circulation, 2004. **110**(8): p. 962-968.
165. Barouch, L.A., et al., *Nitric oxide regulates the heart by spatial confinement of nitric oxide synthase isoforms*. Nature, 2002. **416**(6878): p. 337-339.
166. Vigne, P., et al., *Endothelin mobilizes Ca²⁺ from a caffeine- and ryanodine-insensitive intracellular pool in rat atrial cells*. Journal of Biological Chemistry, 1990. **265**(12): p. 6782-6787.
167. Woo, S.H. and C.O. Lee, *Effects of Endothelin-1 on Ca²⁺ Signaling in Guinea-Pig Ventricular Myocytes: Role of Protein Kinase C*. Journal of Molecular and Cellular Cardiology, 1999. **31**(3): p. 631-643.
168. Jiang, Z. and M. Zhou, *Neuregulin Signaling and Heart Failure*. Current Heart Failure Reports, 2010. **7**(1): p. 42-47.
169. Fishman, M.C. and K.R. Chien, *Fashioning the vertebrate heart: earliest embryonic decisions*. Development, 1997. **124**(11): p. 2099-2117.
170. Lyons, G.E., *In situ analysis of the cardiac muscle gene program during embryogenesis*. Trends in Cardiovascular Medicine. **4**(2): p. 70-77.
171. Reese, D.E., T. Mikawa, and D.M. Bader, *Development of the Coronary Vessel System*. Circulation Research, 2002. **91**(9): p. 761-768.
172. Smith, T.K. and D.M. Bader, *Signals from both sides: Control of cardiac development by the endocardium and epicardium*. Seminars in Cell & Developmental Biology, 2007. **18**(1): p. 84-89.
173. Harris, I. and B. Black, *Development of the Endocardium*. Pediatric Cardiology, 2010. **31**(3): p. 391-399.
174. Bhattacharya, S., S.T. Macdonald, and C.R. Farthing, *Molecular mechanisms controlling the coupled development of myocardium and coronary vasculature*. Clinical Science, 2006. **111**(1): p. 35-46.
175. Rosemblit, N., et al., *Intracellular Calcium Release Channel Expression during Embryogenesis*. Developmental Biology, 1999. **206**(2): p. 163-177.
176. Ades, E.W., et al., *HMEC-1: Establishment of an Immortalized Human Microvascular Endothelial Cell Line*. Journal of Investigative Dermatology, 1992. **99**(6): p. 683-690.
177. Perkel, J., *15 Tips & Tricks for Human Embryonic Stem Cells*. The Scientist, 2005. **19**(13): p. 18-19.

178. Thomas, R.J., et al., *Automated, scalable culture of human embryonic stem cells in feeder-free conditions*. *Biotechnology and Bioengineering*, 2009. **102**(6): p. 1636-1644.
179. Gerecht-Nir, S., S. Cohen, and J. Itskovitz-Eldor, *Bioreactor cultivation enhances the efficiency of human embryoid body (hEB) formation and differentiation*. *Biotechnology and Bioengineering*, 2004. **86**(5): p. 493-502.
180. Mahlstedt, M.M., et al., *Maintenance of pluripotency in human embryonic stem cells cultured on a synthetic substrate in conditioned medium*. *Biotechnology and Bioengineering*, 2010. **105**(1): p. 130-140.
181. Crook, J.M., et al., *The Generation of Six Clinical-Grade Human Embryonic Stem Cell Lines*. *Cell Stem Cell*, 2007. **1**(5): p. 490-494.
182. Mallon, B.S., et al., *Toward xeno-free culture of human embryonic stem cells*. *The International Journal of Biochemistry & Cell Biology*, 2006. **38**(7): p. 1063-1075.
183. Jensen, J., J. Hyllner, and P. Björquist, *Human embryonic stem cell technologies and drug discovery*. *Journal of Cellular Physiology*, 2009. **219**(3): p. 513-519.
184. Bauwens, C.L., et al., *Control of Human Embryonic Stem Cell Colony and Aggregate Size Heterogeneity Influences Differentiation Trajectories*. *Stem Cells*, 2008. **26**(9): p. 2300-2310.
185. Burridge, P.W., et al., *Improved Human Embryonic Stem Cell Embryoid Body Homogeneity and Cardiomyocyte Differentiation from a Novel V-96 Plate Aggregation System Highlights Interline Variability*. *Stem Cells*, 2007. **25**(4): p. 929-938.
186. Carpenedo, R.L., C.Y. Sargent, and T.C. McDevitt, *Rotary Suspension Culture Enhances the Efficiency, Yield, and Homogeneity of Embryoid Body Differentiation*. *Stem Cells*, 2007. **25**(9): p. 2224-2234.
187. Vlodavsky, I., et al., *Endothelial cell-derived basic fibroblast growth factor: synthesis and deposition into subendothelial extracellular matrix*. *Proceedings of the National Academy of Sciences*, 1987. **84**(8): p. 2292-2296.
188. Tu, Q., et al., *Improved Endothelialization of Titanium Vascular Implants by Extracellular Matrix Secreted from Endothelial Cells*. *Tissue Engineering Part A*, 2010. **16**(12): p. 3635-3645.
189. Dubin, D., *Ion Adventure in the Heartland, Volume I*. 2003, Tampa: Cover Publishing Company.
190. Li, X., et al., *Endothelin-1 Induced Arrhythmogenic Ca²⁺ Signaling Is Abolished in Atrial Myocytes of Inositol-1,4,5-Trisphosphate(IP3) Receptor Type 2, Deficient Mice*. *Circulation Research*, 2005. **96**(12): p. 1274-1281.

191. Willam, C., et al., *Tie2 Receptor Expression Is Stimulated by Hypoxia and Proinflammatory Cytokines in Human Endothelial Cells*. *Circulation Research*, 2000. **87**(5): p. 370-377.
192. Nilsson, I., M. Shibuya, and S. Wennström, *Differential activation of vascular genes by hypoxia in primary endothelial cells*. *Experimental Cell Research*, 2004. **299**(2): p. 476-485.
193. Satin, J., et al., *Mechanism of spontaneous excitability in human embryonic stem cell derived cardiomyocytes*. *The Journal of Physiology*, 2004. **559**(2): p. 479-496.
194. Kattman, S.J., T.L. Huber, and G.M. Keller, *Multipotent Flk-1+ Cardiovascular Progenitor Cells Give Rise to the Cardiomyocyte, Endothelial, and Vascular Smooth Muscle Lineages*. *Developmental Cell*, 2006. **11**(5): p. 723-732.
195. Liu, J., et al., *Facilitated maturation of Ca²⁺ handling properties of human embryonic stem cell-derived cardiomyocytes by calsequestrin expression*. *American Journal of Physiology - Cell Physiology*, 2009. **297**(1): p. C152-C159.
196. Jacot, J.G., A.D. McCulloch, and J.H. Omens, *Substrate Stiffness Affects the Functional Maturation of Neonatal Rat Ventricular Myocytes*. *Biophysical Journal*, 2008. **95**(7): p. 3479-3487.
197. Heynen, S., D. Gough, and J. Price, *Optically Stailized Mercury Vapor Short Arc Lamp as UV-Light Source for Microscopy*. *SPIE Photonics West '97*, 1997. **2982**: p. 430-434.
198. Limpert, E., W.A. Stahel, and M. Abbt, *Log-normal distributions across the sciences: keys and clues*. *BioScience*, 2001. **51**(05): p. 341-352.
199. Fu, J.-D., et al., *Crucial role of the sarcoplasmic reticulum in the developmental regulation of Ca²⁺ transients and contraction in cardiomyocytes derived from embryonic stem cells*. *The FASEB Journal*, 2006. **20**(1): p. 181-183.
200. Fu, J.D., et al., *Na⁺/Ca²⁺ Exchanger is a Determinant of Excitation-Contraction Coupling in Human Embryonic Stem Cell-Derived Ventricular Cardiomyocytes*. *Stem Cells and Development*, 2010. **19**(6): p. 773-782.
201. Klitzner, T. and W. Friedman, *A dimisned role for the sarcoplasmic reticulum in newborn myocardial contraction: effects of ryanodine*. *Pediatric Research*, 1989. **26**(2): p. 98-101.
202. Seguchi, M., J.A. Harding, and J.M. Jarmakani, *Developmental change in the function of sarcoplasmic reticulum*. *Journal of Molecular and Cellular Cardiology*, 1986. **18**(2): p. 189-195.

203. Klitzner, T.S., et al., *Calcium current and tension generation in immature mammalian myocardium: Effects of diltiazem*. Journal of Molecular and Cellular Cardiology, 1991. **23**(7): p. 807-815.
204. Kockskamper, J., et al., *Emerging roles of inositol 1,4,5-trisphosphate signaling in cardiac myocytes*. Journal of Molecular and Cellular Cardiology, 2008. **45**(2): p. 128-147.
205. Sedan, O., et al., *Human embryonic stem cell–derived cardiomyocytes can mobilize 1,4,5-inositol trisphosphate–operated $[Ca^{2+}]_i$ stores*. Annals of the New York Academy of Sciences, 2010. **1188**(1): p. 68-77.
206. de Boer, T., et al., *Adrenergic regulation of conduction velocity in cultures of immature cardiomyocytes*. Netherlands Heart Journal, 2008. **16**(3): p. 106-109.
207. Renaud, J., et al., *Differentiation of the fast Na^+ channel in embryonic heart cells: interaction of the channel with neurotoxins*. Proceedings of the National Academy of Sciences, 1981. **78**(9): p. 5348-52.
208. Nathan, R. and R. DeHaan, *In vitro differentiation of a fast Na^+ conductance in embryonic heart cell aggregates*. Proceedings of the National Academy of Sciences, 1978. **75**(6): p. 1776-2780.
209. del Monte, F., et al., *Restoration of Contractile Function in Isolated Cardiomyocytes From Failing Human Hearts by Gene Transfer of SERCA2a*. Circulation, 1999. **100**(23): p. 2308-2311.
210. Binah, O., et al., *Functional and developmental properties of human embryonic stem cells-derived cardiomyocytes*. Journal of Electrocardiology, 2007. **40**(6, Supplement 1): p. S192-S196.
211. Brittsan, A.G. and E.G. Kranias, *Phospholamban and Cardiac Contractile Function*. Journal of Molecular and Cellular Cardiology, 2000. **32**(12): p. 2131-2139.
212. Qu, Y., et al., *Gene expression of Na^+/Ca^{2+} exchanger during development in human heart*. Cardiovascular Research, 2000. **45**(4): p. 866-873.
213. Haddock, P.S., W.A. Coetzee, and M. Artman, *Na^+/Ca^{2+} exchange current and contractions measured under Cl^- -free conditions in developing rabbit hearts*. American Journal of Physiology - Heart and Circulatory Physiology, 1997. **273**(2): p. H837-H846.
214. Nakamura, K., et al., *Complete heart block and sudden death in mice overexpressing calreticulin*. The Journal of Clinical Investigation, 2001. **107**(10): p. 1245-1253.

215. Pavlovic, M., et al., *Age-dependent suppression of SERCA2a mRNA in pediatric atrial myocardium*. Biochemical and Biophysical Research Communications, 2005. **326**(2): p. 344-348.
216. van Tuyn, J., et al., *Fibroblasts from human postmyocardial infarction scars acquire properties of cardiomyocytes after transduction with a recombinant myocardin gene*. The FASEB Journal, 2007. **21**(12): p. 3369-3379.
217. Schroeter, A., et al., *Structure and function of splice variants of the cardiac voltage-gated sodium channel Nav1.5*. Journal of Molecular and Cellular Cardiology, 2010. **49**(1): p. 16-24.
218. Blaustein, M.P. and W.J. Lederer, *Sodium/Calcium Exchange: Its Physiological Implications*. Physiological Reviews, 1999. **79**(3): p. 763-854.
219. Uchida, K., et al., *Gene Knock-Outs of Inositol 1,4,5-Trisphosphate Receptors Types 1 and 2 Result in Perturbation of Cardiogenesis*. PLoS ONE, 2010. **5**(9): p. e12500.
220. Qu, Y. and M. Boutjdir, *Gene Expression of SERCA2a and L- and T-type Ca Channels during Human Heart Development*. Pediatric Research, 2001. **50**(5): p. 569-574.
221. Schroder, E.A., Y. Wei, and J. Satin, *The Developing Cardiac Myocyte*. Annals of the New York Academy of Sciences, 2006. **1080**(1): p. 63-75.
222. Ono, K. and T. Iijima, *Cardiac T-type Ca²⁺ channels in the heart*. Journal of Molecular and Cellular Cardiology, 2010. **48**(1): p. 65-70.
223. Lompre, A.-M., M. Anger, and D. Levitsky, *Sarco(endo)plasmic Reticulum Calcium Pumps in the Cardiovascular System: Function and Gene Expression*. Journal of Molecular and Cellular Cardiology, 1994. **26**(9): p. 1109-1121.
224. Simmerman, H.K.B. and L.R. Jones, *Phospholamban: Protein Structure, Mechanism of Action, and Role in Cardiac Function*. Physiological Reviews, 1998. **78**(4): p. 921-947.
225. Terentyev, D., et al., *Calsequestrin determines the functional size and stability of cardiac intracellular calcium stores: Mechanism for hereditary arrhythmia*. Proceedings of the National Academy of Sciences, 2003. **100**(20): p. 11759-11764.
226. Lynch, J.M., et al., *Assembling Pieces of the Cardiac Puzzle; Calreticulin and Calcium-Dependent Pathways in Cardiac Development, Health, and Disease*. Trends in Cardiovascular Medicine, 2006. **16**(3): p. 65-69.
227. Li, J., et al., *Calreticulin reveals a critical Ca²⁺ checkpoint in cardiac myofibrillogenesis*. The Journal of Cell Biology, 2002. **158**(1): p. 103-113.

228. van Veen, T.A.B., H.V.M. van Rijen, and T. Opthof, *Cardiac gap junction channels: modulation of expression and channel properties*. Cardiovascular Research, 2001. **51**(2): p. 217-229.
229. Kawamoto, A., et al., *Therapeutic potential of ex vivo expanded endothelial progenitor cells for myocardial ischemia*. Circulation, 2001. **103**(5): p. 634-7.
230. Kocher, A.A., et al., *Neovascularization of ischemic myocardium by human bone-marrow-derived angioblasts prevents cardiomyocyte apoptosis, reduces remodeling and improves cardiac function*. Nature Medicine, 2001. **7**(4): p. 430-6.
231. Murohara, T., et al., *Transplanted cord blood-derived endothelial precursor cells augment postnatal neovascularization*. Journal of Clinical Investigation, 2000. **105**(11): p. 1527-36.
232. Urbich, C., et al., *Relevance of monocytic features for neovascularization capacity of circulating endothelial progenitor cells*. Circulation, 2003. **108**(20): p. 2511-6.
233. Fukazawa, R., et al., *Neuregulin-1 protects ventricular myocytes from anthracycline-induced apoptosis via erbB4-dependent activation of PI3-kinase/Akt*. Journal of Molecular Cell Cardiology, 2003. **35**(12): p. 1473-9.
234. Kuramochi, Y., et al., *Cardiac endothelial cells regulate reactive oxygen species-induced cardiomyocyte apoptosis through neuregulin-1beta/erbB4 signaling*. Journal of Biological Chemistry, 2004. **279**(49): p. 51141-7.
235. Remondino, A., et al., *Beta-adrenergic receptor-stimulated apoptosis in cardiac myocytes is mediated by reactive oxygen species/c-Jun NH2-terminal kinase-dependent activation of the mitochondrial pathway*. Circulation Research, 2003. **92**(2): p. 136-8.
236. Minami, E., et al., *Extracardiac progenitor cells repopulate most major cell types in the transplanted human heart*. Circulation, 2005. **112**(19): p. 2951-8.
237. Levenberg, S., et al., *Endothelial cells derived from human embryonic stem cells*. Proceedings of the National Academy of Sciences, 2002. **99**(7): p. 4391-6.
238. Levenberg, S., et al., *Endothelial potential of human embryonic stem cells*. Blood, 2007. **110**(3): p. 806-814.
239. Shaw, J.P., R. Basch, and P. Shamamian, *Hematopoietic stem cells and endothelial cell precursors express Tie-2, CD31 and CD45*. Blood Cells Mol Dis, 2004. **32**(1): p. 168-75.
240. Choi, K., et al., *A common precursor for hematopoietic and endothelial cells*. Development, 1998. **125**(4): p. 725-32.

241. Schlaeger, T., et al., *Uniform vascular-endothelial-cell-specific gene expression in both embryonic and adult transgenic mice*. Proceedings of the National Academy of Sciences, 1997. **94**: p. 3059-3063.
242. Gerecht-Nir, S., et al., *Vascular Development in Early Human Embryos and in Teratomas Derived from Human Embryonic Stem Cells*. Biology of Reproduction, 2004. **71**(6): p. 2029-2036.
243. Zufferey, R., et al., *Self-Inactivating Lentivirus Vector for Safe and Efficient In Vivo Gene Delivery*. Journal of Virology, 1998. **72**(12): p. 9873-9880.
244. Sato, T.N., et al., *Tie-1 and tie-2 define another class of putative receptor tyrosine kinase genes expressed in early embryonic vascular system*. Proceedings of the National Academy of Sciences, 1993. **90**(20): p. 9355-9358.
245. Schlaeger, T.M., et al., *Uniform vascular-endothelial-cell-specific gene expression in both embryonic and adult transgenic mice*. Proceedings of the National Academy of Sciences, 1997. **94**(7): p. 3058-3063.
246. Chen, B.P.C., et al., *DNA microarray analysis of gene expression in endothelial cells in response to 24-h shear stress*. Physiological Genomics, 2001. **7**(1): p. 55-63.
247. Frangos, J., et al., *Flow effects on prostacyclin production by cultured human endothelial cells*. Science, 1985. **227**(4693): p. 1477-9.
248. De Val, S., et al., *Combinatorial Regulation of Endothelial Gene Expression by Ets and Forkhead Transcription Factors*. Cell, 2008. **135**(6): p. 1053-1064.